Ecology and Evolutionary Biology
2025, Vol. 10, No. 2, pp. 34-103
https://doi.org/10.11648/j.eeb.20251002.11

Research Article

Underwater Optical Properties of Lake Texoma (Oklahoma-Texas) Using Secchi Disk, Submarine Photometer, and High-resolution Spectroscopy

David Alan Rolbiecki*

Texas Military Department, Texas National Guard, Camp Mabry, Austin, The United States

Abstract

This research represents the author's thesis, which was completed in 1998, in partial fulfilment of the Master of Science degree in biology from the University of North Texas, Denton, United States, culminating in twelve months of field collection carried out in conjunction with the Lake Texoma Water Quality Monitoring Program (WQMP) funded by the U.S. Army Corps of Engineers, Tulsa District. The purpose of this research was to characterize the underwater light regime in Lake Texoma using secchi disk, submarine photometer, and high-resolution spectroscopy at eleven fixed stations from August 1996 to August 1997. The objectives of this research was to 1) measure Secchi transparency at each station with submarine photometry to characterize seasonal and spatial values of secchi depth (SD); 2) determine vertical attenuation coefficients (η") and depth of euphotic zone (*Zeu*); 3) Compare secchi depth (SD), Zeu, and η" with published data taken from other water bodies; 4) Model SD and η" with water quality parameters taken during the sampling periods; 5) Obtain spectral data in narrow bandwidths from 300 to 800nm using high-resolution spectroscopy; 6) Examine spectral irradiance, reflectance, and attenuation in the green (500-600nm), red (600-700nm), and near-infrared (700-800nm) spectrum; and 7) Model reflectance spectra with water quality parameters taken during the sampling periods. Indices of *Zeu*: SD and η" x SD were compared with universally applied values derived from published research of inland and coastal waters. Turbidity explained 76% of the variation ($p = 0.0001$) of η" among water quality parameters, including chlorophyll-*a*. Spectral signatures of chlorophyll-*a* and turbidity were measured with the spectroradiometer and quantified. Stations with low turbidity exhibited a distinct green reflectance peak around 590-610 nanometers, indicating presence of chlorophyll-*a*. Stations with high turbidity exhibited a reflectance peak shift towards the red spectrum, making it difficult to detect the chlorophyll signature. Derivative analysis of the reflectance signal at 590-610, and 720-780 nanometers allowed discrimination of this chlorophyll signature from those of turbidity ($0.66 < r^2 < 0.99$).

Keywords

Secchi Depth, Depth of the Euphotic Zone, Photosynthetically Available Radiation, Attenuation Coefficients, Spectral Irradiance, Reflectance Spectra, Absorption, Chlorophyll-a, Turbidity, Submarine Photometer, Spectroradiometer, Blue-green-red-infra Red Spectrum, Derivative Analysis

*Corresponding author: david.a.rolbiecki.mil@cfmo.mil.texas.gov (David Alan Rolbiecki)

Received: 7 May 2025; **Accepted:** 6 June 2025; **Published:** 23 June 2025

Copyright: © The Author(s), 2025. Published by Science Publishing Group. This is an **Open Access** article, distributed under the terms of the Creative Commons Attribution 4.0 License (http://creativecommons.org/licenses/by/4.0/), which permits unrestricted use, distribution and reproduction in any medium, provided the original work is properly cited.

1. Introduction

1.1. The Relationship of Light and Water

The radiant energy of the sun is the source of life in the biosphere. The world's climates are controlled by the sun, driving temperature, wind and rain [28]. The basis of productivity in water bodies comes from the sun, which drives metabolic energy through heat and photosynthesis [59]. Juday [31] realized in his time that seasonal changes of solar radiation impinging upon the surface of freshwater lakes were the principal biotic and abiotic factor. For all practical purposes, the sun drives the energy budget of lakes, having a profound influence on temperature, circulation and stratification [59].

The function of light in determining the trophic status and water quality of freshwater lakes, reservoirs, estuaries, and marine environments has been studied extensively [13, 14, 18-20, 23, 31, 44, 49-51, 54]. Present environmental and water quality issues have focused attention on two principal factors affecting light penetration through the water column and subsequently water quality: suspended sediments and chlorophyll concentration [40, 47], both of which absorb and reflect light; e.g., absorption [49]; absorption and reflection [11, 16, 44]; secchi depth and chlorophyll concentration [37]; and algal light shading [29, 54].

In the visible portion of the electromagnetic spectrum, light utilized for photosynthesis or photosynthetically available radiation (PAR) extends from 350 to 750nm [18-20] [1]). The distribution of PAR through the water column has important ecological implications, the most apparent is its effect on a lake's trophic status, which controls gross photosynthetic rates among phytoplankton [29].

Subsurface solar radiation is greatly affected as it penetrates the water column, reducing it to narrow spectral bands of blue, green, or blue-green [3]. As incoming solar radiation strikes the surface of the water, much of it (>50%, initially) is absorbed in the infrared region (>1000nm), transforming energy into heat [59]. Water will transmit or absorb light in the PAR region, as well as in the near infrared region at ~800nm [11]. The degree of absorption in water may be highly wavelength dependent or selectively absorbed by dissolved particles or scattered by suspended sediments [7, 40]. At depth, PAR is affected by both scattering and absorption, depending on the amount of suspended solids and organic matter present [11, 29, 40, 43, 47]. Thus, absorption and scattering properties of the aquatic medium are the inherent optical properties of surface waters [53]. Apparent optical properties of the aquatic medium are dependent upon inherent optical properties of the water body itself and are a function of both the contents in the water and the underwater light field [23]. Examples of apparent optical properties include vertical attenuation and reflectance.

[1] Dubinsky and Berman [18] coined the term "photosynthetically active radiation (PhAR). In Dubinsky and Berman [20], it was changed to 'photosynthetically available radiation (PAR)."

Primary production in water depends upon the depth of which PAR is transmitted. The maximum depth in which light is used for production by phytoplankton is at 1% of photosynthetically available light, often referred to as the euphotic zone [29, 54]. The euphotic zone (*Zeu*) varies between lakes and sites within lakes owing to the different watershed sources of allochthonous and autochthonous inputs [55], both natural and anthropogenetic [15, 29], as well as diurnal and seasonal changes caused by wind-induced mixing and stratification of the water column [29, 59].

1.2. Measuring Photosynthetically Available Radiation

Various methods for measuring PAR and relating it to productivity have been used in limnological research. One of the most basic is secchi depth measurement [22, 35-37, 56] and is used extensively to characterize the clarity of a water body. The secchi disk is a simple device used to estimate visibility through the water column and provides a visual index of the water clarity [7]. Changes in secchi depth have often been related to phytoplankton biomass and fish yield [37], turbidity and dissolved and colloidal organic matter [34], and overall trophic state [8, 9]. Secchi depth, at extremes, represents between 1 to 15-percent light transmission [59]. The depth of the euphotic zone can be estimated using secchi depth, after careful measurements by observers over a range of water conditions using established standards [38]. Ranges in secchi depth run from a few centimeters in turbid or highly colored water, to more than 40 meters in very clear lakes [59]. Thus, it is apparent that in order to use secchi depth as an indicator of algal biomass, turbidity and color in the water needs to be nominal [9, 34, 37].

Submarine photometers are capable of detecting light further into the blue and red regions of the spectrum than the human eye [7, 38]. Using a submarine photometer, the vertical attenuation coefficient (symbolized as η by Wetzel [59]; or k by Carlson [10], and Megard [45] is determined, from which a more precise means of measuring light irradiance available at depth is made (Schwartz et al. 1996). Using both secchi depth and submarine photometer readings, standard conversions between the two measurements can be developed. Based on empirical data $\eta\ m^{-1}$ is about 1.7 ÷ secchi depth; although values from other bodies of water range between 1.16 to 1.45 [34, 56, 59].

More advanced methods of measuring PAR include the use of laboratory-based spectrophotometers [15, 49], and airborne/satellite remote sensing [15, 16, 47]. However, use of airborne and satellite remote sensing platforms have their limitations due to the loss of spectral wavelength resolution from broad, spectral band set imaging and require the use of "ground truthing" with field spectroradiometric and laboratory-based spectrophotometric measurements [1, 15]. Broad-band imaging and interpretation is not practical in the

400-500nm wavelengths due to the highly exponentially increasing spectral absorbency [15], where much absorption of light takes place from the presence of suspended solids. In the 500-800nm region where presence of chlorophyll-*a* can be measured; broadband remote sensing lacks the resolving ability to differentiate between algal pigments and their respective peak absorption wavelengths. Furthermore, broadband imagery lacks the resolution to discriminate between algal chlorophyll and suspended solids, whose optimal ability is in the examination of terrestrial rather than aquatic systems [25]. Detecting small quantities of chlorophyll-*a* and turbidity with remotely sensed satellite data might not be practical in lake management where these quantities, if detected, are less than the magnitude needed for statistical significance [8]. Therefore, the use of high-resolution spectral imaging is needed in order to discriminate between these features [1, 11, 16, 25], to allow more accurate and statistically significant predictors of water quality parameters.

High-resolution spectral imaging has incorporated the use of spectroradiometers with resolutions of 2-10nm for limnological and coastal studies [1, 11, 15, 18-20]. With the different spectral absorption characteristics of species-specific chlorophyta whose absorption peaks cover a very narrow spectral band width, high-resolution spectroradiometric measurements have a far superior ability to predict chlorophyll concentrations and other ecological water parameters than the broad-band remote sensing abilities of airborne and satellite platforms [1, 15].

1.3. Lake Texoma Water Quality Monitoring Program

This research is a culmination of twelve months of field collection carried out in conjunction with the Lake Texoma Water Quality Monitoring Program (WQMP) by the University of North Texas. The WQMP, a proposed, five-year study funded by the U.S. Army Corps of Engineers, is designed to establish a base line of physical-chemical-biological data over time in order to evaluate any changes to water quality in Lake Texoma due to the planned, phased reduction of chlorides. Chloride control is intended to remove salts from the Red River for the benefit of downstream uses in Lake Texoma, such as drinking water and agricultural irrigation [2].

Far too often today, however, water quality is associated only for human consumption and does not address the biological aspects of water quality. For example, Lake Texoma has a large population of reproducing striped bass, and therefore, boasts a well-established striped bass fishery [2, 41, respectively]. With the introduction of chloride control to Lake Texoma, there is concern for what the impact will have on the aquatic wildlife in the lake; specifically, the "bottom-up" effect on the food chain. The potential impact on the "bottom-up" trophic interaction would be an increase in turbidity due to the absence of a "flocculating" electrolyte such as chloride [22]. Decreases in chloride would allow clay particles to remain in suspension longer and thereby increase turbidity and reduce the amount of light for phytoplanktonic primary producers. This could affect populations of organisms at higher trophic levels. Thus, the issues to be addressed by the Lake Texoma Water Quality Program include examining the effectiveness of the chloride control project; and examine the relationships between chloride concentration, turbidity and phytoplankton.

1.4. Purpose and Objectives

The purpose of this thesis is to characterize the underwater light regime in Lake Texoma using secchi disk and photometer estimates as well as high-resolution spectroscopy. A total of 11 sampling sites – two for each of five delineated zones (3 in Red River Transition Zone) of historical physical-chemical-biological significance were chosen for this characterization in order to investigate the relationships between ecologically important water quality parameters and the underwater spectral characteristics of photosynthetically active radiation unique to each site. Twelve months of field data collecting (August 1996-August 1997) coincided with regular, monthly scheduled sampling trips made by the Lake Texoma Water Quality Monitoring Program.

The objectives of this thesis are to:

1. Determine the depth of the euphotic zone (*Zeu*) at each station and the attenuation coefficient (η").
2. Determine secchi transparency at each station.
3. Compare secchi depth (SD), *Zeu*, and η" with published data taken from other water bodies.
4. Model SD and η" with water quality parameters taken during the sampling periods.
5. Obtain spectral data in narrow bandwidths from 300 to 800nm using high-resolution spectroscopy.
6. Examine spectral irradiance, reflectance, and attenuation in the green (500-600nm), red (600-700nm), and near-infrared (700-800nm) spectrum.
7. Model reflectance spectra with water quality parameters taken during the sampling periods.

Table 1. *Locations of fixed sampling stations.*

station	zone	sampling intensity	depth (meters)	latitude	longitude
1	RR	routine	6	33 °54' 44"N	96 °54' 04"W
3	RR	intensive	13	33 °52' 26"N	96 °50' 01"W

station	zone	sampling intensity	depth (meters)	latitude	longitude
7	BM	routine	9	33 °47' 59"N	96 °48' 16"W
8	RRT	routine	17	33 °49' 38"N	96 °46' 09"W
9	RRT	intensive	19	33 °50' 08"N	96 °42' 18"W
17	ML	intensive	25	33 °49' 29"N	96 °36' 00"W
19	ML	routine	24	33 °53' 21"N	96 °35' 06"W
20	WRT	routine	15	33 °55' 49"N	96 °33' 22"W
22	WRT	intensive	19	34 °00' 03"N	96 °37' 34"W
24	WR	intensive	12	34 °01' 42"N	96 °34' 11"W
25	WR	routine	7	34 °02' 34"N	96 °34' 02"W

RR = Red River BM = Big Mineral RRT = Red River Transition ML = Main Lake
WR = Washita River WRT = Washita River Transition

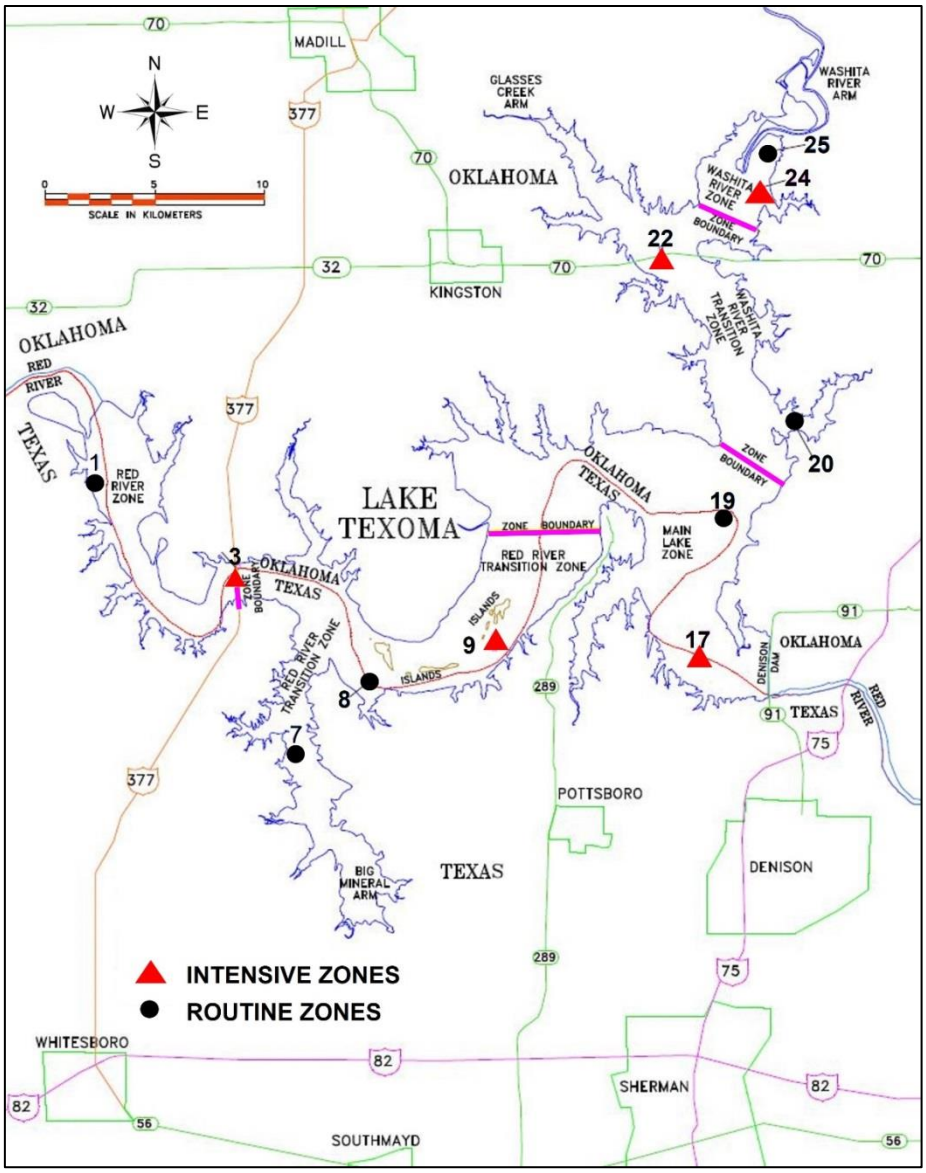

Figure 1. *Sampling stations at Lake Texoma.*

2. Materials and Methods

2.1. Study Area

Lake Texoma, fed by the Red and Washita rivers, is situated on the border of north central Texas and southeastern Oklahoma (Figure 1). The watershed encompasses a 102,870-km^2 area consisting of primarily agricultural land use [41]. Lake Texoma is documented to have four distinct zones based on historical water quality studies [2]: 1.) Red River Zone (riverine); 2.) Red River Transition Zone (riverine transitional); 3.) Main Lake Zone (lacustrine); and 4.) Washita River Zone (riverine). These zones were identified *a priori* from sampling based on historical research done on Lake Texoma [12]. The Washita River Transition Zone (riverine transitional), not previously reported in the historical data, was added in order to delineate the lake from the Washita River Zone to the Main Lake Zone [2]. The Red and Washita Rivers influence Lake Texoma with the downstream transport of chemicals [2] indicating a gradient of chemical parameters running from the upstream to the downstream sections of the reservoir. The Red River and Washita River arms are reported to be shallow (~ 18 m), and the Main Lake Zone being the deepest (22-26 m) at the confluence of the two arms at Denison Dam [41]. Lake Texoma is shown to have high nutrient input from runoff of nitrogen and phosphorus from stormwater runoff and agricultural activities and is classified to range from eutrophic to hyper-eutrophic [27]; however, the research from Clyde [12], indicated the trophic classification of Lake Texoma ranges from mesotrophic to hyper-eutrophic, depending upon concentrations of total phosphorous and chlorophyll-*a* in the epilimnion.

2.2. Sampling Frequency

Light data was collected from a boat from August 1996 to September 1997. Sampling was done at eleven fixed sampling stations, with ten located in each historical zone. An additional fixed sampling station was added to the Big Mineral Arm (Table 1). Sampling trips were carried out concurrently with the WQMP each month except for the months of October, December, and February where these months typically have low discharge events and therefore regarded to be insignificant by the WQMP. Two trips were made on the first and third weeks of May and June 1997 during spring mixing of the of the epilimnion, thermocline, and hypolimnion [57] to monitor the periods of high discharge and subsequently high chloride loading.

With the exception of Stations 3 and 22 (which are located next to bridges), the remaining stations are located offshore with no visible landmark to aid in navigating to the same spot each sampling trip. An on-board global positioning system (GPS) enabled me to reach each station without the use of landmarks to a horizontal positional accuracy of 30 meters.

2.3. Vertical Profile Measurements

Light visibility and vertical illumination was recorded from secchi disk and submarine photometer readings taken at each station. Averaging the depths when the secchi disk disappears when lowered in the water from the shaded side of the boat and when it reappears after raising it determined Secchi depth in meters [38]. Three sets were taken, and an overall average was determined. A Protomatic submarine photometer measured light energy (in foot-candles) starting with the surface followed by one-meter intervals [56] down to one percent of the surface reading.

A light profile was made for each station by regressing percent light transmission against depth. The true depth of the euphotic zone (Z_{eu}) was determined by inverse prediction of the regression equation [63]:

$$Z_{eu} = \frac{(Ln\%) - a}{b} \quad (1)$$

where Ln% = the natural logarithm of one percent (the amount of light at Z_{eu}), a = the y-intercept, and b = the slope of the regression equation.

Dividing Z_{eu} by secchi depth will obtain a factor in which to multiply secchi depths taken in the future, when a submarine photometer is not available [38]. Z_{eu} can therefore be determined by multiplying secchi depth by this constant. Additionally, the Protomatic enabled me to calculate light attenuation of the entire PAR spectrum. By applying Beer's Law, the attenuation coefficient (η) at depth (z) below the surface are calculated [1, 20, 43, 52, 59]:

$$\eta = \frac{LnIo - LnIz}{z} \quad (2)$$

where Io = irradiance at 0.1 meter, and Iz = irradiance at depth, z.

The vertical attenuation coefficient (η") over the entire light-depth profile can therefore be calculated by least square estimate [38]:

$$\eta'' = \frac{LnIo(\sum z) - \sum[z(LnIz)]}{\sum z^2} \quad (3)$$

where $\eta'' = \eta_w + \eta_p + \eta_c$: the composite of the components of water, suspended particles, and dissolved, colored components, respectively [59].

In assessing the underwater light regime, standard conversion factors from the Z_{eu}: secchi depth (SD) ratio and η" x SD were developed and compared with published literature [7, 34, 38].

2.4. High-resolution Spectroscopy

High-resolution spectroscopy was done at five fixed intensive sampling stations; one located in each zone (Table 1). The intensive stations are designed to collect more replicate samples in order to take into account the between-replicate variability that is associated with parameters such as chlorophyll-*a*, turbidity, phytoplankton, and zooplankton. For this reason, I chose to sample only the intensive stations in each zone in order to correlate my data with the greater number replicate samples of turbidity and chlorophyll-*a*. Present water quality data collected from these five intensive stations are thereby linked to the historical data of these zones [2].

Downwelling PAR spectra [18, 19, 20] was collected at 0.1, 0.5, 1.0, and 1.5-meter depths via a cosine-corrected 200 µm-diameter underwater glass fiber optic cable connected to the master channel of an Ocean Optics SD-1000 spectroradiometer. The instrument has a spectral bandwidth resolution (FWHM; full width at half the maximum peak) of 10nm when used with a 200 µm-diameter fiber, with a sampling interval of 0.5nm (manufacturers' specifications) over wavelength ranges of 262-854nm. A submersible PVC platform held the underwater fiber steady during the measurements. Simultaneously, another 200 µm glass fiber optic cable with a cosine corrector collected surface irradiance reflected off a Spectralon white-body panel which was fed to the SD-1000 slave channel. Data collected by the spectroradiometer was filed in binary format and stored on diskette in a microcomputer on the boat and later converted to ASCII format for post-processing. Every effort was made to measure light with the spectroradiometer between 0900h and 1400h local time to coincide with the sun's maximum daily irradiance [28, 54, 59].

Spectral data post-processing consisted of importing the ASCII file for each depth into a spreadsheet program. Percent transmission for each wavelength was calculated by dividing the master channel data by the slave channel data [62] after subtraction from their respective minimum values. Reflectance values were also calculated for each wavelength from the ratio of upwelling spectral irradiance to downwelling spectral irradiance [14, 15, 53, 61]. A 7-point moving average was applied to smooth the raw values of spectral irradiance [1] in order to reduce random noise and increase the signal-to-noise ratio [11, 16, 25]. Light attenuation varies with wavelength therefore vertical attenuation coefficients (η) were calculated at each wavelength (λ) [19] using Beer's Law (Equation 2).

To differentiate between turbidity and chlorophyll-*a* concentrations, I chose to run derivative analysis on reflectance values from 350-800nm. Derivative spectroscopy uses the change in the slope of a line (in this case reflectance) with wavelength (λ) to a first order or higher order [11, 25]. Geometrically, the derivative is the slope of the tangent of a curve, estimated by calculating the slope of the secant line through one or more points on both sides of x [58]:

$$\frac{f(x+h)-f(x-h)}{h} \quad (4)$$

where f = the function of x, the center point of the tangent, and h = the interval between x and points preceding and succeeding x.

The greatest advantage in using derivatives is its ability to resolve or enhance small peaks from larger peaks of percent transmission and light attenuation due to background noise [17]. A seven-point algorithm was used to estimate derivatives at the midpoint and both endpoints of any seven, contiguous and evenly spaced points [1, 25]. In this case, the seven points are at 1-nm intervals anywhere from 350-800nm:

$$\frac{df(x_3)}{d(\lambda)} = \frac{f(x_0)+9f(x_1)-45f(x_2)+45f(x_4)-9f(x_5)+f(x_6)}{60h} \quad (5)$$

where the derivative of the center point (x_3) is calculated using the preceding points (x_0, x_1, x_2) and the succeeding points (x_4, x_5, x_6), and h = the wavelength interval.

Lake Texoma exhibits dramatic inflow events, especially in the spring and early summer resulting in high turbidity [42]. Consequently, turbidity "masks" the spectral signature of chlorophyll-*a*. The spectral signature of the combination of turbidity and chlorophyll-*a* is more complex than either clear or turbid water [25]. Both turbidity and chlorophyll-*a* show up in the zero-order spectral pattern; however, derivatives differentiate between these components of the original (0^{th}-order) signal, as will be presented in Chapter 3. Location of the chlorophyll and turbidity signatures were accomplished by examining the distinctive reflectance peaks and troughs found at specific wavelengths [11, 25].

2.5. Water Quality Parameters

Replicate samples of water quality parameters taken at a depth of one meter were collected at the time of spectroradiometric readings. Ten replicates of turbidity and chlorophyll-*a*, and three replicates of total suspended solids (TSS) and total dissolved solids (TDS) were collected per station. Turbidity, TSS, and TDS were analyzed in accordance with Standard Methods at TRAC Labs, Denton, Texas. Dark bottles containing the chlorophyll-*a* samples were immediately chilled and processed at the University of North Texas within 24 hours. Chlorophyll-*a* was filtered and extracted with acetone in accordance with standard trichromatic methods and analyzed with a spectrometer for absorption in the 470 and 670nm wavelengths [19, 32, 61, 62].

2.6. Statistical Analysis

One-way parametric and nonparametric ANOVA [63] compared the spatial and temporal differences ($p < 0.05$) in mean water quality parameters along with η", SD, and Z_{eu} (Ho: $\mu_1 = \mu_2 = \mu_3 \ldots$). Following this analysis, parametric and

non-parametric multiple comparison tests were run to determine if there were any distinct sampling periods. Water quality parameters versus η" and SD were analyzed using simple and multiple linear regression. A one-tailed F-test ($p < 0.05$) determined if the regression variables were significantly related (*Ho*: $\beta = 0$).

Regression with replication [63] of high-resolution derivative spectra versus water quality parameters was run following a trimmed mean analysis of the bottom and top 30% of chlorophyll-*a* and turbidity values. I chose this method due to high replicate variability of chlorophyll-*a* and turbidity in the data sets, and to be able to match the three-replicate sets of TSS and TDS when I compared all four-water quality parameters together. During regression analysis, I used multiple linear regression models to predict chlorophyll-*a* and turbidity concentrations using second-order derivatives of reflectance spectra as the independent variable ($p < 0.05$).

3. Results

3.1. Apparent Optical Properties

Optical values of SD, η", and *Zeu* taken at each station during the entire sampling year are presented in Table 2. Median values of η" ranged from 0.54-5.55m^{-1} when considering the whole lake over the course of the sampling year. Attenuation coefficients by station shows a decrease from the Red and Washita River zones to the Main Lake zone (Figure 2), with η" being the highest at Stations 1 and 25 (2.44 and 2.30m^{-1}, respectively), and the lowest at Station 17 (0.78m^{-1}). A comparison between August 1996 and August 1997 reveals nearly identical values of η" for all stations. An inverse relationship is apparent for secchi depth, where median SD is lowest at Stations 1 and 25 (0.40 and 0.32 m, respectively), and highest at Station 17 (1.69m). When the entire lake was classified, median SD was 0.90m (range 0.15 - 0.92m). Median *Zeu* was lowest at Stations 1 and 25 (1.84 and 1.83m, respectively), and the highest at Station 17 (5.60 m). Median *Zeu* for the entire sampling year was 3.48 m (range 0.81-8.58 m).

Changes in SD, η", and *Zeu* are again apparent when they are examined by zone and season (Table 3). Median values of η" were greatest in the Red and Washita River zones (2.02 and 1.88m^{-1}, respectively), and lowest in the Main Lake zone (0.81 m^{-1}). Seasonal values of η" were greatest in the fall and spring (1.69 and 1.55m^{-1}, respectively), probably due to mixing and rainfall events typical of these seasons. The lowest median values of η" occurred in summer and winter (1.04 and 1.10m^{-1}, respectively). An inverse relationship of SD to η" is also apparent for zones and seasons. Median SD by zone was lowest in the Red and Washita River zones (0.54 and 0.45m, respectively), and highest in the Main Lake zone (1.64m). Fall and spring sampling periods had the lowest median SD values by season zones (0.82 and 0.75 m, respectively), with summer and winter having the highest (1.03 and 1.15m, respectively). Median *Zeu* by zone was lowest in the Big Mineral Arm, and the Red and Washita River zones (2.44, 2.45, and 1.92m, respectively), and highest in the Main Lake zone (5.60 m). Fall and spring seasons had the lowest Median *Zeu* values (2.82 and 2.91m, respectively), and summer and winter having the highest values (4.38 and 4.26 m, respectively.

Significant differences both spatially and temporally were found in the variables, SD, η", and *Zeu* using ANOVA on ranked data (Table 4). A Tukey-type multiple comparison test separated zonal SD, η", and *Zeu* into the following three groups: Group 1 – Red River, Big Mineral, and Washita River; Group 2 – Red River Transition, and Washita River Transition; Group 3 – Main Lake. Similarly, the Tukey-type test separated seasonal SD, η", and *Zeu* into two statistically distinct groups: Group 1 – winter and summer; Group 2 – fall and spring.

3.2. Conversion Factors Using SD, η", and Zeu

The ratio of *Zeu*: SD and the product of η" x SD by station, zone, and season are presented in Tables 5 and 6. Median ratios of *Zeu*: SD by station ranged from 3.40 at Station 17, to 4.71 at Station 25 (Table 5), increasing from zones of low turbidity to zones of high turbidity. Median values of η" x SD were different among stations, ranging from 0.97 at Station 25, to 1.37 at Station 17. Similarly, median ratios of *Zeu*: SD were greater in the river zones of Lake Texoma, and lesser in the river transition and main zones of the lake (Table 6). Red River zone exhibited the greatest ratio (4.28), with Red River Transition and Main Lake zones having the lowest (3.61, and 3.62, respectively). Median values of η" x SD ranged from 1.04 in the Washita River zone, to 1.29 in the Main Lake zone. In this study, ratios of *Zeu*: SD which decrease from zones of higher turbidity to zones of lower turbidity followed a similar pattern found by Koenings and Edmundson [34]. Conversely, the same of η" x SD held as well; where they increased from high turbidity zones to low turbidity zones. Seasonally, ratios of *Zeu*: SD and η" x SD values remained fairly constant over the sampling year (Table 6). Winter had the smallest median *Zeu*: SD ratio of 3.71, increasing to summer, fall, then spring, which had the highest ratio of 4.10. The highest median η" x SD value was winter, decreasing to summer, fall, and then spring, which had the lowest value of 1.13. The median *Zeu*: SD ratio for the entire sampling year was 3.98, which agreed with the constant factor of 4.0 multiplied by SD in order to obtain *Zeu* at Lake Texoma (K. L. Dickson, personal communication). The overall median η" x SD value was 1.15, which agreed with the empirical value of 1.16 given by French et al. [21] taken from data of 11 turbid reservoirs in the Midwest and southeast United States.

3.3. Percent Transmission of PAR at Secchi Depth

The percent transmission of PAR (% PAR) at the secchi depth varied by station and by zone (Table 7). Median% PAR

was lowest at Stations 17 and 19 (18.2 and 21.0, respectively), and greatest at Stations 1 and 25 (38.3 and 36.2, respectively). In comparing lake zones, Red River and Washita river zones exhibited the greatest% PAR (31.9 and 25.7, respectively), compared to the lowest value in the Main Lake zone which was 20.0. The% PAR values in this study agreed with those of Beeton [4] and Koenings and Edmundson [34] in that% PAR at SD was greatest in turbid waters than in clear waters, suggesting suspended matter in turbid waters scatter and reflect more light.

3.4. Relationships Between SD, η", Zeu, and Water Quality Parameters

Water quality parameters taken at eleven fixed sampling stations at Lake Texoma from August 1996 to August 1997 are presented in Table A1, in the Appendix. Secchi depth (SD), vertical attenuation coefficients (η" m^{-1}) and depth of euphotic zone (Z_{eu}) taken at eleven fixed sampling stations at Lake Texoma from August 1996 to August 1997 are presented in Table A2, in the Appendix.

Figure 3 shows that turbidity is in fact greatest in the river zones of Lake Texoma, as seen from the mean values for the five intensive sampling stations over the entire sampling year. Mean values of η" follow closely to the turbidity curves for all intensive sampling stations, and mean *Zeu* values show an inverse relationship. Mean values of chlorophyll-*a* differed by station and usually decreased when turbidity increased. At Station 17, chlorophyll-*a* was approximately parallel with the turbidity curves except during the summer months, where chlorophyll-*a* values peaked.

Correlation among water quality parameters at the five intensive stations is presented in Table 8. Turbidity shows a strong, positive association with total suspended solids (TSS) at all but one station (Station 9), and a mild, negative association with total dissolved solids (TDS). Chlorophyll-*a* is generally positively correlated with TDS and negatively correlated with turbidity, suggesting absorption properties in Lake Texoma are mildly influenced by the presence of Chlorophyll-*a*. Overall, turbidity exhibited a strong, positive correlation with TSS (r = 0.88), suggesting turbidity contributes strongly to reflectance and scattering of light in Lake Texoma. Reservoirs are known to have greater turbidity due to silts and clays [21], thus, the optical properties in Lake Texoma appear to be dependent upon turbidity, since the lake is an artificial impoundment.

Regression and Spearman correlation (r_s) of *Zeu* versus SD was done by lake zone and season (Table 9). A strong correlation (r_s = 0.94; p = 0.0001) between *Zeu* and SD was found for the Red River zone (*Zeu* = 0.588 + 3.419 (SD); r^2 = 0.71; *p* = 0.0001). *Zeu* and SD were not significantly correlated in the Main Lake zone. The remainder of the lake zones had mild, but significant correlation between *Zeu* and SD (Figure 4). Fall produced the best regression model (*rs* = 0.90; *p* = 0.0001) between *Zeu* and SD (*Zeu* = 0.989 + 2.638 (SD); r^2 = 0.83; *p* = 0.0001). There was no significant correlation between *Zeu* and SD in the winter. A strong correlation existed between *Zeu* and SD for the spring and summer sampling periods (*rs* = 0.93 and 0.84, respectively; *p* = 0.0001). When the entire sampling year was considered, *Zeu* was strongly correlated (*rs* = 0.89; *p* = 0.0001) with SD (*Zeu* = 1.250 + 2.557 (SD); r^2 = 0.63; *p* = 0.0001).

Variations in SD and η" were related to the water quality parameters, chlorophyll-*a*, turbidity, TSS, and TDS. Using multiple linear regression (maximum r^2 improvement), there was no significant correlation between the variables SD, η", and Chlorophyll-*a* by zone, or for the entire data set. Turbidity accounted for the majority of variation among SD and η" in the best one and two-variable models (Table 10). The slope for the dependent variable, SD was negative, indicating a decrease in SD with an increase in turbidity. The best one-variable model for SD came from the Big Mineral Arm, where turbidity explained 84% of the variation (*p* = 0.0001). When all zones were combined, turbidity explained only 43% of the variation (*p* = 0.0001) in SD. The coefficient of determination (r^2) increased only slightly when the best multi-variable was produced, accounting for only 50% of the variation (*p* = 0.0001) of SD among all four water quality parameters. The best one-variable model for η" came from the Washita River zone where TDS explained 80% of the variation (*p* = 0.0001). The regression slope for the dependent variable, η" was positive in all single-variable models, indicating an increase in η" with an increase in turbidity. Overall, turbidity explained 76% of the variation (*p* = 0.0001) in η" from the best one-variable model. 78% of the variation (*p* = 0.0001) was accounted for when all four water quality parameters were run together.

3.5. High-resolution Spectroradiometric Measurements

Spectral values from 350-800nm were measured with the spectroradiometer at the five intensive stations from August 1996 to July 1997. Percent transmission of incident solar radiation and diffuse attenuation coefficients (η) were calculated at 0.5-m intervals beginning at 0.1 m below the surface. Reflectance spectra were calculated using the downwelling and upwelling irradiance taken at 0.1 m. Percent transmission spectra at Stations 3, 9, 17, 22, and 24 are presented in Figures 5a to 5e, respectively. As incident solar radiation passes through the water column, percent light transmission is significantly reduced at the 0.5-m depth and below for all stations. During the months when turbidity is low, e.g., September and November, percent light transmission is generally higher than the months having high turbidity (Figure 3). What becomes readily apparent is the shift in broad-width percent transmission peaks from the green spectrum (500-600nm) to more narrow peaks in the red-infrared spectrum (~680-800nm) at depths of 0.5 meters and below [6, 7, 24]. Loss of light with increasing depth becomes apparent at selected wavelengths in

all five intensive stations (Figure 6). For the sake of brevity, one station from each zone representing a sampling month is shown from September to July. Near-linear plots of log-transformed percent light transmission as a function of depth show that blue light at 450nm is quickly removed from the surface as depth increases. Stations located in zones of high turbidity (e.g., Stations 3 and 24) show that green light (550nm) is the next spectral band to be removed, followed by red (650nm), and infrared (710nm), respectively. Zones exhibiting moderate-to-low turbidity values in the months shown (Stations 9, 17, and 22) show that blue and infrared wavelengths are the first to be removed followed by red then green. From this graphical representation, it becomes apparent to the observer that inference to understanding the varying degree of spectral displays exhibited by each station throughout the year can be made when referring back to Figures 5a to 5e.

Diffuse attenuation coefficients (η) from downwelling light were calculated at 0.5-meter intervals for each intensive station (Figures 7a to 7e). Increasing turbidity concentrations result in high η values from 0.5-1.5 m in the blue (400-450nm) and infrared (730-800nm) spectrums [55]. Attenuation remained fairly constant from ~500-700nm for all stations. Strong winds and rough surface waters had a tendency to increase η at the first half-meter interval. When surface conditions were more stable, η increased with depth.

3.6. Reflectance Spectra, and Their First and Second-order Derivatives

Reflectance values were obtained from upwelling irradiance taken just below the water surface at 0.1 meter. Zero-order reflectance curves from 400-800nm and their corresponding first and second-order derivatives are presented in Figures 8a to 8e. Prominent reflectance peaks can be seen at 590-610nm, 725-735nm, and 765-775nm in most cases. Reflection troughs are apparent at 450nm, 670nm, 750nm, and 780nm although not as sharp as reflectance peaks. Reflectance peaks are associated with low absorption and backscattering, while reflectance troughs are associated with absorption [14, 15]. Reflectance increases around 700-800nm when turbidity (Figure 3) increases (e.g., Station 3 and 24 in March 1997, Station 24 during the first sampling trip in May 1997). The high reflectance at longer wavelengths appears to be caused by backscattering from turbidity [14, 15]. When chlorophyll-*a* values are high, as is the case at Station 3 in the months of September 1996 and April 1997, reflectance increases in the green-yellow spectrum (590-610nm). Station 22 had the highest reflectance centered around 655 and 735nm when chlorophyll-*a* was high in September. Station 17 exhibited the lowest reflectance values due to lower chlorophyll-*a* and turbidity concentrations, which are typical in the Main Lake zone. Absorption by chlorophyll-*a* in the regions of 670 and 750nm has been previously reported [16, 25]; however, absorption at 750nm may also be from water [14, 15].

First-order derivatives increase in absolute value as they approach 700nm (Figures 8a through 8b). The peaks of first-order derivatives correspond to half the height of the reflectance peaks where the reflectance curve changes direction at the point of reverse curvature. First-order derivatives are positive on the ascending side of the reflectance curve, reaching a value of zero when the reflectance curve peaks, becoming a negative value on the descending side of the reflectance curve; their values once again are zero at the trough of the reflectance curve. Second-order derivatives of reflectance spectra were used in order to remove the effects of water and turbidity in the first-order derivatives [25]. Positive and negative second-order peaks correspond to reflectance troughs and peaks, respectively, and occur at locations where first-order values become zero. Compared to first-order curves, second-order curves show much smaller absolute values; however, an orderly spectral pattern still emerges. The distinct reflectance peak and trough patterns, along with their corresponding second-order derivatives were used to determine if a linear relationship existed between reflectance spectra and turbidity, TSS, TDS, and chlorophyll-*a*.

3.7. Modeling the Effects of Water Quality Parameters on Derivatives of Reflectance Spectra

The reflectance peak in the green-yellow region of the spectrum was found to have a strong chlorophyll signature. Second-order derivatives of these reflectance peaks versus chlorophyll-*a* were analyzed via multiple linear regression (maximum r^2 improvement) in order to find the single best model among these wavelengths (Table 11). Monthly Chlorophyll-*a* values correlated well with derivatives at 590, 605, and 610nm ($rs > 0.81$). The best single variable model was in April and July, using derivatives at 610nm ($r^2 = 0.97$ and 0.98, respectively, $p = 0.0001$). Improvement in the regression coefficient ($0.84 < r^2 < 0.99$) was gained in all the months when derivatives at 590, 605, and 610nm were combined in the best multi-variable model.

The chlorophyll signature correlated well ($0.88 < rs < 0.99$) with second-order reflectance derivatives in the 670-800nm range (Table 12), especially in the presence of turbidity. Regression coefficients of single-variable models for every month except May 97b (statistically non-significant) were very high in the absorption wavelengths at 670, 720, 750, 760, and 780nm. The best single-variable models between chlorophyll-*a* and second-order derivatives were in September (720nm - $r^2 = 0.98$; $p = 0.0001$), November (780nm - $r^2 = 0.99$; $p = 0.0001$), and July (725nm - $r^2 = 0.98$; $p = 0.0001$). The two reflectance peaks at 730 and 770nm were not significantly related to the chlorophyll signature except when they appeared in the multi-variable models, where improvements in the regression coefficient ($0.94 < r^2 < 0.99$) were always gained.

Turbidity was correlated with the reflectance peak at 730nm and its corresponding second derivative in September, January, and the second May trip ($0.74 < rs < 0.96$) (Table 13). The best single-variable model for 730nm was September ($r^2 = 0.92$; $p = 0.0001$). Turbidity was also related to absorption at 670nm (July), 720nm (April) and 750nm (November and June). April yielded the best single-variable model for turbidity at 750nm ($r^2 = 0.96$; $p = 0.0001$). Single-variable models for March and the first May trip were not statistically significant. Like the multiple-variable models using chlorophyll-*a*, improvement of the regression coefficient using turbidity was gained ($0.58 < r^2 < 0.99$).

Correlation of light absorption and water quality parameters is presented in Table 14. From September to March, a strong positive correlation ($0.92 < rs < 0.99$) exists between chlorophyll-*a* and derivatives from 720 to 780nm. Strong negative to weak positive correlation with turbidity and TSS and positive correlation with TDS suggest absorption was dependent upon dissolved organic matter during these months. April and the first May trip have a strong negative correlation (rs = -0.88 and -0.92, respectively) with the generally low chlorophyll-*a* concentrations throughout the lake. Negative correlation at 670nm in April between turbidity, TSS and TDS also suggest absorption was dependent upon dissolved organic matter. The one-variable model for the second May trip was not significantly related to chlorophyll-*a*; however, it shows a positive correlation (rs = 0.73) with turbidity, and a very strong negative correlation (rs = -0.95) with TDS suggesting presence of both seston and tripton. June was strongly correlated with chlorophyll-*a* at 670nm (rs = 0.96) and negatively correlated with turbidity and TSS suggesting absorption by algal pigments. Finally, chlorophyll-*a*, turbidity and TSS correlated strongly (rs = 0.98, 0.90 and 0.83, respectively) with derivatives at 725nm in July suggesting absorption by water sedimentation was dependent upon plankton biomass.

Table 2. *Results for η", SD, and Zeu by station from August 1996 to August 1997 showing sample size, mean, standard deviation, median, range, and normal probability values. RR = Red River Zone, BM = Big Mineral Arm, RRT =Red River Transition Zone, ML = Main Lake Zone, WRT = Washita River Transition Zone, WR = Washita River Zone.*

station	n	mean	std dev	median	range	*p* (normal)
η"· m^{-1} by station						
1 (RR)	12	2.63	0.915	2.44	1.56-5.13	<0.02
3 (RR)	12	1.69	0.793	1.49	1.00-3.73	<0.01
7 (BM)	12	2	0.623	1.9	1.21-2.89	>0.10
8 (RRT)	12	1.45	0.391	1.43	0.89-2.17	>0.50
9 (RRT)	12	1.11	0.376	1.01	0.82-2.20	<0.01
17 (ML)	12	0.8	0.169	0.78	0.54-1.21	>0.10
19 (ML)	12	0.82	0.126	0.83	0.58-1.04	>0.99
20 (WRT)	12	1.11	0.379	1.02	0.60-2.07	<0.05
22 (WRT)	12	1.28	0.323	1.25	0.80-1.90	>0.50
24 (WR)	12	1.92	0.744	1.76	1.11-3.58	>0.10
25 (WR)	11	2.59	1.183	2.3	1.44-5.55	<0.05
η"· m^{-1} stations combined						
	131	1.57	0.859	1.29	0.54-5.55	0.0001
SD (m) by station						
1 (RR)	12	0.39	0.169	0.4	0.15-0.75	>0.50
3 (RR)	12	0.85	0.261	0.92	0.35-1.25	>0.50
7 (BM)	12	0.64	0.243	0.66	0.23-1.05	>0.50
8 (RRT)	12	0.9	0.263	0.92	0.45-1.5	>0.50
9 (RRT)	12	1.21	0.417	1.26	0.51-1.85	>0.50

station	n	mean	std dev	median	range	*p* (normal)
17 (ML)	12	1.76	0.568	1.69	1.15-3.38	<0.01
19 (ML)	12	1.52	0.382	1.56	0.60-2.15	>0.10

station	n	mean	std dev	median	range	*p* (normal)
20 (WRT)	12	1.01	0.203	1.06	0.55-1.21	<0.01
22 (WRT)	12	0.92	0.293	0.78	0.57-1.45	<0.05
24 (WR)	12	0.65	0.31	0.5	0.35-1.23	>0.05
25 (WR)	11	0.44	0.256	0.32	0.15-0.92	<0.05
SD (m) stations combined						
	131	0.94	0.513	0.9	0.15-3.38	0.0001
Z_{eu} (m) by station						
1 (RR)	12	1.88	0.505	1.84	0.92-2.85	>0.90
3 (RR)	12	3.54	1.296	3.32	1.69-6.70	>0.10
7 (BM)	12	2.5	0.796	2.44	1.51-3.82	>0.10
8 (RRT)	12	3.37	0.91	3.18	2.20-4.98	>0.10
9 (RRT)	12	4.41	1.033	4.53	2.13-5.72	>0.10
17 (ML)	12	5.94	1.225	5.6	3.76-8.58	>0.10
19 (ML)	12	5.67	0.946	5.51	4.39-7.90	>0.10
20 (WRT)	12	4.49	1.366	4.49	2.14-7.60	>0.10
22 (WRT)	12	3.78	0.958	3.67	2.34-5.73	>0.90
24 (WR)	12	2.54	1.043	2.15	1.22-4.14	>0.10
25 (WR)	11	1.9	0.618	1.83	0.81-2.65	>0.10
Z_{eu} (m) stations combined						
	131	3.65	1.647	3.48	0.81-8.58	0.001

Table 3. *Results for η", SD, and Zeu by zone and by season showing sample size, mean, standard deviation, median, range, and normal probability values. RR = Red River Zone, BM = Big Mineral Arm, RRT =Red River Transition Zone, ML = Main Lake Zone, WRT = Washita River Transition Zone, WR = Washita River Zone.*

zone	n	mean	std dev	median	range	*p* (normal)
η"· m^{-1} by zone						
RR	24	2.16	0.967	2.02	0.995-5.134	0.02
BM	12	2	0.623	1.9	1.206-2.889	0.173
RRT	24	1.28	0.413	1.17	0.818-2.196	0.011
ML	24	0.81	0.146	0.81	0.538-1.207	0.6
WRT	24	1.2	0.355	1.12	0.605-2.070	0.127
WR	23	2.24	1.015	1.88	1.109-5.554	0.003

zone	n	mean	std dev	median	range	*p* (normal)
η"· m $^{-1}$ by season						
Fall	22	1.71	0.664	1.69	0.734-2.904	0.194
Winter	11	1.12	0.313	1.1	0.746-1.727	0.326
Spring	55	1.82	1.062	1.55	0.538-5.554	0
Summer	43	1.3	0.604	1.04	0.585-3.281	0
SD (m) *by* zone						
RR	24	0.62	0.316	0.54	0.150-1.250	0.283
BM	12	0.64	0.242	0.66	0.230-1.050	0.824
RRT	24	1.05	0.376	0.96	0.450-1.850	0.396
ML	24	1.64	0.488	1.64	0.600-3.380	0.001
WRT	24	0.96	0.252	1.03	0.550-1.450	0.456
WR	23	0.55	0.3	0.45	0.150-1.230	0.017
SD (m) by season						
Fall	22	0.81	0.465	0.82	0.200-1.680	0.091
Winter	11	1.2	0.462	1.15	0.650-2.150	0.367
Spring	55	0.84	0.578	0.75	0.150-3.380	0
Summer	43	1.06	0.417	1.03	0.250-1.950	0.506
Z_{eu} (m) by zone						
RR	24	2.71	1.284	2.45	0.920-6.700	0.016
BM	12	2.5	0.796	2.44	1.510-3.820	0.391
RRT	24	3.89	1.091	3.9	2.130-5.720	0.441
ML	24	5.8	1.079	5.6	3.760-8.580	0.255
WRT	24	4.14	1.211	4.1	2.140-7.600	0.42
WR	23	2.24	0.909	1.92	0.810-4.140	0.086
Z_{eu} (m) by season						
Fall	22	3.13	1.344	2.82	1.540-6.250	0.086
Winter	11	4.64	1.37	4.26	2.620-6.700	0.714
Spring	55	3.28	1.7	2.91	0.810-8.580	0.006
Summer	43	4.14	1.581	4.38	1.430-7.900	0.336

Table 4. *Probabilities (p) from ANOVA done on ranked data for the variables η", SD, and Zeu, followed by a Tukey-type multiple comparison test for significantly different zones and seasons. RR = Red River Zone, BM =Big Mineral Arm, RRT =Red River Transition Zone, ML =Main Lake Zone, WRT = Washita River Transition Zone, WR =Washita River Zone. Lines beneath zones indicate groups not significantly Different.*

variable	n	*p*	multiple range test					
by zone:								
η" m^{-1}	131	0.0001	WR	BM	RR	RRT	WRT	ML

variable	n	*p*	multiple range test					
SD (m)	131	0.0001	ML	RRT	WRT	BM	RR	WR
Z_{eu} (m)	131	0.0001	ML	WRT	RRT	RR	BM	WR
by season:								
η" m^{-1}	131	0.0041	Fall			Summer		
SD (m)	131	0.0047	Winter			Spring		
Z_{eu} (m)	131	0.0017	Winter			Spring		

Table 5. *Results for Zeu: SD and η" x SD by station showing sample size, mean, standard deviation, and median values. RR = Red River Zone, BM = Big Mineral Arm, RRT = Red, River Transition Zone, ML = Main Lake Zone, WRT = Washita River Transition Zone, WR = Washita River Zone.*

station	n	mean	std dev	median
Z_{eu}: SD (by station)				
1 (RR)	12	5.23	1.535	3.98
3 (RR)	12	4.26	1.028	4.1
7 (BM)	12	4.22	1.378	3.82
8 (RRT)	12	3.82	0.677	3.66
9 (RRT)	12	3.91	1.199	3.6
17 (ML)	12	3.6	1.087	3.4
19 (ML)	12	4.02	1.468	3.72
20 (WRT)	12	4.52	1.408	4.13
22 (WRT)	12	4.23	0.6	4.14
24 (WR)	12	4.18	1.341	4.03
25 (WR)	11	5.1	2.102	4.71
η" x SD (by station)				
1 (RR)	12	0.93	0.235	1.15
3 (RR)	12	1.27	0.281	1.24
7 (BM)	12	1.18	0.377	1.16
8 (RRT)	12	1.22	0.193	1.25
9 (RRT)	12	1.24	0.295	1.25
17 (ML)	12	1.38	0.447	1.37
19 (ML)	12	1.24	0.351	1.24
20 (WRT)	12	1.09	0.281	1.08
22 (WRT)	12	1.11	0.176	1.09
24 (WR)	12	1.14	0.477	1.11
25 (WR)	11	1	0.421	0.97

Table 6. *Results for Zeu: SD and η" x SD by zone and season showing sample size, mean, standard deviation, and median values. RR = Red River Zone, BM = Big Mineral Arm, RRT = Red River Transition Zone, ML = Main Lake Zone, WRT = Washita River Transition Zone, WR = Washita River Zone.*

zone	n	mean	std dev	median
Zeu: SD (by zone)				
RR	24	4.74	1.371	4.28
BM	12	4.22	1.378	3.82
RRT	24	3.87	0.953	3.61
ML	24	3.81	1.281	3.62
WRT	24	4.37	1.069	4.14
WR	23	4.62	1.769	4.15
Z_{eu}: SD (by season)				
Fall	22	4.47	1.621	4
Winter	11	4.22	1.727	3.71
Spring	55	4.35	1.321	4.1
Summer	43	4.09	1.129	3.98
Z_{eu}: SD (by year)				
zones combined	131	4.27	1.346	3.98
η" x SD (by zone)				
RR	24	1.1	0.308	1.11
BM	12	1.18	0.377	1.16
RRT	24	1.23	0.244	1.25
ML	24	1.31	0.399	1.29
WRT	24	1.1	0.229	1.09
WR	23	1.07	0.447	1.04
η" x SD (by season)				
Fall	22	1.14	0.366	1.15
Winter	11	1.26	0.315	1.26
Spring	55	1.14	0.357	1.13
Summer	43	1.19	0.329	1.15
η" x SD (by year)				
zones combined	131	1.17	0.344	1.15

Table 7. *Percent transmission of PAR at secchi depth by station and zone from August 1996 to August 1997 showing sample size, mean, standard deviation, median, and range. RR = Red River Zone, BM = Big Mineral Arm, RRT =Red River Transition Zone, ML = Main Lake Zone, WRT = Washita River Transition Zone, WR = Washita River Zone.*

station / zone	n	mean	std dev	median	range
% transmission at secchi depth by station					
1 (RR)	12	38.9	13.19	38.3	21.1 - 56.6

station / zone	n	mean	std dev	median	range
3 (RR)	12	30.9	15.69	26.9	17.8 - 76.8
7 (BM)	12	26.1	10.43	25.1	12.0 - 49.5
8 (RRT)	12	26.1	13.83	22.2	13.3 - 61.5
9 (RRT)	12	25.8	12.7	22.4	10.2 - 52.1
17 (ML)	12	23.7	14.21	18.2	4.1 - 48.2
19 (ML)	12	21.8	9.99	21	11.5 - 44.7
20 (WRT)	12	27.1	10.99	24.1	13.8 - 49.3
22 (WRT)	12	27	8.09	26.6	11.0 - 39.5
24 (WR)	12	28.7	12.9	25.3	6.4 - 55.7
25 (WR)	11	30.8	13.19	36.2	12.0 - 52.9
% transmission at secchi depth by zone					
RR	24	34.9	14.76	31.9	17.8 - 76.8
BM	12	26.1	10.43	25.1	12.0 - 49.5
RRT	24	25.9	12.99	22.2	10.2 - 61.5
ML	24	22.7	12.05	20	4.1 - 48.2
WRT	24	27	9.44	25	11.0 - 49.5
WR	23	29.7	12.79	25.7	6.4 - 55.7

Table 8. *Correlation (R) among water quality parameters at five intensive stations from September 1996 to August 1997. Station 3: TSS/Turbidity, R = 0.85; Station 9: TDS/Turbidity, R = - 0.57; Station 17: TSS/Turbidity, R = 0.66; Station 22: TSS/Turbidity, R = 0.51; Station 24: TSS/Turbidity, R = 0.66.*

	Station 3				**Station 9**			
	TSS	**TDS**	**Turbidity**	**Chl-*a***	**TSS**	**TDS**	**Turbidity**	**Chl-*a***
TSS	1				1			
TDS	-0.09	1			0.05	1		
Turbidity	0.85	-0.38	1		0.26	-0.57	1	
Chl-*a*	-0.32	0.62	-0.62	1	0.15	0.37	-0.46	1
	Station 17				Station 22			
	TSS	TDS	Turbidity	Chl-*a*	TSS	TDS	Turbidity	Chl-*a*
TSS	1				1			
TDS	-0.16	1			-0.03	1		
Turbidity	0.66	-0.18	1		0.51	0.05	1	
Chl-*a*	0.7	-0.06	0.12	1	0.39	0.05	0.05	1
	Station 24				zones combined			
	TSS	TDS	Turbidity	Chl-*a*	TSS	TDS	Turbidity	Chl-*a*
TSS	1				1			

	Station 3				Station 9			
	TSS	**TDS**	**Turbidity**	**Chl-*a***	**TSS**	**TDS**	**Turbidity**	**Chl-*a***
TDS	-0.42	1			-0.34	1		
Turbidity	0.91	-0.61	1		0.88	-0.42	1	
Chl-*a*	-0.24	0.58	-0.45	1	0.09	0.22	-0.19	1

Table 9. *Regression and Spearman correlation of Zeu (m) versus SD (m) by zone and season. RR = Red River Zone, BM = Big Mineral Arm, RRT =Red River Transition Zone, ML =Main Lake Zone, WRT = Washita River Transition Zone, WR = Washita River Zone. Nonsignificant correlations (ns) were $p > 0.05$.*

group	**n**	**linear regression**	**spearman correlation**
		by zone	
RR	24	Z_{eu} = 0.588 + 3.419 (SD) r^2 = 0.708 p = 0.0001	r_s = 0.941 p = 0.0001
BM	12	Z_{eu} = 1.070 + 2.226 (SD) r^2 = 0.461 p = 0.0153	r_s = 0.667 p = 0.0179
RRT	24	Z_{eu} = 1.473 + 2.290 (SD) r^2 = 0.622 p = 0.0001	r_s = 0.785 p = 0.0001
ML	24	ns	ns
WRT	24	Z_{eu} = 1.241 + 3.003 (SD) r^2 = 0.390 p = 0.0011	r_s = 0.640 p = 0.0008
WR	23	Z_{eu} = 1.019 + 2.214 (SD) r^2 = 0.533 p = 0.0001	r_s = 0.809 p = 0.0001
		by season	
Fall	22	Z_{eu} = 0.989 + 2.638 (SD) r^2 = 0.833 p = 0.0001	r_s = 0.902 p = 0.0001
Winter	11	ns	ns
Spring	55	Z_{eu} = 1.253 + 2.396 (SD) r^2 = 0.663 p = 0.0001	r_s = 0.926 p = 0.0001
Summer	43	Z_{eu} = 1.162 + 2.815 (SD) r^2 = 0.552 p = 0.0001	r_s = 0.838 p = 0.0001
		by year	
combined	131	Z_{eu} = 1.250 + 2.557 (SD) r^2 = 0.634 p = 0.0001	r_s = 0.887 p = 0.0001

Table 10. *Variation in a) secchi depth (SD); and b) vertical attenuation coefficient (η") explained by simple and multiple (max r^2 improvement) regression. RR = Red River, BM = Big Mineral, RRT = Red River, Transition, ML = Main Lake, WR = Washita River, WRT = Washita River Transition.*

zone	best one-variable model	best two-variable model	best multi-variable model
RR n = 22	*Y* = 0.933 - 0.018 (turbidity) r^2 = 0.677 *p* = 0.0001	*Y* = 0.947 + 0.234 (TDS) - 0.040 (turbidity) r^2 = 0.712 *p* = 0.0001	*Y* = 1.518 + 0.0003 (Chl-*a*) - 0.0004 (TSS) + 0.0389 (TDS) - 0.056 (turbidity) r^2 = 0.782 *p* = 0.0001
BM n = 11	*Y* = 1.267 - 0.061 (TDS) r^2 = 0.840 *p* = 0.0001	*Y* = 1.782 - 0.0005 (TSS) - 0.041 (turbidity) r^2 = 0.855 *p* = 0.0004	*Y* = 1.661 - 0.0018 (Chl-*a*) - 0.0004 (TSS) - 0.014 (TDS) - 0.031 (turbidity) r^2 = 0.877 *p* = 0.0068
RRT n = 22	*Y* = 1.586 - 0.079 (turbidity) r^2 = 0.593 *p* = 0.0001	*Y* = 1.734 - 0.062 (TDS) - 0.054 (turbidity) r^2 = 0.715 *p* = 0.0001	*Y* = 3.005 - 0.0092 (Chl-*a*) - 0.0008 (TSS) - 0.0489 (TDS) - 0.084 (turbidity) r^2 = 0.797 *p* = 0.0001
ML n = 22	*Y* = 2.566 - 0.272 (turbidity) r^2 = 0.312 *p* = 0.0069	*Y* = 2.558 - 0.0185 (Chl-*a*) - 0.202 (turbidity) r^2 = 0.414 *p* = 0.0063	*Y* = 3.287 - 0.0199 (Chl-*a*) - 0.0006 (TSS) - 0.0061 (TDS) - 0.221 (turbidity) r^2 = 0.459 *p* = 0.0266
WRT n = 22	*Y* = 1.355 - 0.065 (turbidity) r^2 = 0.546 *p* = 0.0001	*Y* = 1.222 + 0.0001 (TSS) - 0.062 (turbidity) r^2 = 0.553 *p* = 0.0005	*Y* = 1.248 - 0.0029 (Chl-*a*) + 0.0001 (TSS) + 0.0104 (TDS) - 0.070 (turbidity) r^2 = 0.562 *p* = 0.0051
WR n = 21	*Y* = 0.777 - 0.012 (turbidity) r^2 = 0.482 *p* = 0.0014	*Y* = 0.818 + 0.018 (TDS) - 0.031 (turbidity) r^2 = 0.482 *p* = 0.0027	*Y* = 0.918 + 0.0008 (Chl-*a*) - 0.0002 (TSS) + 0.0185 (TDS) - 0.031 (turbidity) r^2 = 0.485 *p* = 0.0240
all zones n = 120	*Y* = 1.262 - 0.029 (turbidity) r^2 = 0.431 *p* = 0.0001	*Y* = 1.459 - 0.0112 (Chl-*a*) - 0.0303 (turbidity) r^2 = 0.492 *p* = 0.0001	*Y* = 1.469 - 0.0124 (Chl-*a*) + 0.00002 (TSS) + 0.0185 (TDS) - 0.045 (turbidity) r^2 = 0.500 *p* = 0.0001

Table 11. *Multiple linear regression (max r^2 improvement) and spearman correlation (r_s) of second-order derivatives of reflectance spectra versus chlorophyll-a concentrations ($\mu g \cdot l^{-1}$) in the green spectrum (590-610nm) for combined stations 3, 9, 17, 22, and 24 from September 1996 to July 1997. Station 17 was not sampled in September because of bad weather. Station 9 is missing for April due to bad spectral data. A broken fiber-optic wire prevented data collection for the June 1997b sampling trip.*

month	best one-variable model, and spearman correlation	best two-variable model
Sep-96 n = 12	Chl-*a* = 14.665 + 78951.9 (*d*590) r^2 = 0.899 *p* = 0.0001 r_s = 0.948 *p* = 0.0001	Chl-*a* = 15.011 - 264619.1 (*d*605) + 225960.9 (*d*610) r^2 = 0.921 *p* = 0.0001
Nov-96 n = 15	Chl-*a* = 13.790 - 298889.7 (*d*590) r^2 = 0.809 *p* = 0.0001 r_s = -0.899 *p* = 0.0001	Chl-*a* = 11.851 - 361219.6 (*d*590) + 29065.1 (*d*605) r^2 = 0.835 *p* = 0.0001
Jan-7 n = 15	Chl-*a* = 1.290 + 302921.9 (*d*605) r^2 = 0.662 *p* = 0.0001 r_s = 0.814 *p* = 0.0002	Chl-*a* = 2.830 + 229129.5 (*d*605) - 84512.9 (*d*610) r^2 = 0.775 *p* = 0.0001
Apr-97 n = 12	Chl-*a* = 11.618 + 270758.6 (*d*610) r^2 = 0.974 *p* = 0.0001 r_s = 0.987 *p* = 0.0001	Chl-*a* = 15.167 - 90903.9 (*d*605) + 221180.3 (*d*610) r^2 = 0.996 *p* = 0.0001
May-97a n = 15	Chl-*a* = 11.085 + 34718.7 (*d*590) r^2 = 0.721 *p* = 0.0001 r_s = 0.849 *p* = 0.0001	Chl-*a* = 10.620 + 62293.2 (*d*590) + 18681.9 (*d*610) r^2 = 0.898 *p* = 0.0001
May-97b n = 15	Chl-*a* = 18.550 - 57682.8 (*d*605) r^2 = 0.902 *p* = 0.0001 r_s = -0.950 *p* = 0.0001	Chl-*a* = 18.451 - 53362.8 (*d*605) + 10461.9 (*d*610) r^2 = 0.914 *p* = 0.0001
Jun-97a n = 15	Chl-*a* = 19.864 + 164192.5 (*d*605) r^2 = 0.804 *p* = 0.0001 r_s = 0.896 *p* = 0.0001	Chl-*a* = 20.255 + 137722.3 (*d*605) + 27926.8 (*d*610) r^2 = 0.860 *p* = 0.0001
Jul-97 n = 15	Chl-*a* = 2.752 + 426045.4 (*d*610) r^2 = 0.952 *p* = 0.0001 r_s = 0.976 *p* = 0.0001	Chl-*a* = 3.551 + 416193.4 (*d*590) + 285041.2 (*d*610) r^2 = 0.998 *p* = 0.0001
month	best three-variable model	
Sep-96 n = 12	Chl-*a* = 28.128 - 1757697.7 (*d*590) - 4943167.8 (*d*605) + 4265536.2 (*d*610) r^2 = 0.982 *p* = 0.0001	
Nov-96 n = 15	Chl-*a* = 9.961 - 365542.8 (*d*590) + 49480.8 (*d*605) + 7308.6 (*d*610) r^2 = 0.835 *p* = 0.0001	
Jan-97 n = 15	Chl-*a* = 1.326 + 101305.6 (*d*590) + 264902.7 (*d*605) - 256071.9 (*d*610) r^2 = 0.878 *p* = 0.0001	
Mar-97 n = 15	Chl-*a* = 6.510 + 50154.8 (*d*590) - 14273.4 (*d*605) - 17780.6 (*d*610) r^2 = 0.977 *p* = 0.0001	

month	best one-variable model, and spearman correlation	best two-variable model
Apr-97 n = 12	Chl-*a* = 14.292 - 142385.9 (*d*590) - 300678.0 (*d*605) + 248492.3 (*d*610) r^2 = 0.999 *p* = 0.0001	
May-97a n = 15	Chl-*a* = 8.519 + 96179.0 (*d*590) - 47440.3 (*d*605) + 61819.0 (*d*610) r^2 = 0.944 *p* = 0.0001	
May-97b n = 15	Chl-*a* = 13.440 + 155639.0 (*d*590) - 161744.6 (*d*605) + 68350.8 (*d*610) r^2 = 0.965 *p* = 0.0001	
Jun-97a n = 15	Chl-*a* = 20.734 - 14170.5 (*d*590) + 132148.6 (*d*605) + 21393.6 (*d*610) r^2 = 0.862 *p* = 0.0001	
Jul-97 n = 15	Chl-*a* = 3.307 + 421073.4 (*d*590) + 20531.1 (*d*605) + 303516.9 (*d*610) r^2 = 0.998 *p* = 0.0001	

Table 12. *Multiple linear regression (max r^2 improvement) and spearman correlation (r_s) of second-order derivatives of reflectance spectra versus chlorophyll-a concentrations ($\mu g \cdot l^{-1}$) in the red-near-IR spectrum (670-780nm) for combined stations 3, 9, 17, 22, and 24 from September 1996 to July 1997. Station 17 was not sampled in September because of bad weather. Station 9 is missing for April due to bad spectral data. A broken fiber-optic wire prevented data collection for the June 1997b sampling trip.*

month	best one-variable model, and spearman correlation	best two-variable model
Sep-96 n = 12	Chl-*a* = 16.089 + 12069.1 (*d*720) r^2 = 0.982 *p* = 0.0001 r_s = 0.991 *p* = 0.0001	Chl-*a* = 15.932 + 13441.3 (*d*720) + 1389.6 (*d*730) r^2 = 0.982 *p* = 0.0001
Nov-96 n = 15	Chl-*a* = 4.284 + 13009.1 (*d*780) r^2 = 0.990 *p* = 0.0001 r_s = 0.995 *p* = 0.0001	Chl-*a* = 4.353 - 1143.4 (*d*760) + 9415.2 (*d*780) r^2 = 0.997 *p* = 0.0001
Jan-97 n = 15	Chl-*a* = 4.861 + 2827.5 (*d*755) r^2 = 0.856 *p* = 0.0001 *rs* = 0.925 *p* = 0.0001	Chl-*a* = 6.636 + 18275.4 (*d*730) - 2527.7 (*d*760) r^2 = 0.977 *p* = 0.0001
Mar-97 n = 15	Chl-*a* = 4.324 + 4549.6 (*d*780) r^2 = 0.953 *p* = 0.0001 r_s = 0.976 *p* = 0.0001	Chl-*a* = 4.401 + 112.2 (*d*770) + 5102.9 (*d*780) r^2 = 0.968 *p* = 0.0001
Apr-97 n = 12	Chl-*a* = 23.131 - 13080.2 (*d*760) r^2 = 0.777 *p* = 0.0002 r_s = 0.881 *p* = 0.0002	Chl-*a* = 27.683 - 41607.3 (*d*770) - 55157.6 (*d*780) r^2 = 0.975 *p* = 0.0001
May-97a n = 15	Chl-*a* = 10.937 - 34841.7 (*d*670) r^2 = 0.841 *p* = 0.0001 r_s = -0.917 *p* = 0.0001	Chl-*a* = 11.049 - 25364.1 (*d*670) - 2370.5 (*d*750) r^2 = 0.886 *p* = 0.0001
May-97b n = 15	ns	Chl-*a* = 21.219 - 12021.0 (*d*750) - 11471.9 (*d*770) r^2 = 0.844 *p* = 0.0001
Jun-97a n = 15	Chl-*a* = 20.660 + 103618.5 (*d*670) r^2 = 0.918 *p* = 0.0001 r_s = 0.958 *p* = 0.0001	Chl-*a* = 32.726 + 4036.8 (*d*730) - 12569.0 (*d*780) r^2 = 0.971 *p* = 0.0001
Jul-97 n = 15	Chl-*a* = 11.5452 + 57202.2 (*d*725) r^2 = 0.952 *p* = 0.0001 r_s = 0.985 *p* = 0.0001	Chl-*a* = 14.073 - 98344.6 (*d*670) + 42837.8 (*d*725) r^2 = 0.993 *p* = 0.0001

month	best multi-variable model
Sep-96 n = 12	Chl-*a* = 15.872 + 12728.1 (*d*720) + 1533.2 (*d*730) + 896.9 (*d*780) r^2 = 0.982 *p* = 0.0001
Nov-96 n = 15	Chl-*a* = 6.121 + 8837.5 (*d*730) + 1195.8 (*d*750) + 7078.4 (*d*780) r^2 = 0.9997 *p* = 0.0001
Jan-97 n = 15	Chl-*a* = 7.316 + 25503.4 (*d*730) - 3114.0 (*d*755) - 5659.7 (*d*760) r^2 = 0.997 *p* = 0.0001
Mar-97 n = 15	Chl-*a* = 5.216 - 14971.2 (*d*735) - 2858.7 (*d*750) - 1216.1 (*d*780) r^2 = 0.987 *p* = 0.0001
Apr-97 n = 12	Chl-*a* = 27.024 + 81798.6 (*d*760) - 210491.5 (*d*770) - 323203.5 (*d*780) r^2 = 0.9998 *p* = 0.0001
May-97a n = 15	Chl-*a* = 10.082 - 3952.9 (*d*730) - 4218.9 (*d*750) - 482.0 (*d*770) r^2 = 0.944 *p* = 0.0001
May-97b n = 15	Chl-*a* = 42.782 - 19118.6 (*d*730) - 23368.1 (*d*750) - 22684.1 (*d*770) - 104103.9 (*d*780) r^2 = 0.998 *p* = 0.0001
Jun-97a n = 15	Chl-*a* = 32.749 + 4359.4 (*d*730) + 4098.2 (*d*750) - 157.6 (*d*770) - 15236.8 (*d*780) r^2 = 0.974 *p* = 0.0001
Jul-97 n = 15	Chl-*a* = 13.346 + 33551.0 (*d*725) - 20145.5 (*d*750) - 3305.1 (*d*770) r^2 = 0.9999 *p* = 0.0001

Table 13. *Multiple linear regression (max r^2 improvement) and spearman correlation (r_s) of second-order derivatives of reflectance spectra versus turbidity concentrations (NTU) in the red-near-IR spectrum (670-780nm) for combined stations 3, 9, 17, 22, and 24 from September 1996 to July 1997. Station 17 was not sampled in September because of bad weather. Station 9 is missing for April due to bad spectral data. A broken fiber-optic wire prevented data collection for the June 1997b sampling trip.*

month	best one-variable model, and spearman correlation	best two-variable model
Sep-96 n = 12	Chl-*a* = 16.089 + 12069.1 (*d*720) r^2 = 0.982 *p* = 0.0001 r_s = 0.991 *p* = 0.0001	Chl-*a* = 15.932 + 13441.3 (*d*720) + 1389.6 (*d*730) r^2 = 0.982 *p* = 0.0001
Nov-96 n = 15	Chl-*a* = 4.284 + 13009.1 (*d*780) r^2 = 0.990 *p* = 0.0001 r_s = 0.995 *p* = 0.0001	Chl-*a* = 4.353 - 1143.4 (*d*760) + 9415.2 (*d*780) r^2 = 0.997 *p* = 0.0001
Jan-97 n = 15	Chl-*a* = 4.861 + 2827.5 (*d*755) r^2 = 0.856 *p* = 0.0001 *rs* = 0.925 *p* = 0.0001	Chl-*a* = 6.636 + 18275.4 (*d*730) - 2527.7 (*d*760) r^2 = 0.977 *p* = 0.0001
Mar-97 n = 15	Chl-*a* = 4.324 + 4549.6 (*d*780) r^2 = 0.953 *p* = 0.0001 r_s = 0.976 *p* = 0.0001	Chl-*a* = 4.401 + 112.2 (*d*770) + 5102.9 (*d*780) r^2 = 0.968 *p* = 0.0001
Apr-97 n = 12	Chl-*a* = 23.131 - 13080.2 (*d*760) r^2 = 0.777 *p* = 0.0002 r_s = 0.881 *p* = 0.0002	Chl-*a* = 27.683 - 41607.3 (*d*770) - 55157.6 (*d*780) r^2 = 0.975 *p* = 0.0001
May-97a n = 15	Chl-*a* = 10.937 - 34841.7 (*d*670) r^2 = 0.841 *p* = 0.0001 r_s = -0.917 *p* = 0.0001	Chl-*a* = 11.049 - 25364.1 (*d*670) - 2370.5 (*d*750) r^2 = 0.886 *p* = 0.0001
May-97b n = 15	ns	Chl-*a* = 21.219 - 12021.0 (*d*750) - 11471.9 (*d*770) r^2 = 0.844 *p* = 0.0001
Jun-97a n = 15	Chl-*a* = 20.660 + 103618.5 (*d*670) r^2 = 0.918 *p* = 0.0001 r_s = 0.958 *p* = 0.0001	Chl-*a* = 32.726 + 4036.8 (*d*730) - 12569.0 (*d*780) r^2 = 0.971 *p* = 0.0001
Jul-97 n = 15	Chl-*a* = 11.5452 + 57202.2 (*d*725) r^2 = 0.952 *p* = 0.0001 r_s = 0.985 *p* = 0.0001	Chl-*a* = 14.073 - 98344.6 (*d*670) + 42837.8 (*d*725) r^2 = 0.993 *p* = 0.0001
month	best multi-variable model	
Sep-96 n = 12	Chl-*a* = 15.872 + 12728.1 (*d*720) + 1533.2 (*d*730) + 896.9 (*d*780) r^2 = 0.982 *p* = 0.0001	
Nov-96 n = 15	Chl-*a* = 6.121 + 8837.5 (*d*730) + 1195.8 (*d*750) + 7078.4 (*d*780) r^2 = 0.9997 *p* = 0.0001	
Jan-97 n = 15	Chl-*a* = 7.316 + 25503.4 (*d*730) - 3114.0 (*d*755) - 5659.7 (*d*760) r^2 = 0.997 *p* = 0.0001	
Mar-97 n = 15	Chl-*a* = 5.216 - 14971.2 (*d*735) - 2858.7 (*d*750) - 1216.1 (*d*780) r^2 = 0.987 *p* = 0.0001	
Apr-97 n = 12	Chl-*a* = 27.024 + 81798.6 (*d*760) - 210491.5 (*d*770) - 323203.5 (*d*780) r^2 = 0.9998 *p* = 0.0001	
May-97a n = 15	Chl-*a* = 10.082 - 3952.9 (*d*730) - 4218.9 (*d*750) - 482.0 (*d*770) r^2 = 0.944 *p* = 0.0001	
May-97b n = 15	Chl-*a* = 42.782 - 19118.6 (*d*730) - 23368.1 (*d*750) - 22684.1 (*d*770) - 104103.9 (*d*780) r^2 = 0.998 *p* = 0.0001	
Jun-97a n = 15	Chl-*a* = 32.749 + 4359.4 (*d*730) + 4098.2 (*d*750) - 157.6 (*d*770) - 15236.8 (*d*780) r^2 = 0.974 *p* = 0.0001	
Jul-97 n = 15	Chl-*a* = 13.346 + 33551.0 (*d*725) - 20145.5 (*d*750) - 3305.1 (*d*770) r^2 = 0.9999 *p* = 0.0001	

Table 14. *Spearman correlation (r_s) among water quality parameters and second-order derivatives of reflectance spectra at the five intensive station for each sampling month. Wavelengths shown are from the best one-variable models in Table 12.*

spearman correlation coefficient, r_s				
sampling month	**chl-*a***	**turbidity**	**TSS**	**TDS**
September (720nm)	0.991	-0.898	-0.956	0.589
November (780nm)	0.995	-0.423	-0.369	0.853
January (755nm)	0.925	0.392	0.391	0.571
March (780nm)	0.976	0.311	0.247	0.308

spearman correlation coefficient, r_s				
sampling month	**chl-*a***	**turbidity**	**TSS**	**TDS**
April (760nm)	-0.881	-0.341	-0.512	-0.661
May (a) (670nm)	-0.917	0.004	-0.128	0.424
May (b) (750nm)	-0.27	0.726	0.39	-0.953
June (a) (670nm)	0.958	-0.823	-0.615	-0.281
July (725nm)	0.985	0.896	0.829	-0.582

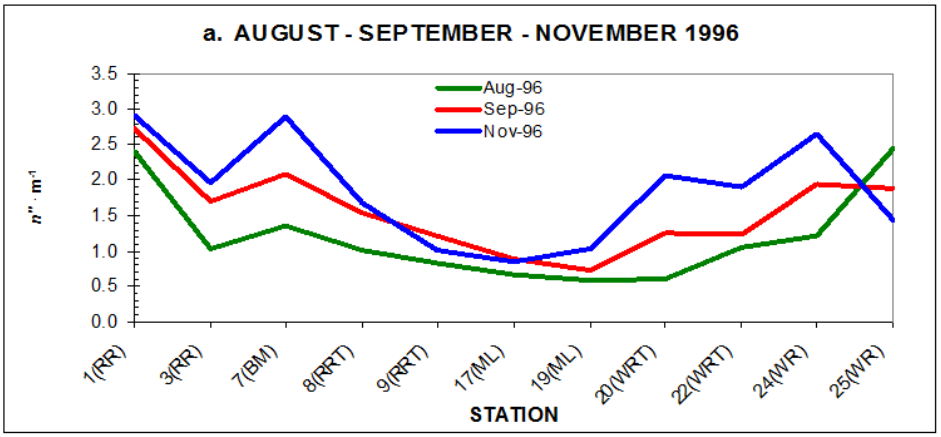

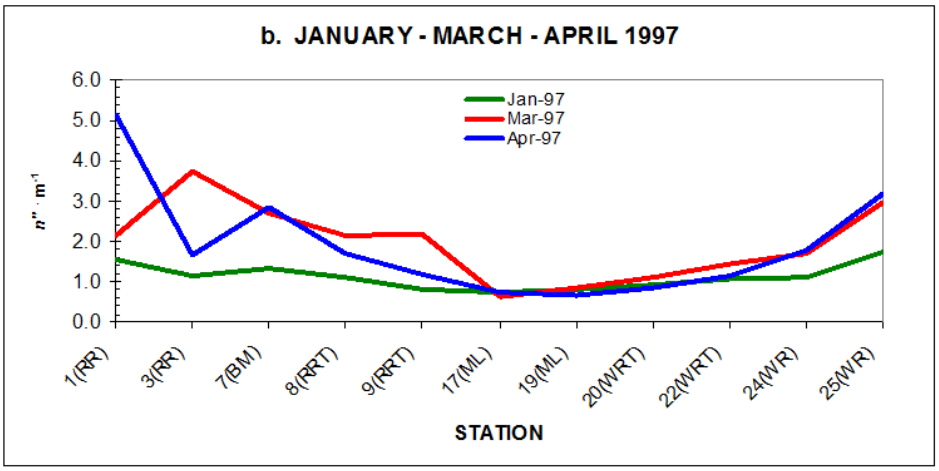

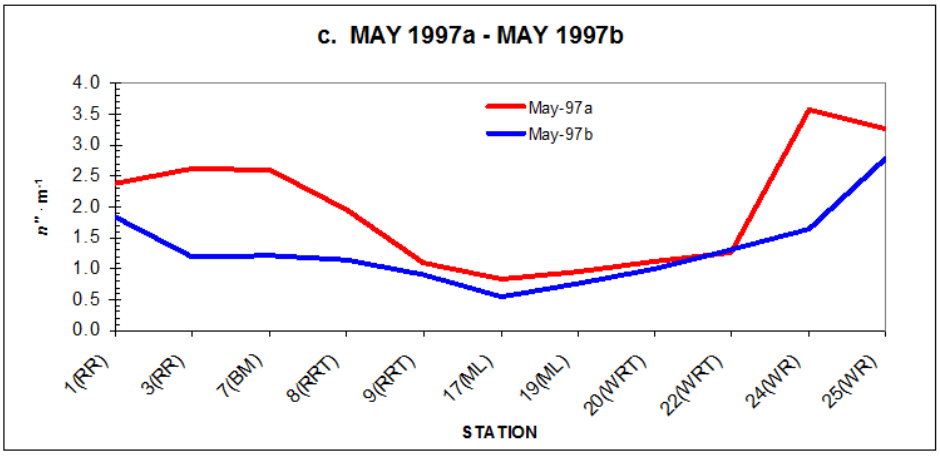

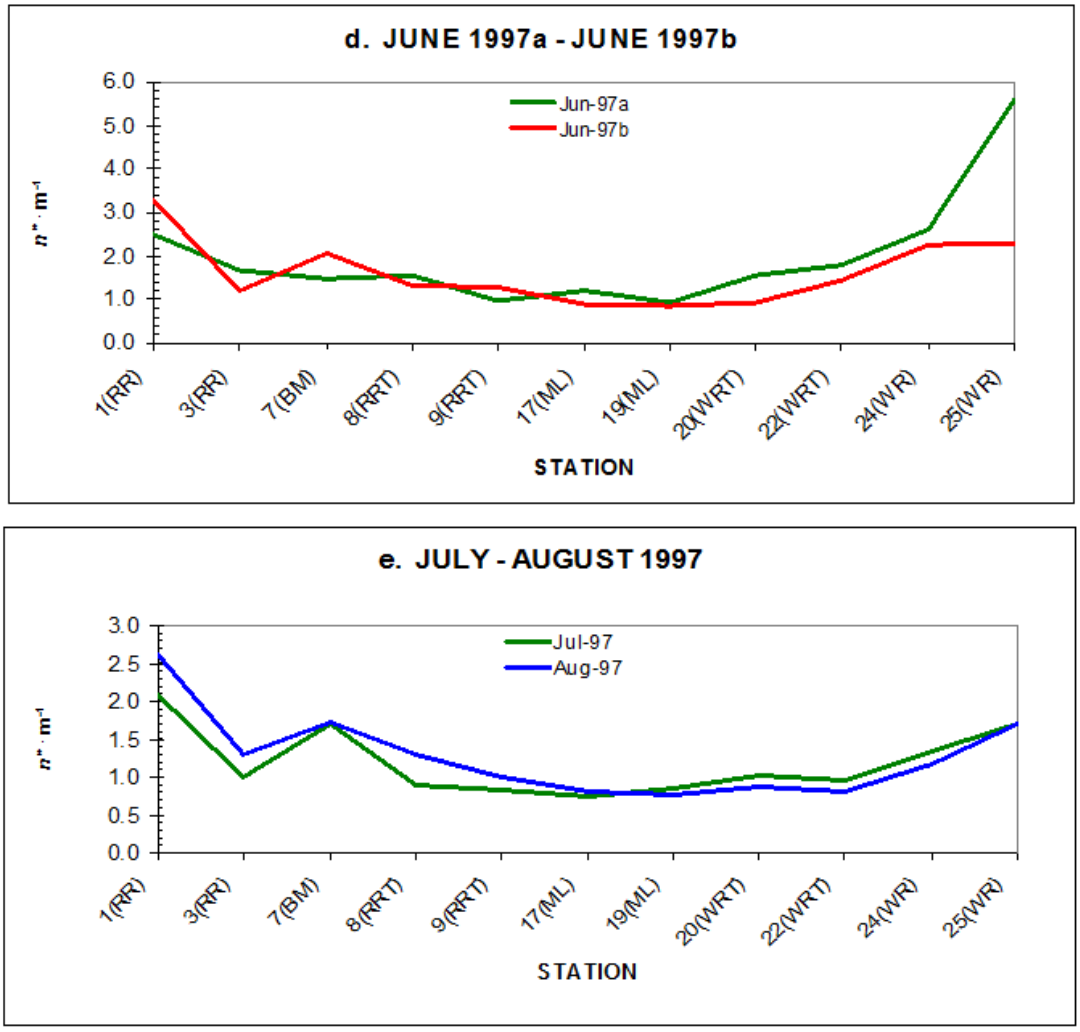

Figure 2. *Longitudinal gradient of attenuation coefficients ($\eta'' \cdot m^{-1}$) at eleven fixed sampling stations from Red River and Washita zones to the Main Lake zone. a) August-November 1996; b) January-April 1997; c) May 1997a-May 1997b; d) June 1997a-June 1997b; e) July-August 1997; f) August 1996 and August 1997. Zones of Lake Texoma: RR = Red River; RRT = Red River Transition; BM = Big Mineral; ML = Main Lake; WRT = Washita River Transition; WR = Washita River.*

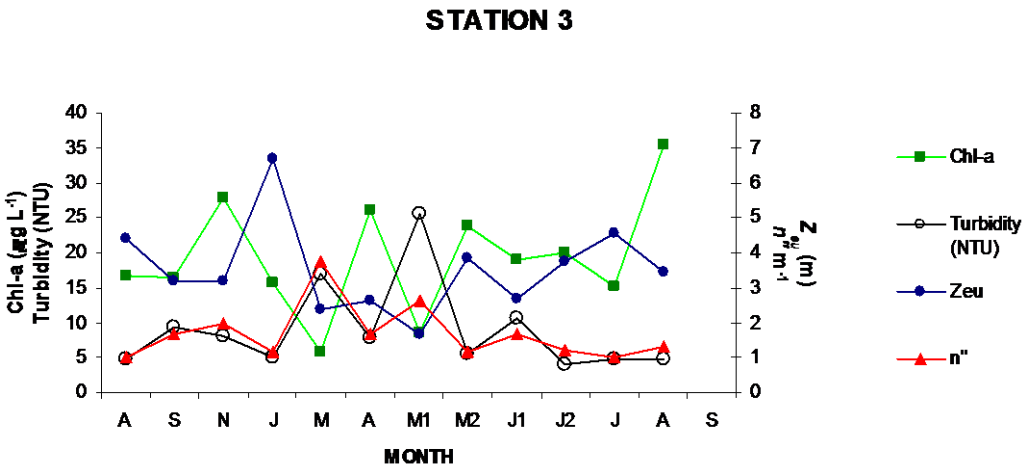

STATION 9

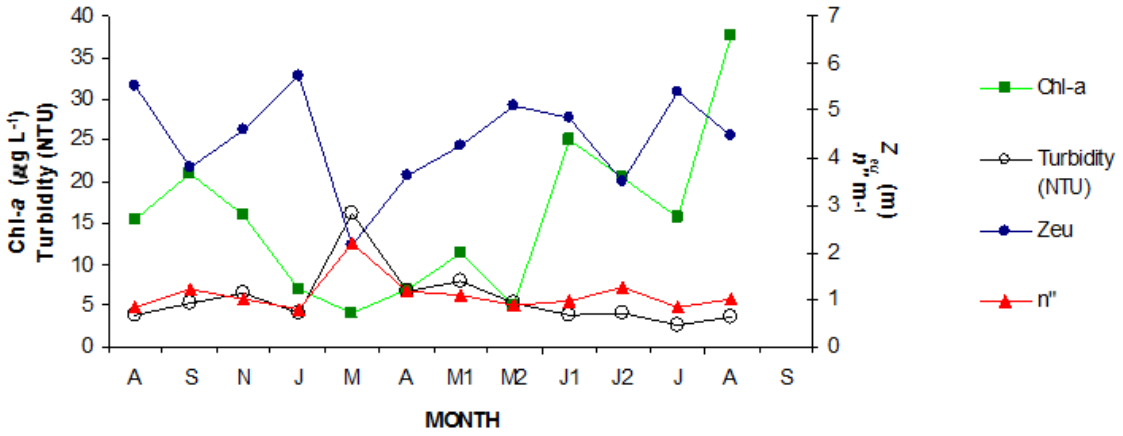

STATION 17

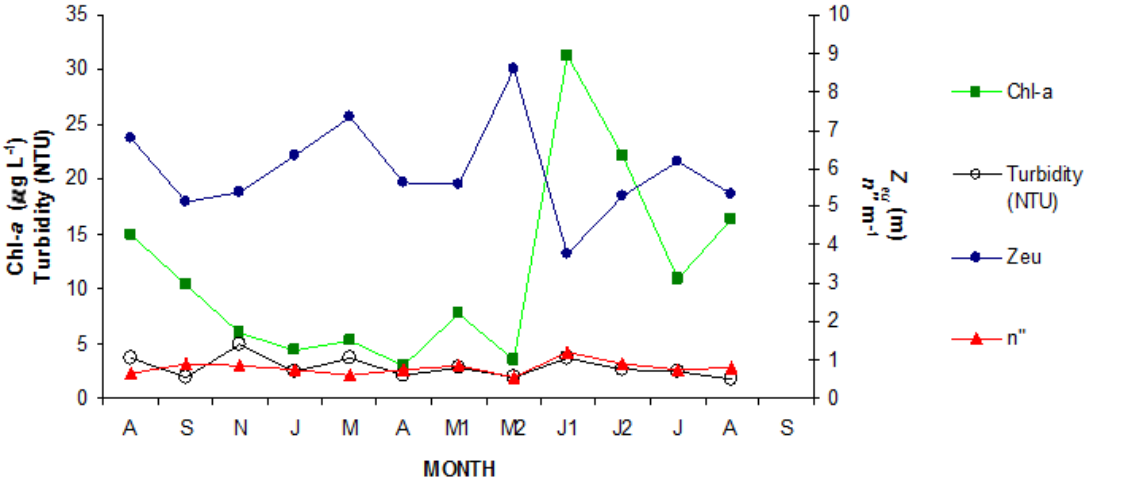

STATION 22

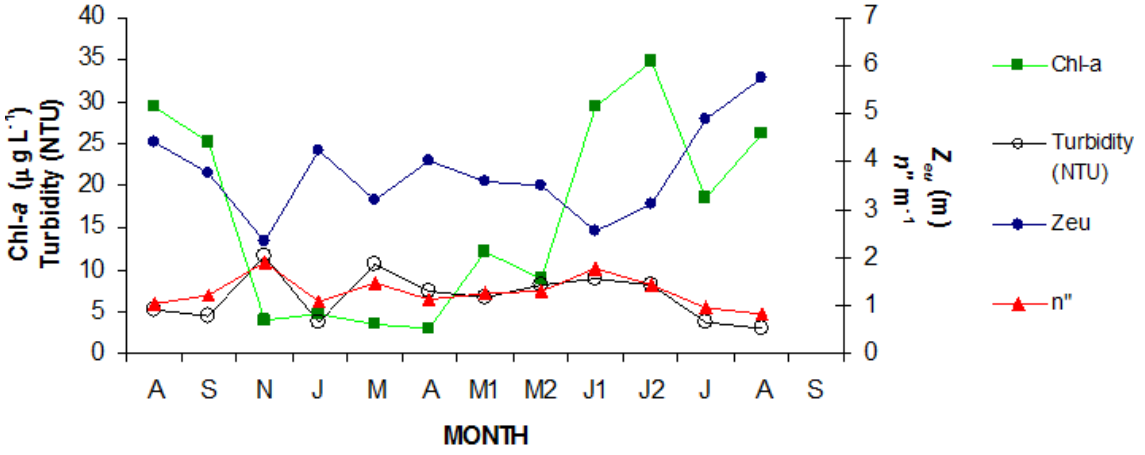

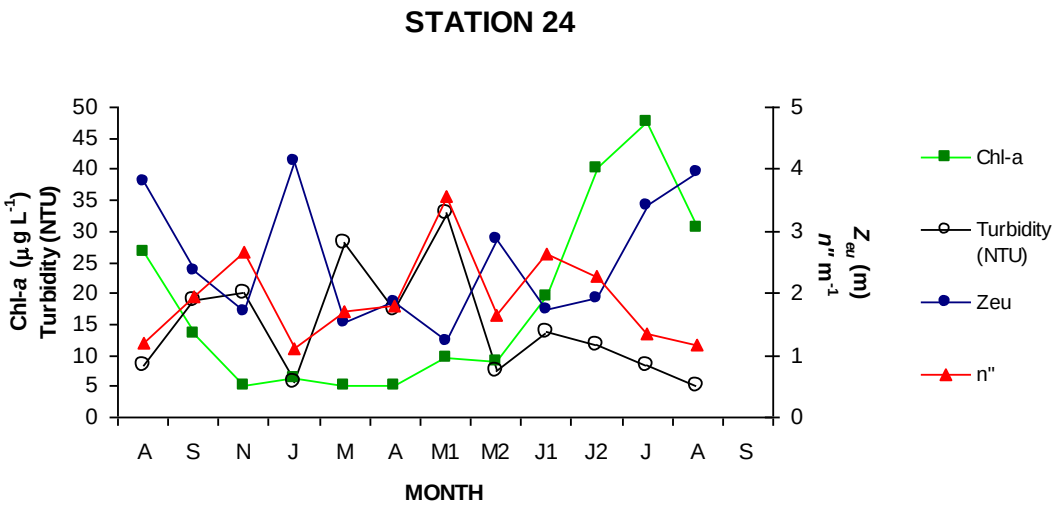

Figure 3. *Depth of euphotic zone (Zeu), vertical attenuation coefficient (η"), mean turbidity and chlorophyll-a at Stations 3, 9, 17, 22 and 24, Lake Texoma from August 1996 to September 1997. May and June had two sampling dates, designated as M1, M2 and J1, J2, respectively.*

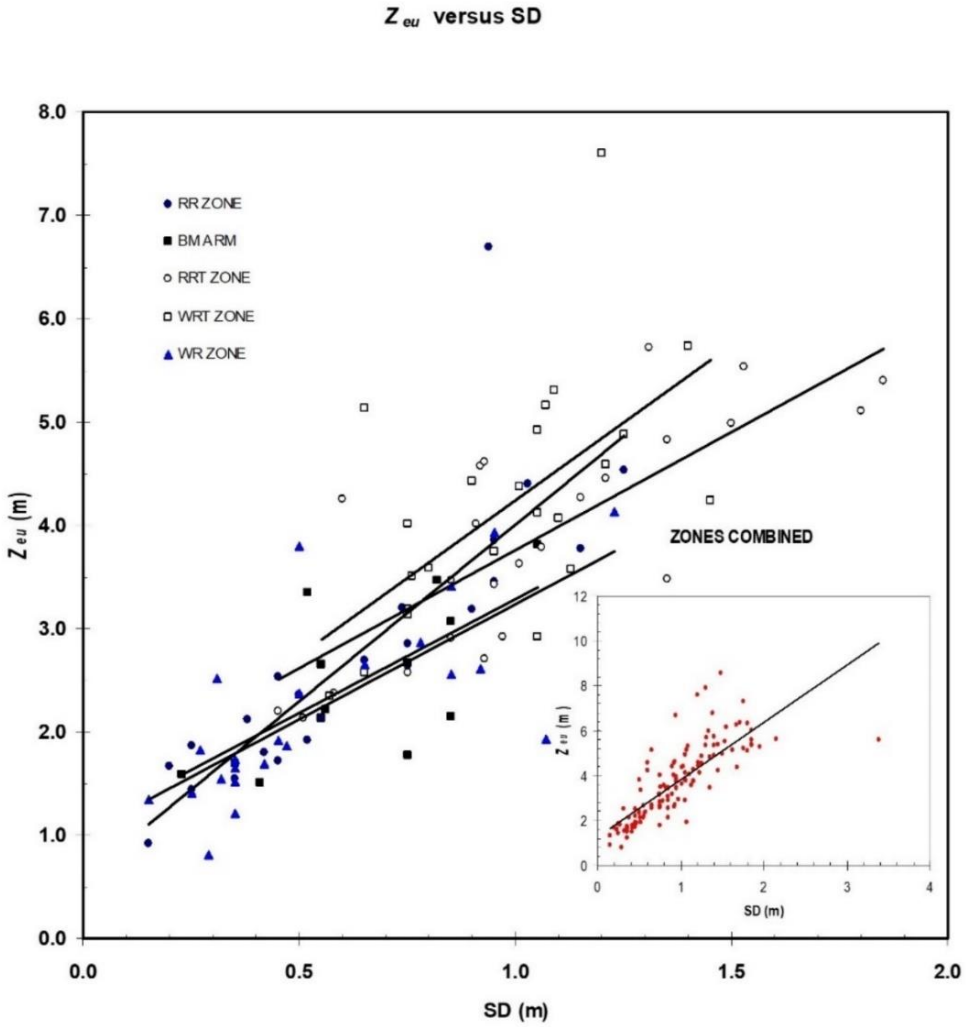

Figure 4. *Z_{eu} versus SD at five zones in Lake Texoma took over the course of the sampling year. Inset figure shows regression line through all zones combined (Z_{eu} = 1.250 + 2.557 (SD); r^2 = 0.63; p = 0.0001).*

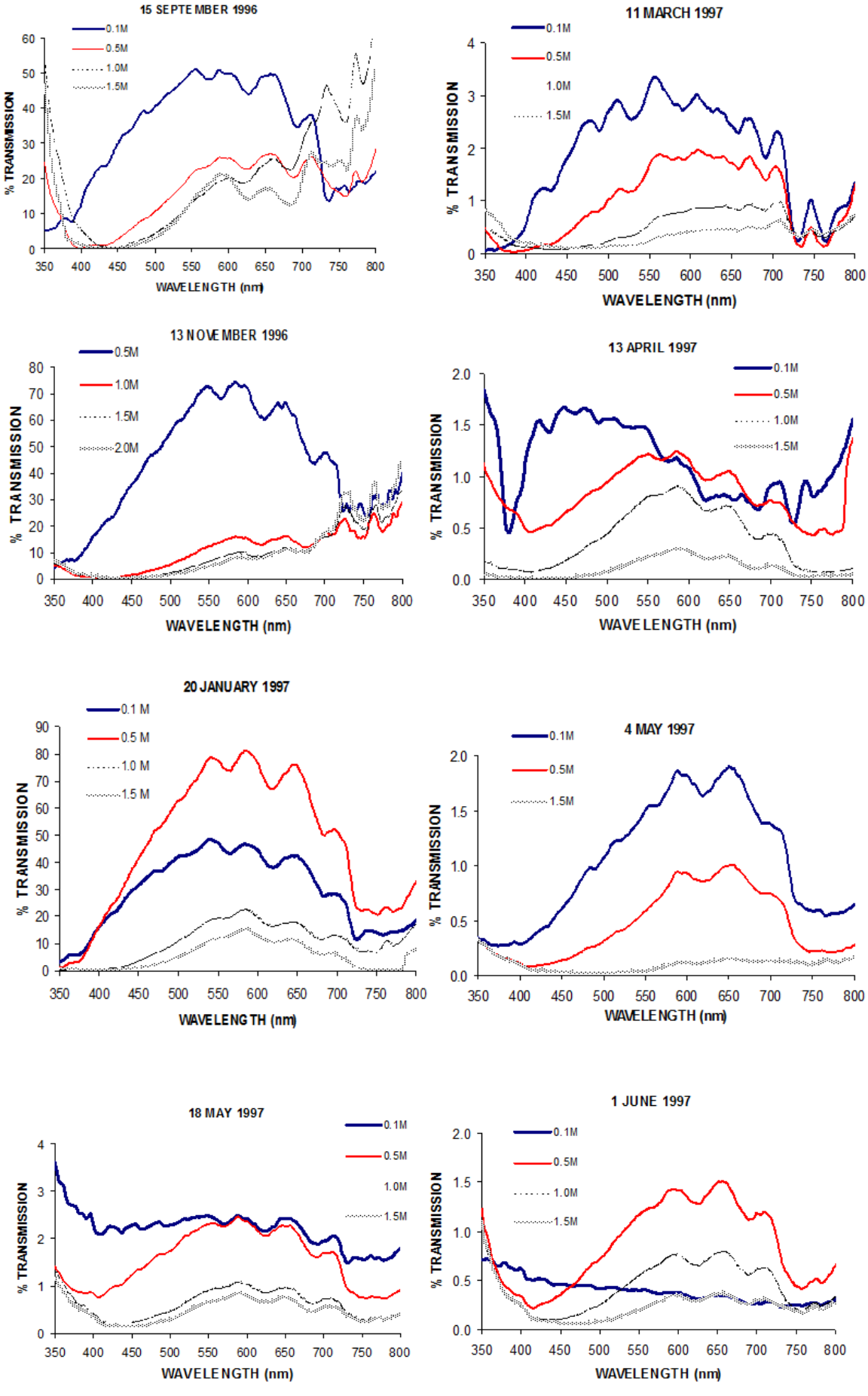
15 SEPTEMBER 1996
0.1M
0.5M
1.0M
1.5M
% TRANSMISSION
WAVELENGTH (nm)
11 MARCH 1997
0.1M
0.5M
1.0M
1.5M
% TRANSMISSION
WAVELENGTH (nm)
13 NOVEMBER 1996
0.5M
1.0M
1.5M
2.0M
% TRANSMISSION
WAVELENGTH (nm)
13 APRIL 1997
0.1M
0.5M
1.0M
1.5M
% TRANSMISSION
WAVELENGTH (nm)
20 JANUARY 1997
0.1 M
0.5 M
1.0 M
1.5 M
% TRANSMISSION
WAVELENGTH (nm)
4 MAY 1997
0.1M
0.5M
1.5M
% TRANSMISSION
WAVELENGTH (nm)
18 MAY 1997
0.1M
0.5M
1.0M
1.5M
% TRANSMISSION
WAVELENGTH (nm)
1 JUNE 1997
0.1M
0.5M
1.0M
1.5M
% TRANSMISSION
WAVELENGTH (nm)

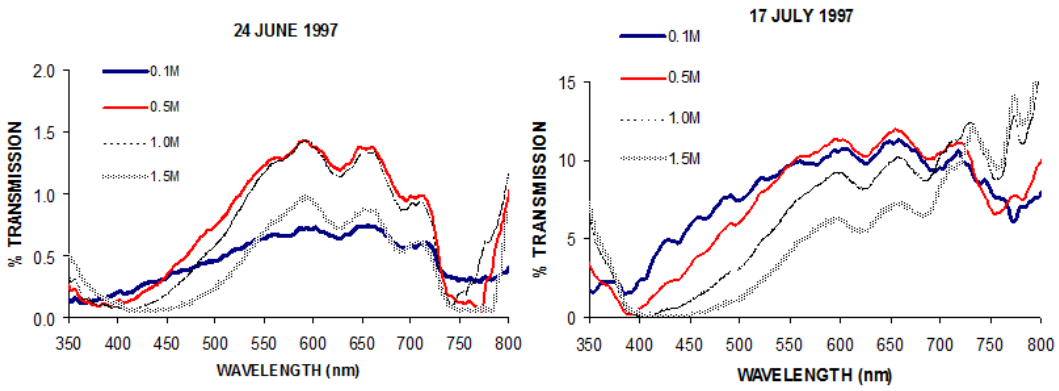

Station 3 (Figure 5a.)

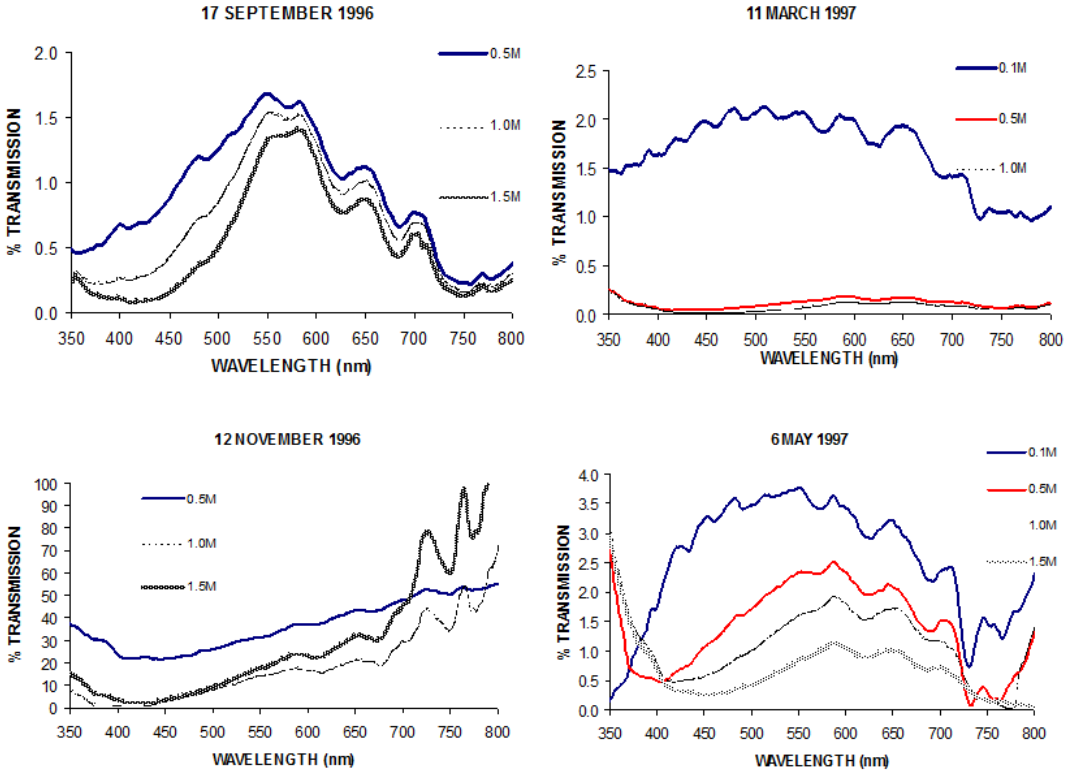

Station 3 (Figure 5a.)

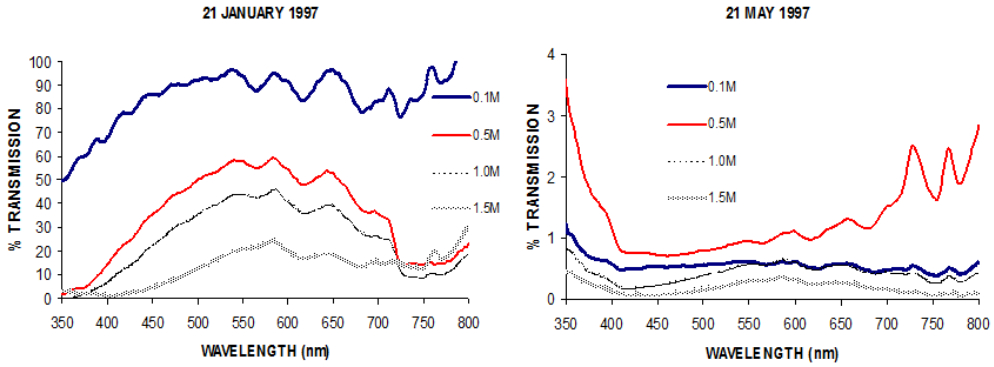

Station 9 (Figure 5b.)

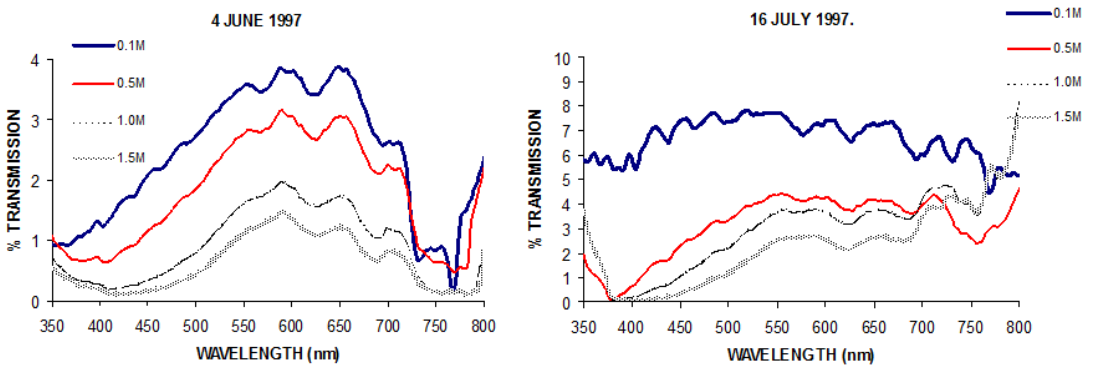

Station 9 (Figure 5b.)

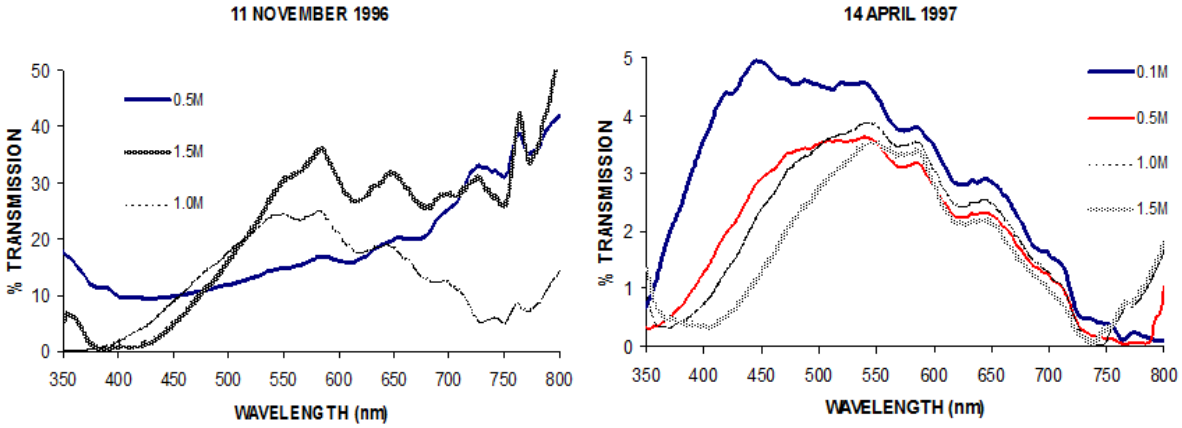

Station 17 (Figure 5c.)

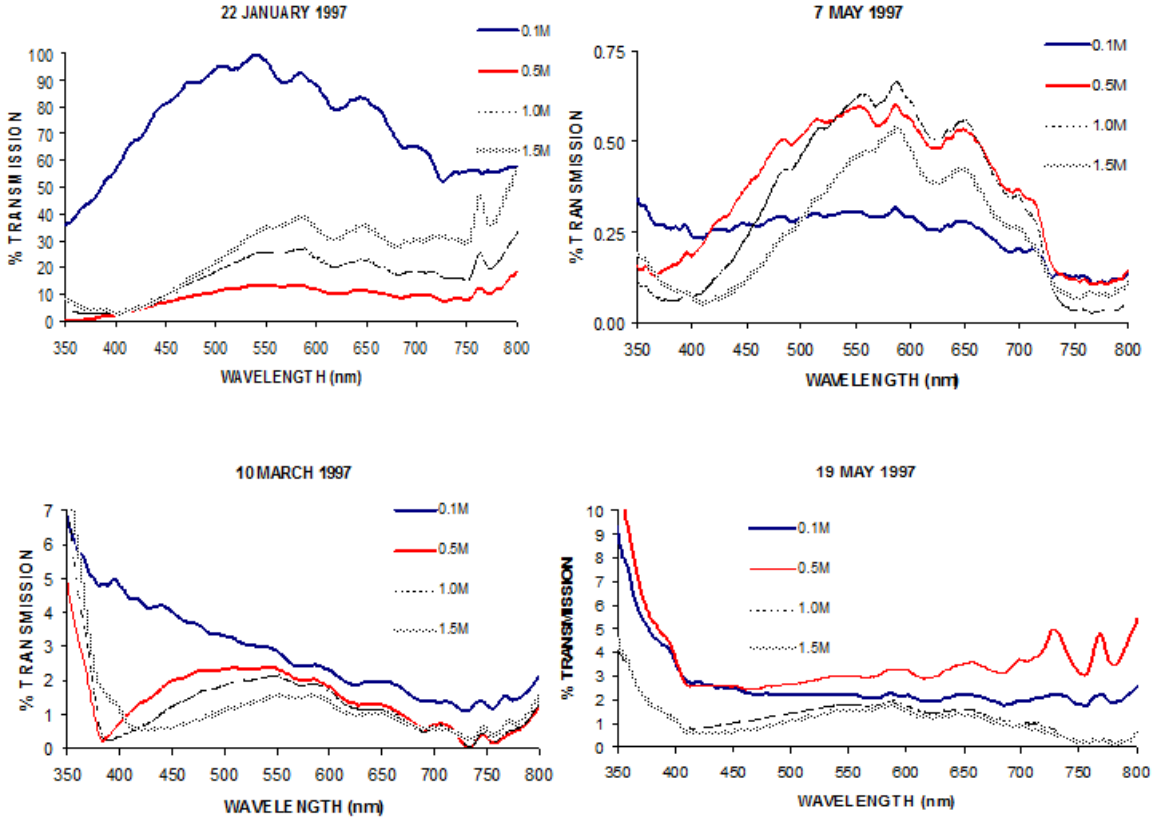

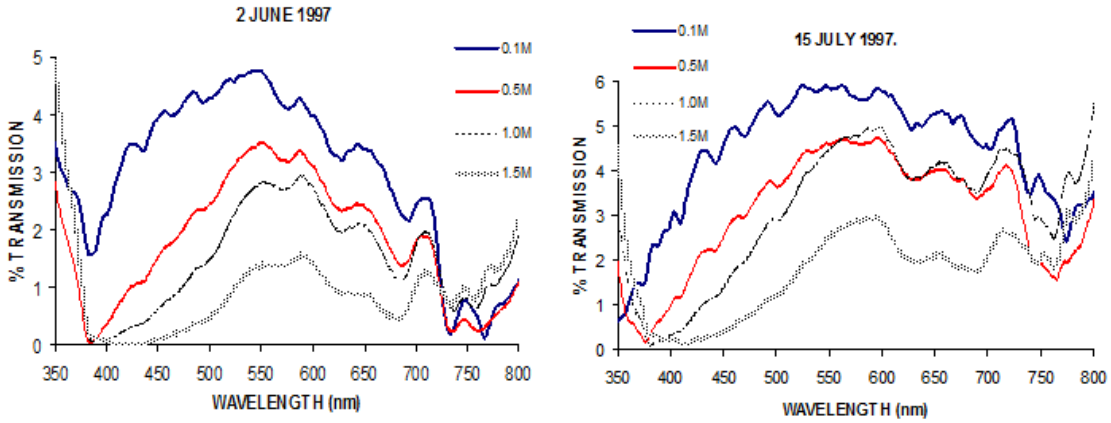

Station 17 (Figure 5c.)

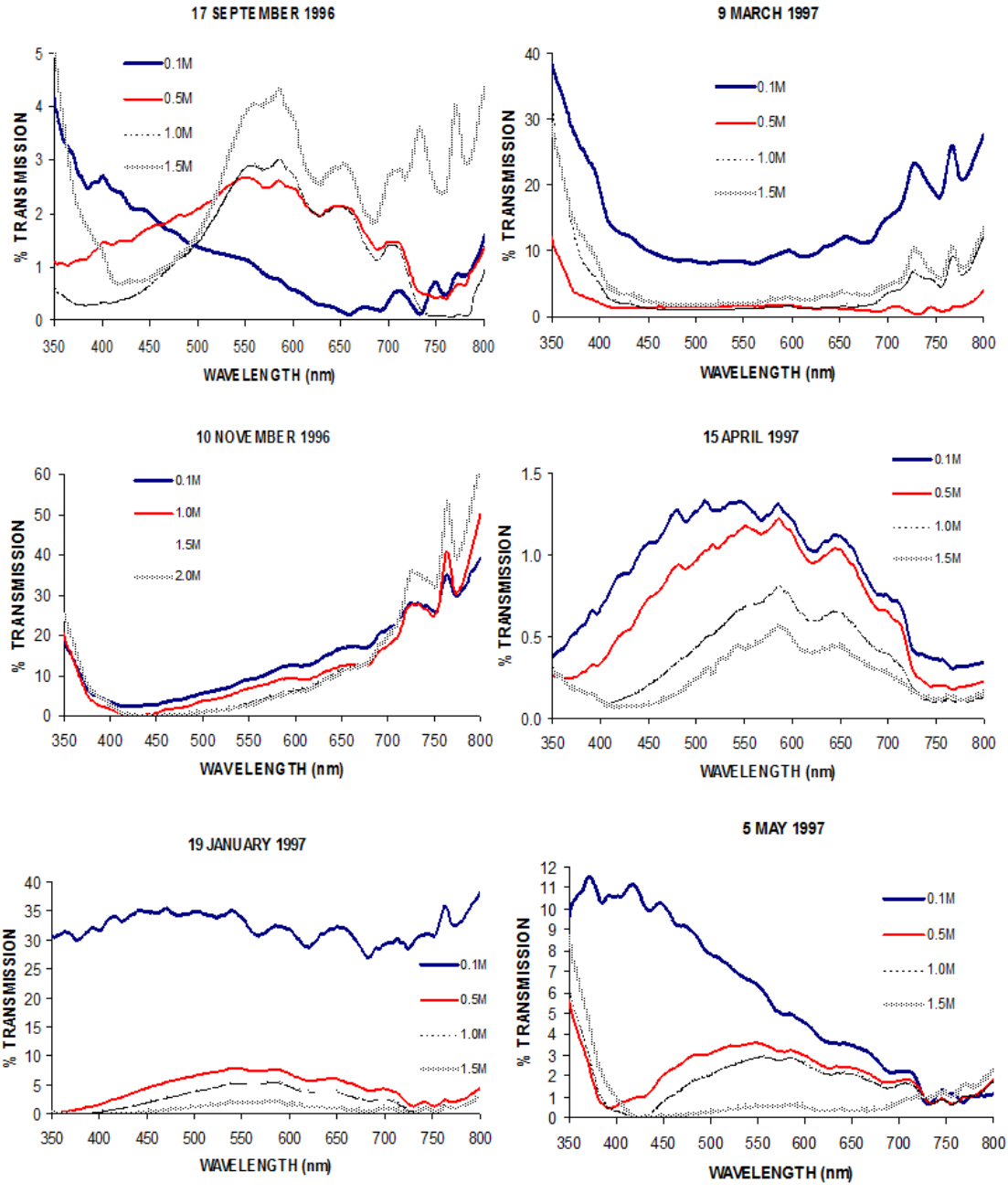

Station 22 (Figure 5d.)

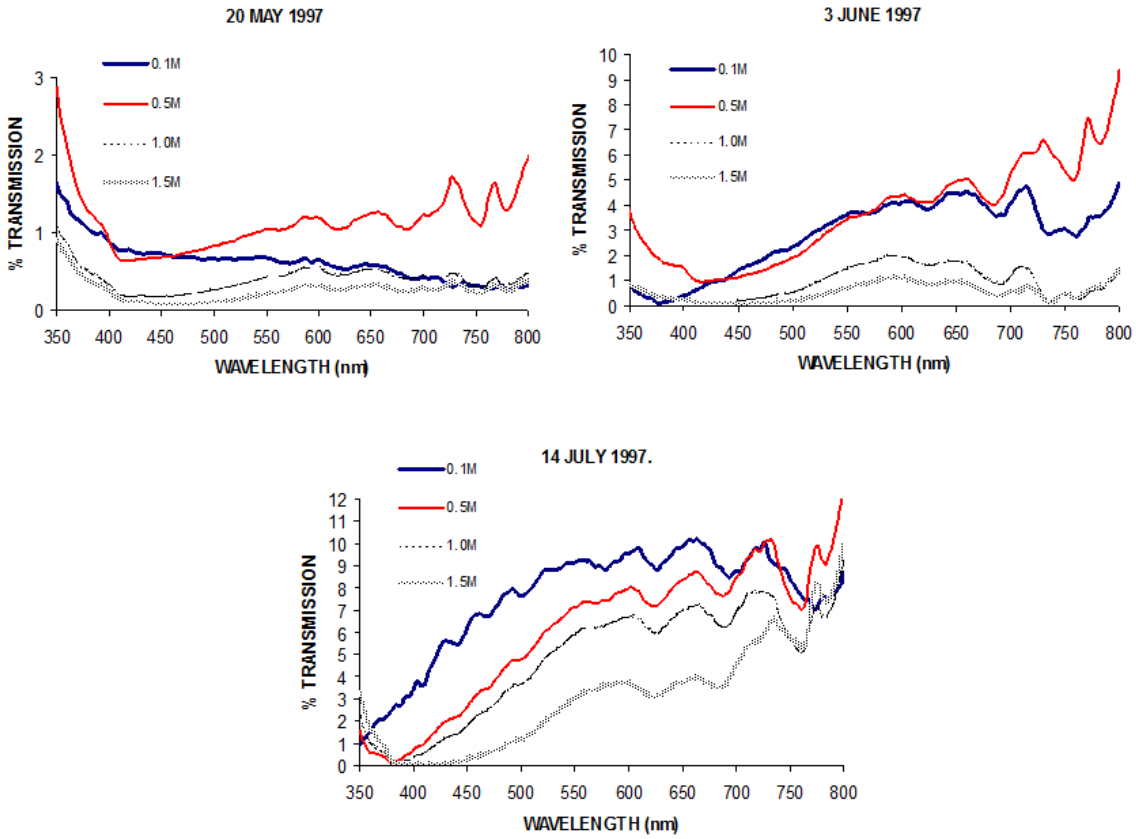

Station 22 (Figure 5d.)

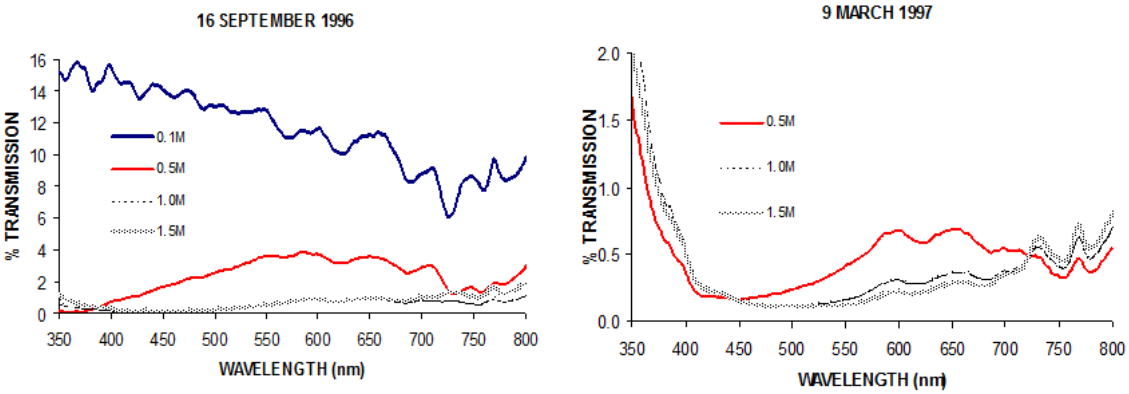

Station 24 (Figure 5e.)

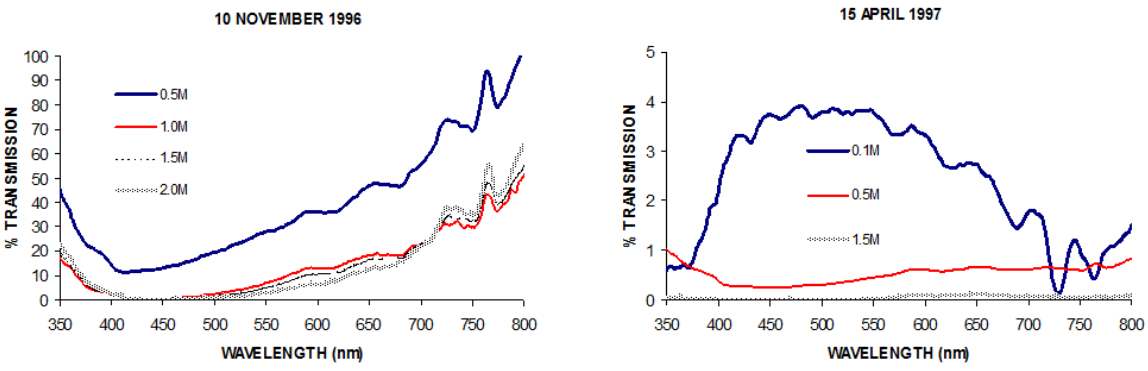

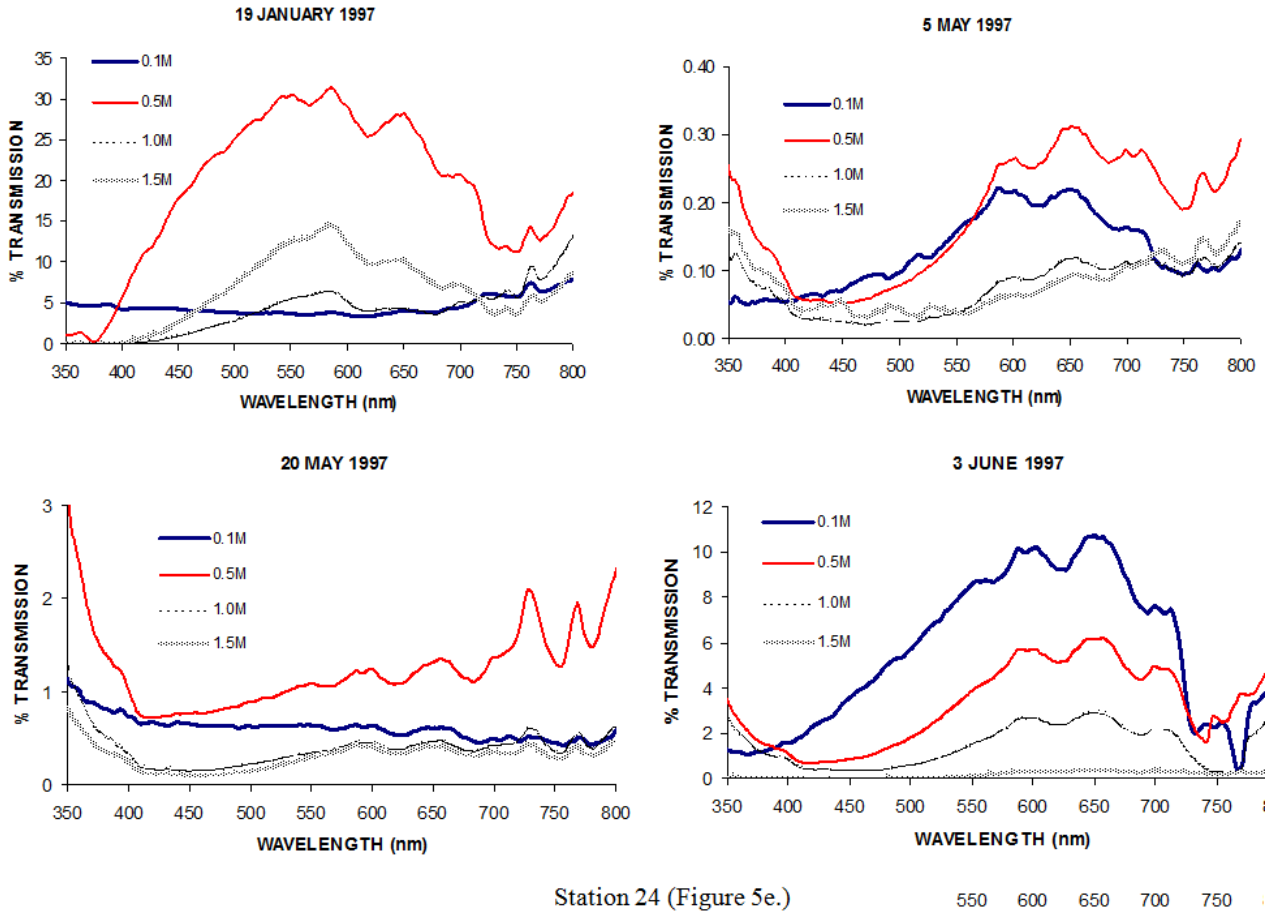

Station 24 (Figure 5e.)

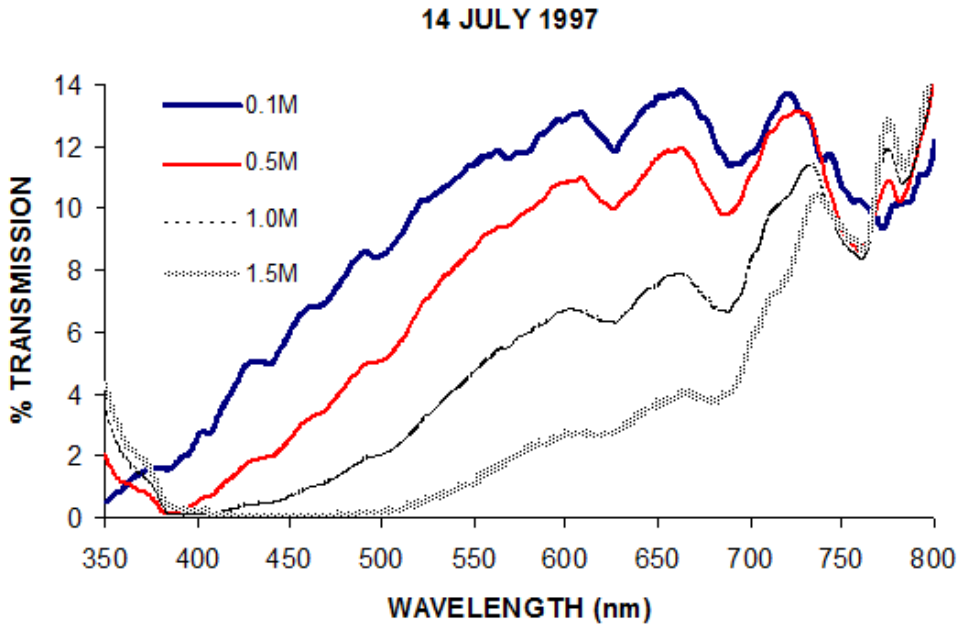

Station 24 (Figure 5e.)

Figure 5. *Percent transmission spectra at 0.5-meter intervals at Stations 3, 9, 17, 22 and 24, Lake Texoma from September 1996 to July 1997. The following figures correspond to each station. Figure 5a: Station 3. Figure 5b: Station 9. Figure 5c: Station 17. Figure 5d: Station 22. Figure 5e: Station 24.*

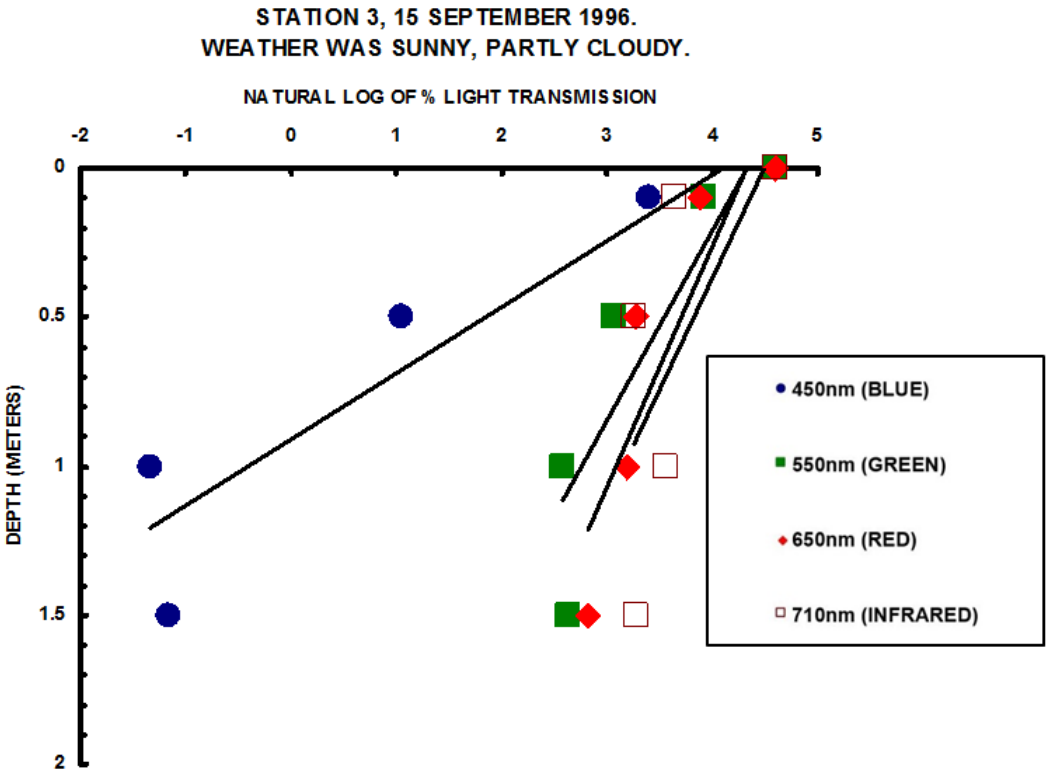
STATION 3, 15 SEPTEMBER 1996.
WEATHER WAS SUNNY, PARTLY CLOUDY.
NATURAL LOG OF % LIGHT TRANSMISSION
-2
-1
0
1
2
3
4
5
0
0.5
1
1.5
2
DEPTH (METERS)
450nm (BLUE)
550nm (GREEN)
650nm (RED)
710nm (INFRARED)

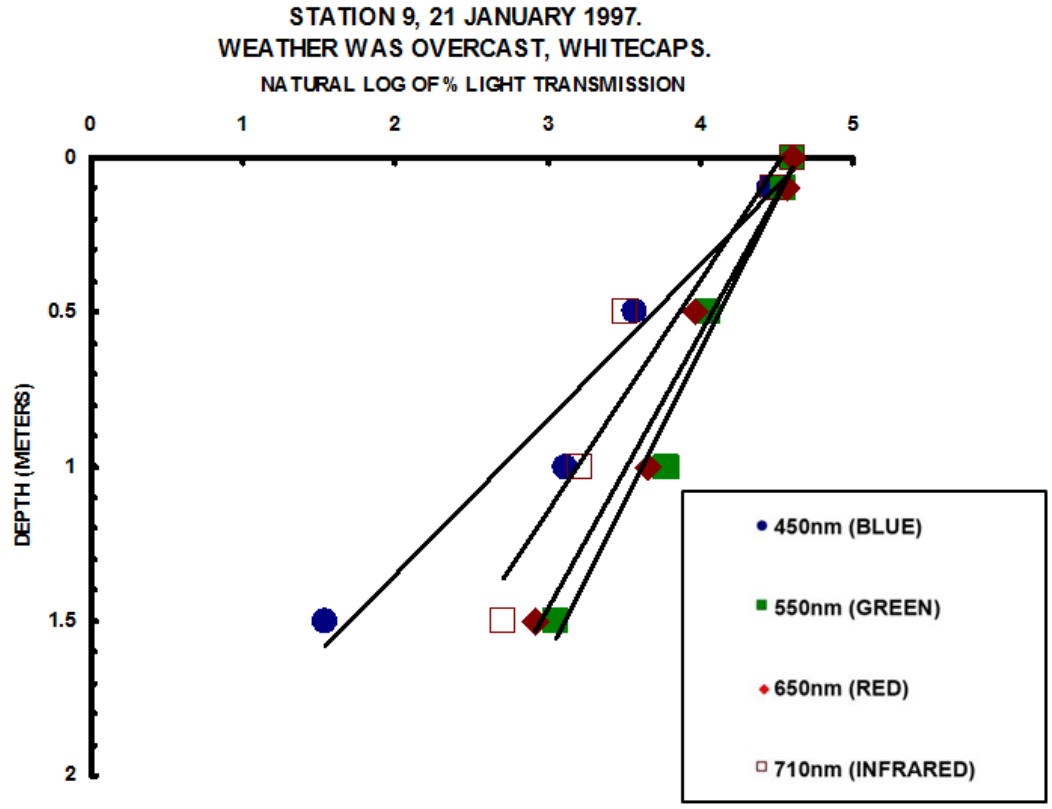
STATION 9, 21 JANUARY 1997.
WEATHER WAS OVERCAST, WHITECAPS.
NATURAL LOG OF % LIGHT TRANSMISSION
0
1
2
3
4
5
0
0.5
1
1.5
2
DEPTH (METERS)
450nm (BLUE)
550nm (GREEN)
650nm (RED)
710nm (INFRARED)

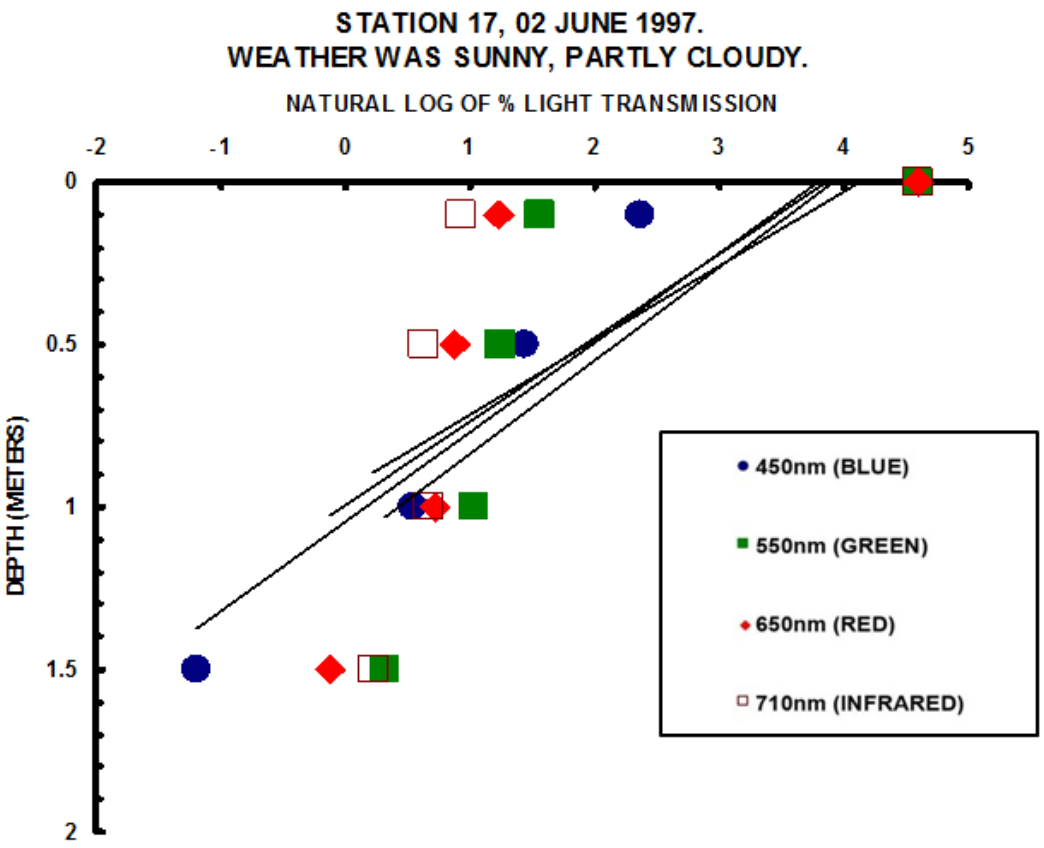
STATION 17, 02 JUNE 1997.
WEATHER WAS SUNNY, PARTLY CLOUDY.
NATURAL LOG OF % LIGHT TRANSMISSION
-2
-1
0
1
2
3
4
5
0
0.5
1
1.5
2
DEPTH (METERS)
450nm (BLUE)
550nm (GREEN)
650nm (RED)
710nm (INFRARED)

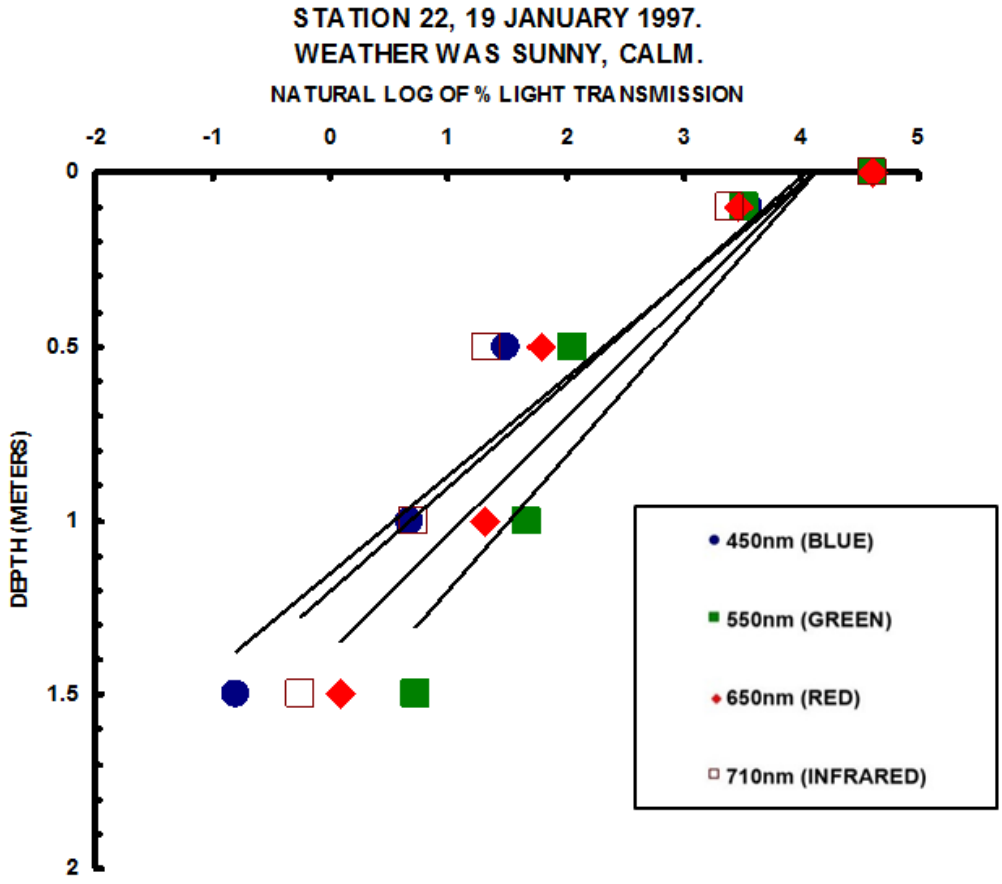
STATION 22, 19 JANUARY 1997.
WEATHER WAS SUNNY, CALM.
NATURAL LOG OF % LIGHT TRANSMISSION
-2
-1
0
1
2
3
4
5
0
0.5
1
1.5
2
DEPTH (METERS)
450nm (BLUE)
550nm (GREEN)
650nm (RED)
710nm (INFRARED)

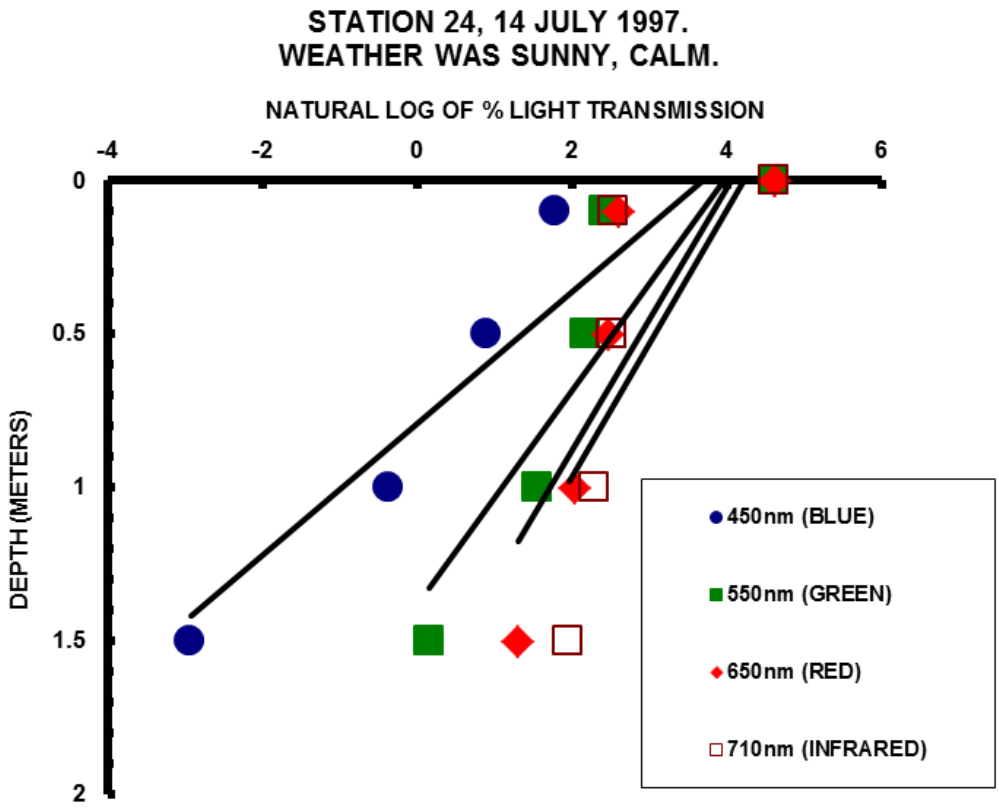

Figure 6. *Light intensity versus depth at five intensive sampling stations.*

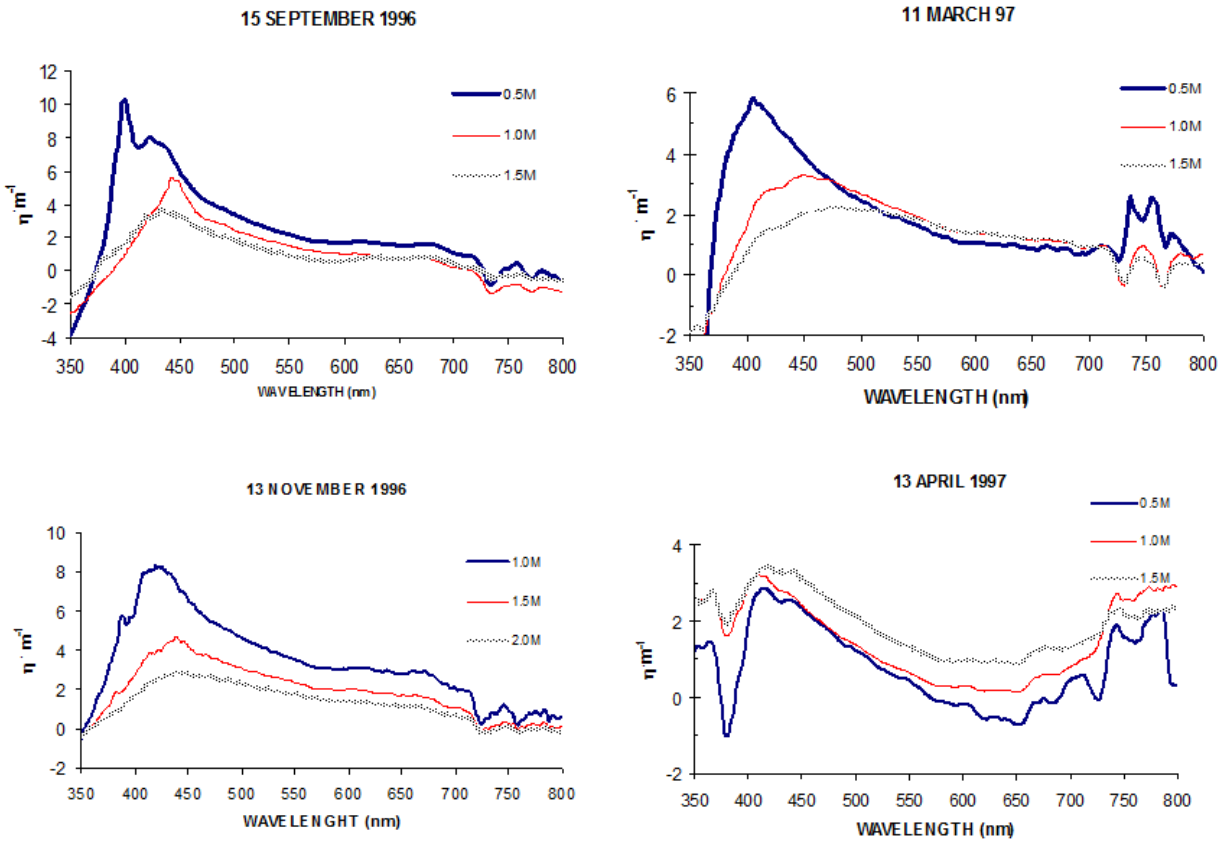

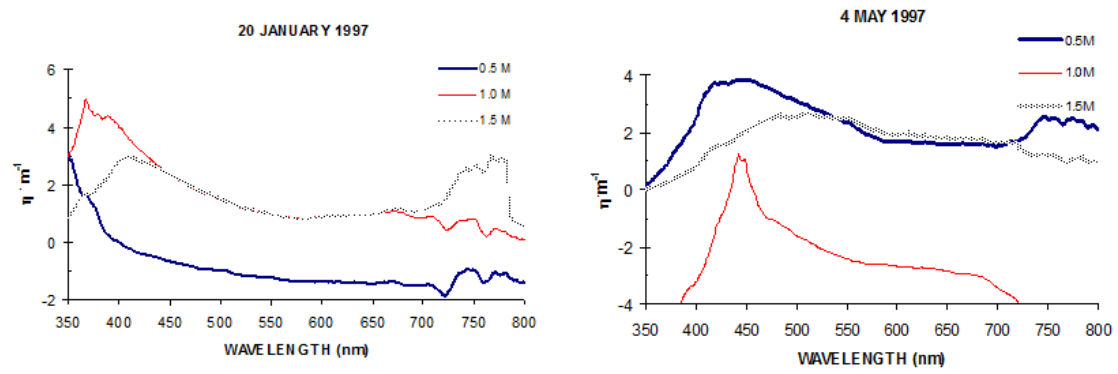

Station 3

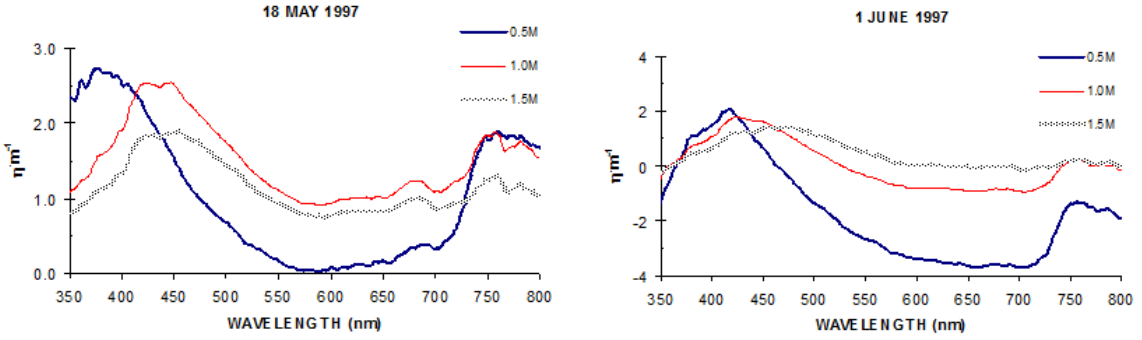

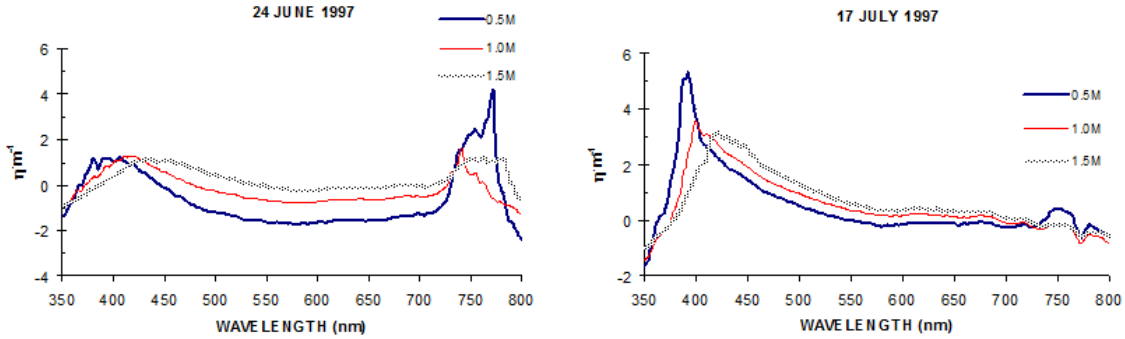

Station 3

a. Attenuation coefficients (η. m^{-1}) at Station 3, September 1996-July 1997.

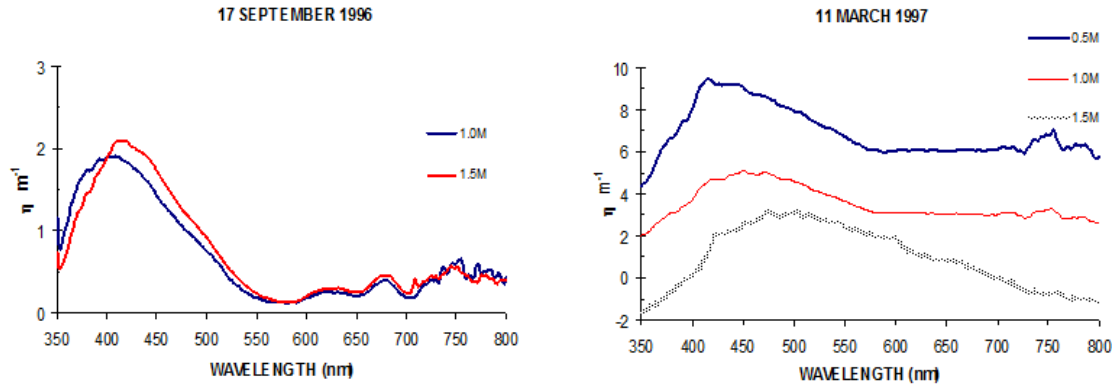

Station 9

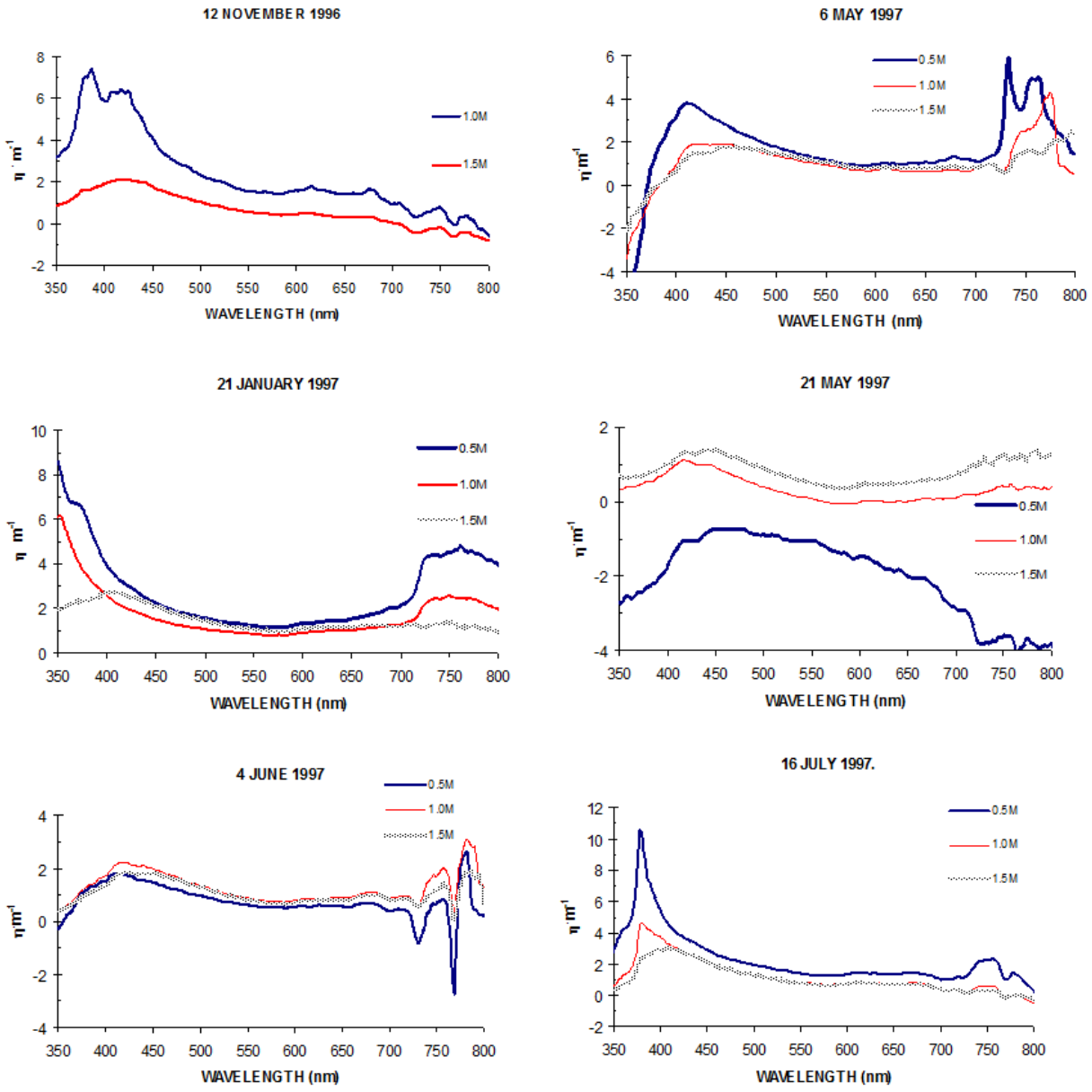

Station 9

b. Attenuation coefficients (η. m-1) at Station 9, September 1996-July 1997.

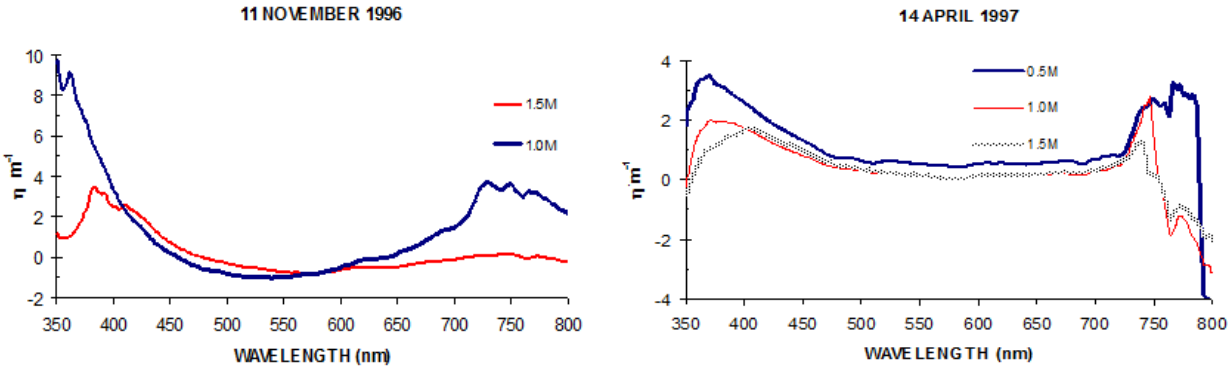

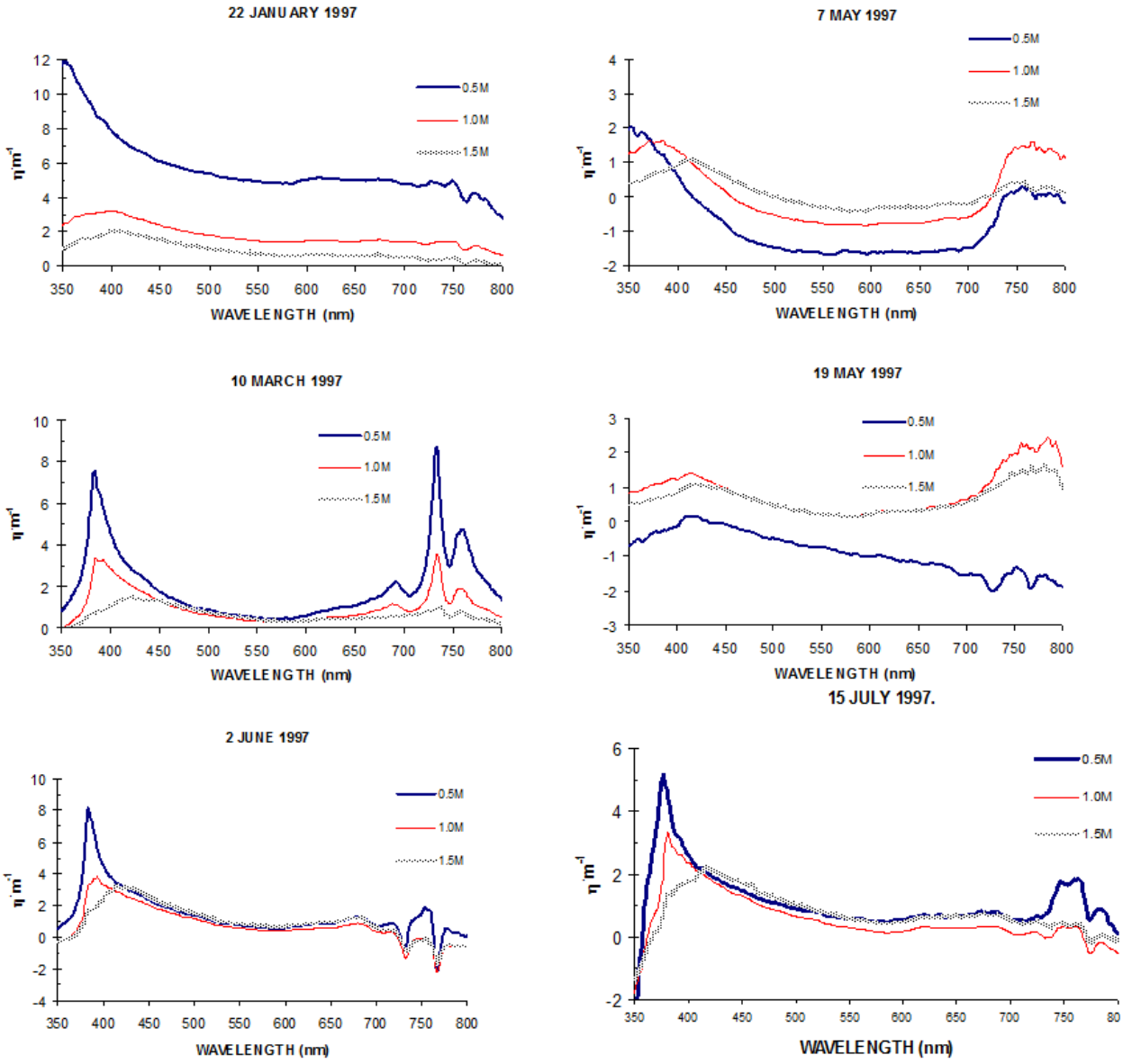

Station 17

c. Attenuation coefficients ($\eta . m^{-1}$) at Station 17, September 1996-July 1997.

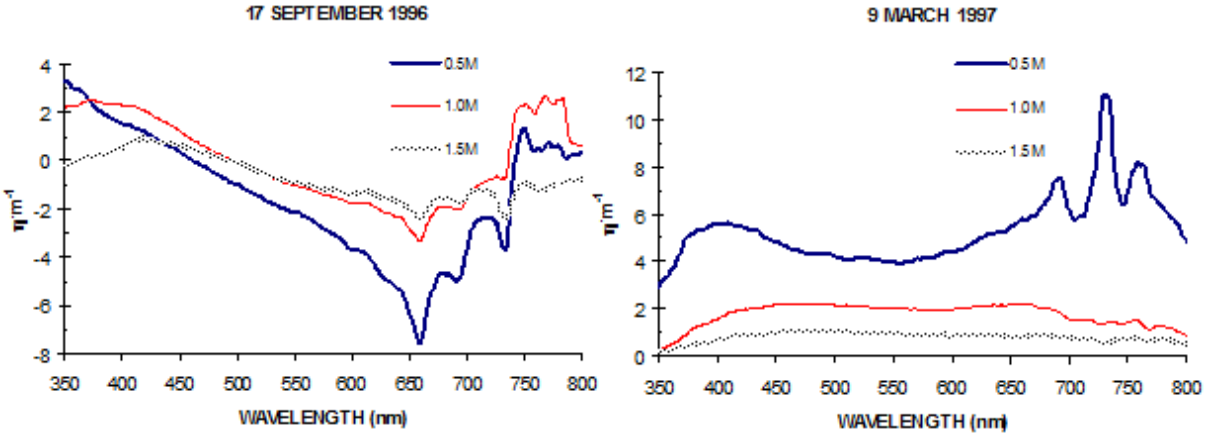

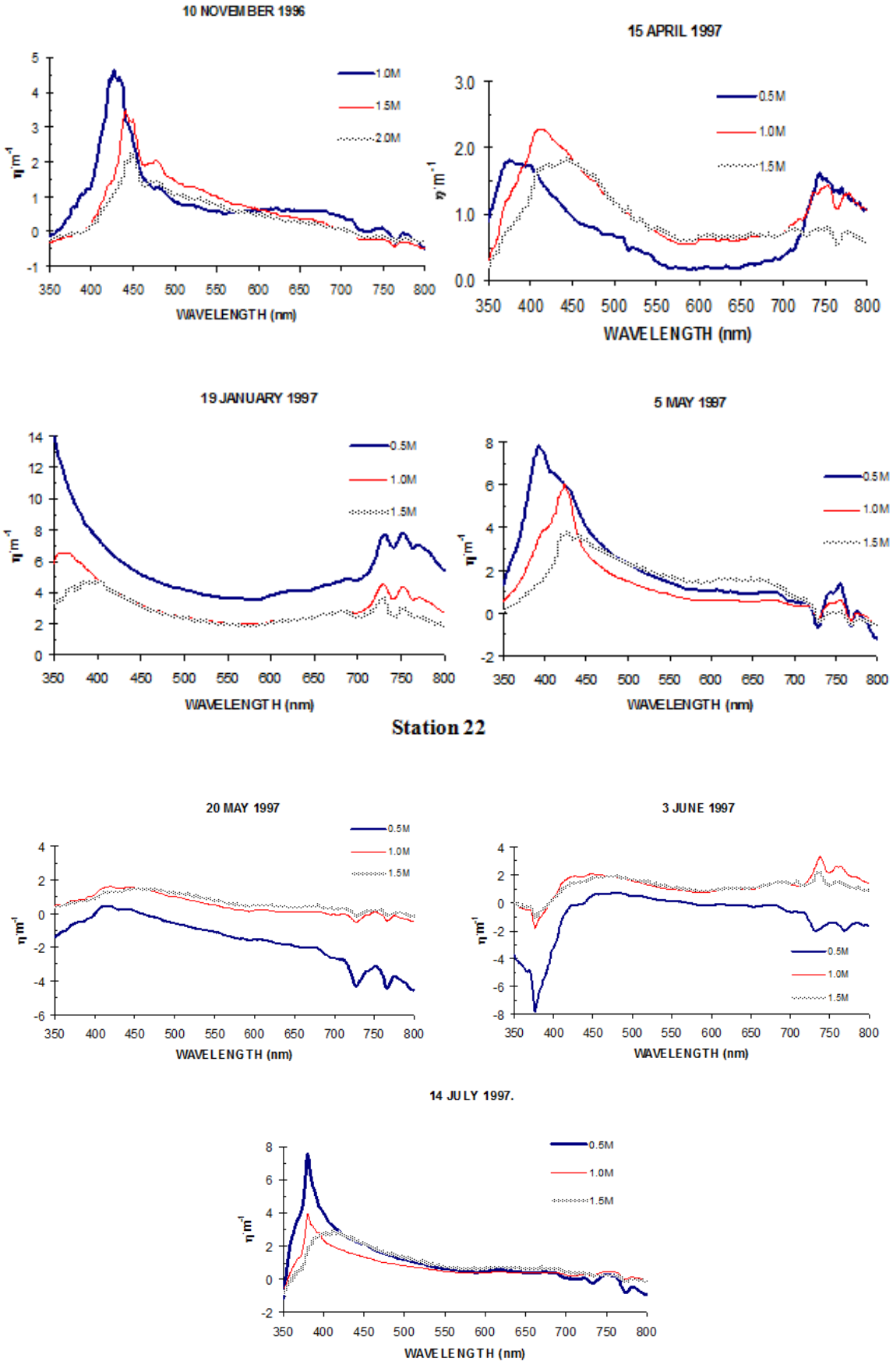

Station 22

d. Attenuation coefficients (η. m^{-1}) at Station 22, September 1996-July 1997.

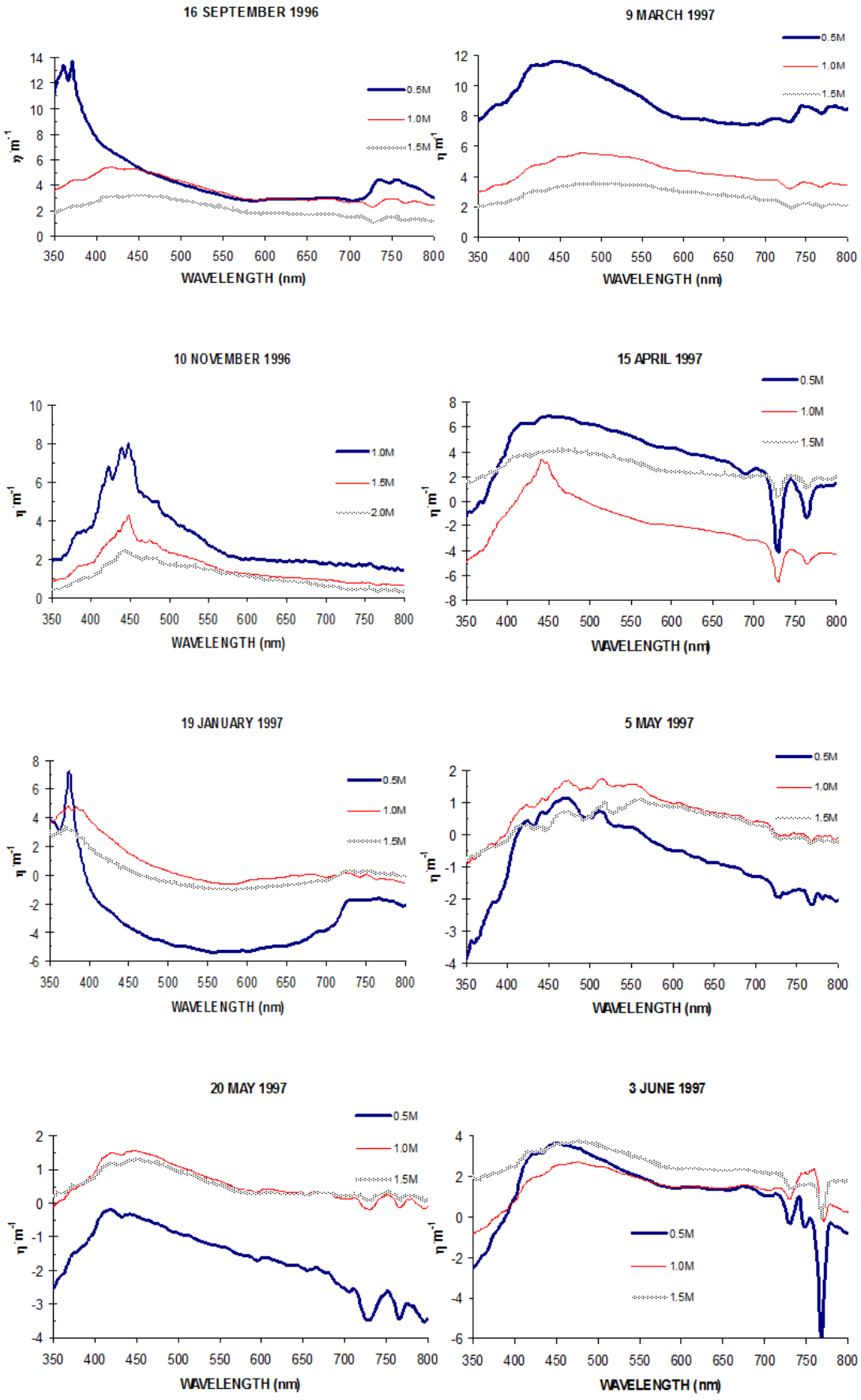
16 SEPTEMBER 1996
9 MARCH 1997
10 NOVEMBER 1996
15 APRIL 1997
19 JANUARY 1997
5 MAY 1997
20 MAY 1997
3 JUNE 1997
η m-1
WAVELENGTH (nm)
0.5M
1.0M
1.5M
2.0M

Station 24

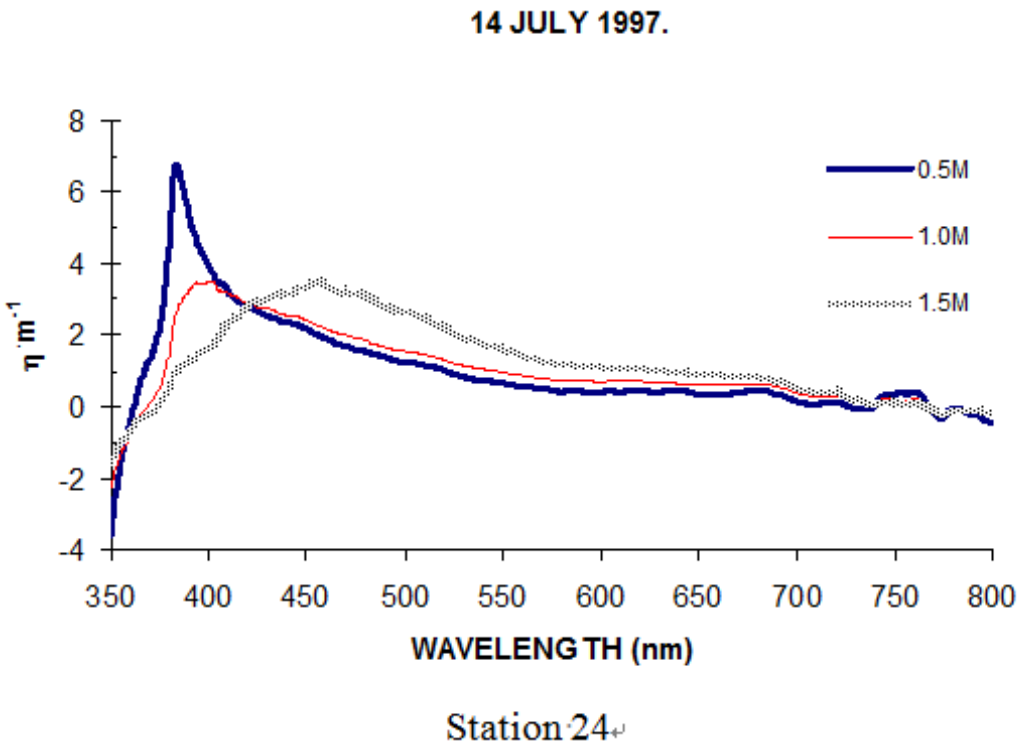

Station 24

e. Attenuation coefficients (η. m^{-1}) at Station 24, September 1996-July 1997.

Figure 7. *Attenuation coefficients (η. m^{-1}) at 0.5-meter interval at Stations 3, 9, 17, 22 and 24, Lake Texoma from September 1996 to July 1997. The following figures correspond to each station. Figure 7a: Station 3. Figure 7b: Station 9. Figure 7c: Station 17. Figure 7d: Station 22. Figure 7e: Station 24.*

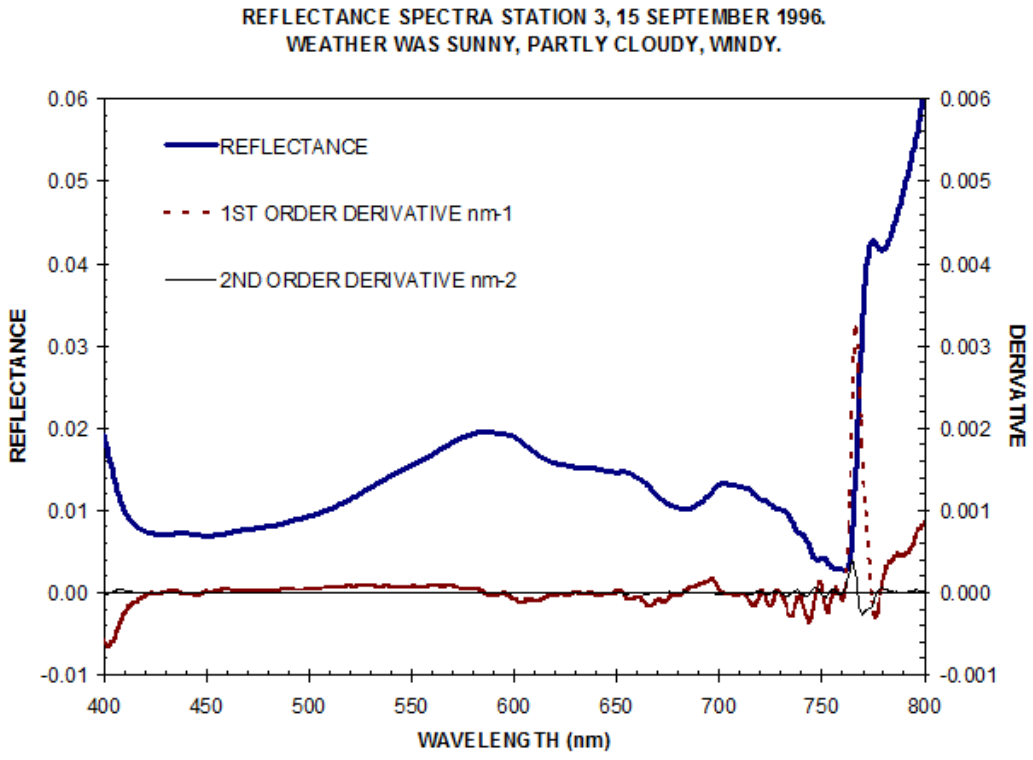

Station 3

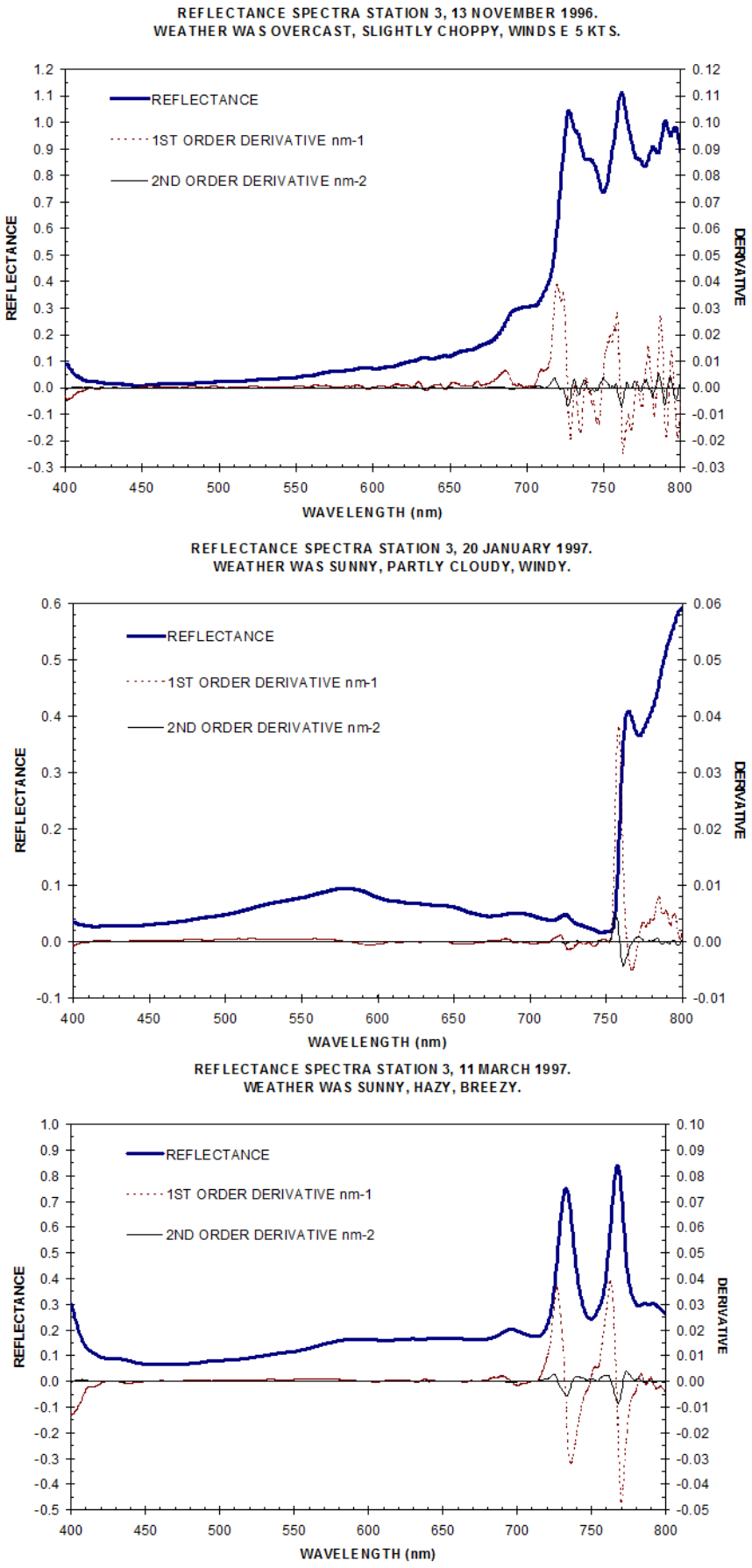
REFLECTANCE SPECTRA STATION 3, 13 NOVEMBER 1996.
WEATHER WAS OVERCAST, SLIGHTLY CHOPPY, WINDS E 5 KTS.
REFLECTANCE
1ST ORDER DERIVATIVE nm-1
2ND ORDER DERIVATIVE nm-2
REFLECTANCE
DERIVATIVE
WAVELENGTH (nm)
REFLECTANCE SPECTRA STATION 3, 20 JANUARY 1997.
WEATHER WAS SUNNY, PARTLY CLOUDY, WINDY.
REFLECTANCE
1ST ORDER DERIVATIVE nm-1
2ND ORDER DERIVATIVE nm-2
REFLECTANCE
DERIVATIVE
WAVELENGTH (nm)
REFLECTANCE SPECTRA STATION 3, 11 MARCH 1997.
WEATHER WAS SUNNY, HAZY, BREEZY.
REFLECTANCE
1ST ORDER DERIVATIVE nm-1
2ND ORDER DERIVATIVE nm-2
REFLECTANCE
DERIVATIVE
WAVELENGTH (nm)

Station 3

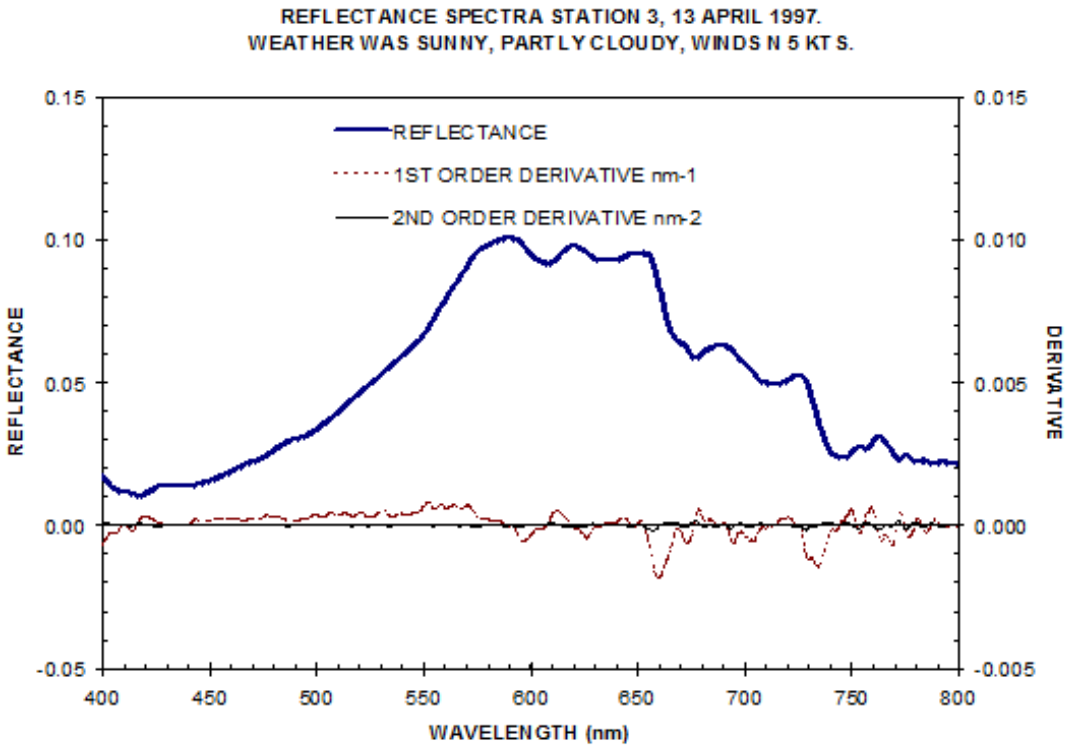
REFLECTANCE SPECTRA STATION 3, 13 APRIL 1997.
WEATHER WAS SUNNY, PARTLY CLOUDY, WINDS N 5 KTS.
REFLECTANCE
1ST ORDER DERIVATIVE nm-1
2ND ORDER DERIVATIVE nm-2
REFLECTANCE
DERIVATIVE
WAVELENGTH (nm)
0.15
0.10
0.05
0.00
-0.05
0.015
0.010
0.005
0.000
-0.005
400
450
500
550
600
650
700
750
800

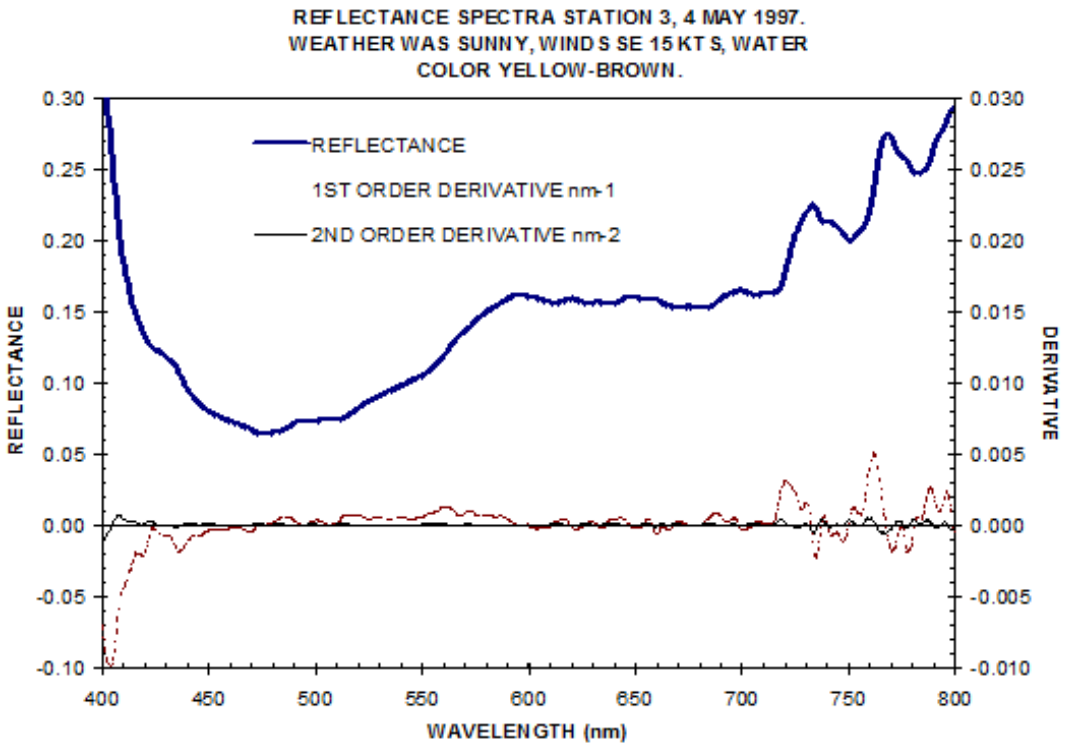
REFLECTANCE SPECTRA STATION 3, 4 MAY 1997.
WEATHER WAS SUNNY, WINDS SE 15 KTS, WATER
COLOR YELLOW-BROWN.
REFLECTANCE
1ST ORDER DERIVATIVE nm-1
2ND ORDER DERIVATIVE nm-2
REFLECTANCE
DERIVATIVE
WAVELENGTH (nm)
0.30
0.25
0.20
0.15
0.10
0.05
0.00
-0.05
-0.10
0.030
0.025
0.020
0.015
0.010
0.005
0.000
-0.005
-0.010
400
450
500
550
600
650
700
750
800

Station 3

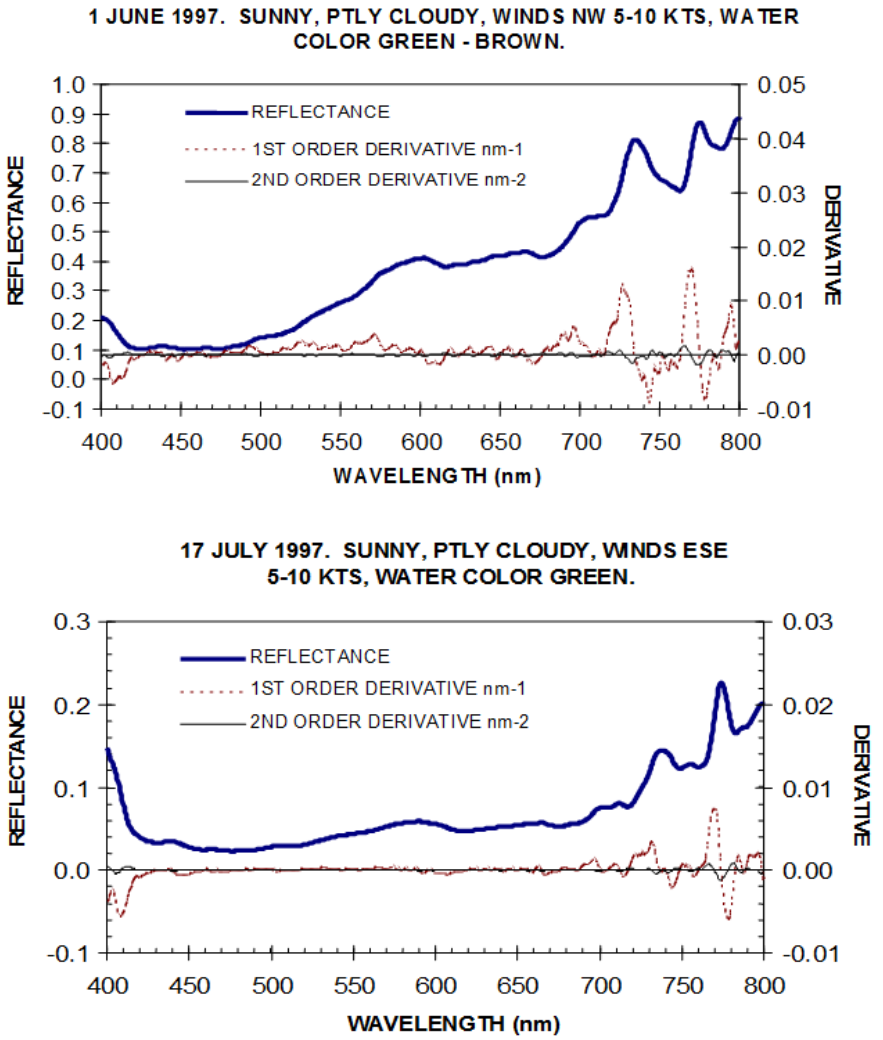

a. Reflectance spectra and their first and second-order derivatives at Station 3, September 1996-July 1997.

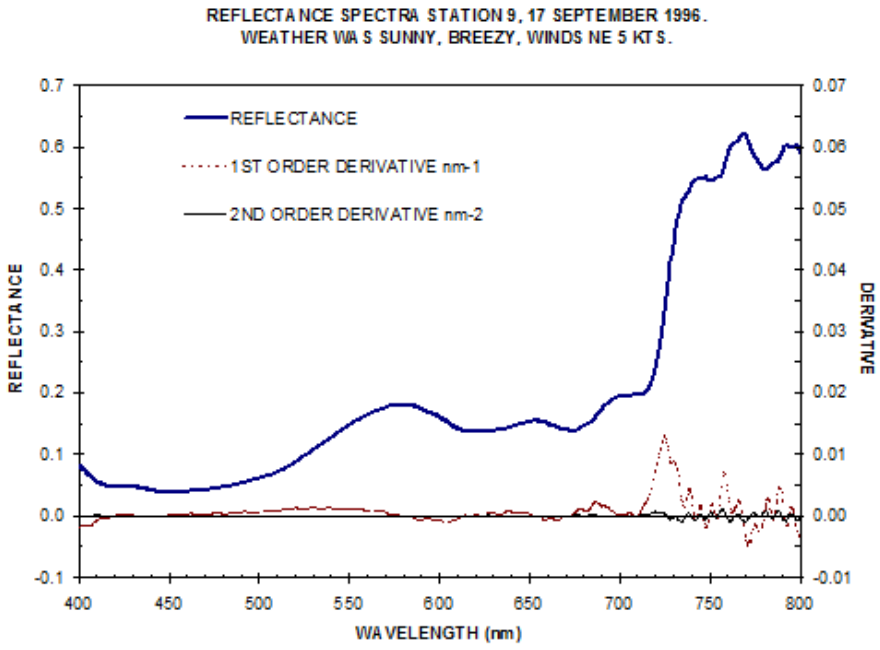

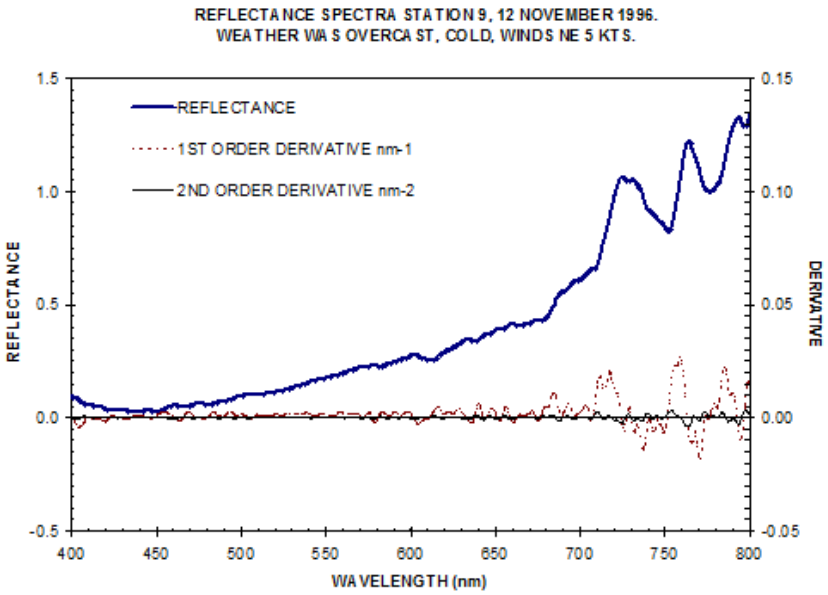

Station 9

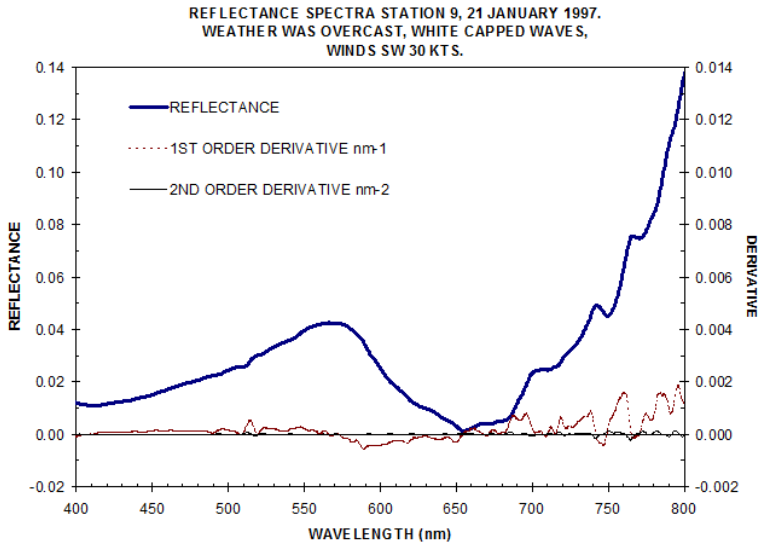

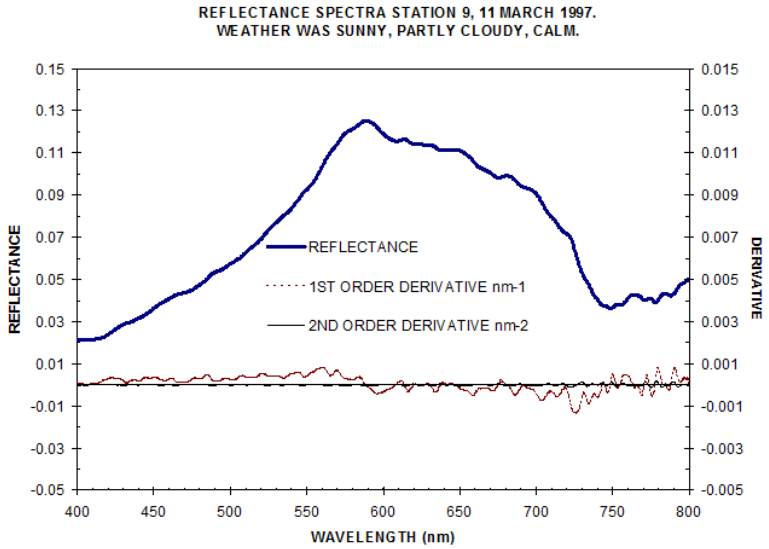

Station 9

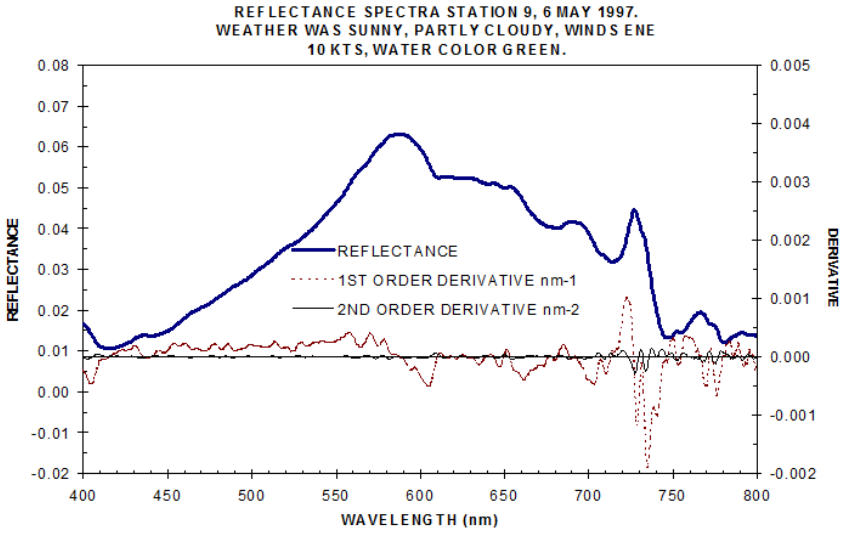
REFLECTANCE SPECTRA STATION 9, 6 MAY 1997.
WEATHER WAS SUNNY, PARTLY CLOUDY, WINDS ENE
10 KTS, WATER COLOR GREEN.
REFLECTANCE
1ST ORDER DERIVATIVE nm-1
2ND ORDER DERIVATIVE nm-2
REFLECTANCE
DERIVATIVE
WAVELENGTH (nm)

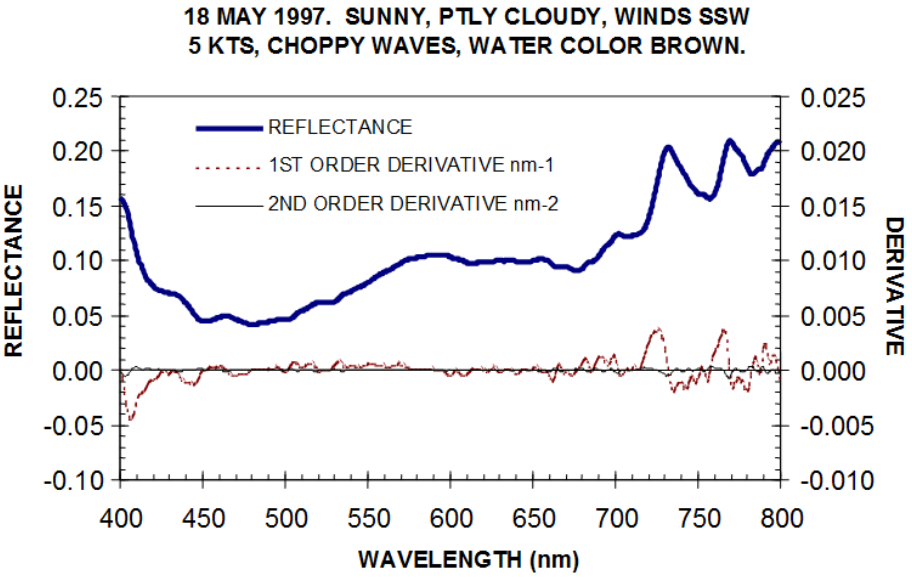
18 MAY 1997. SUNNY, PTLY CLOUDY, WINDS SSW
5 KTS, CHOPPY WAVES, WATER COLOR BROWN.
REFLECTANCE
1ST ORDER DERIVATIVE nm-1
2ND ORDER DERIVATIVE nm-2
REFLECTANCE
DERIVATIVE
WAVELENGTH (nm)

Station 9

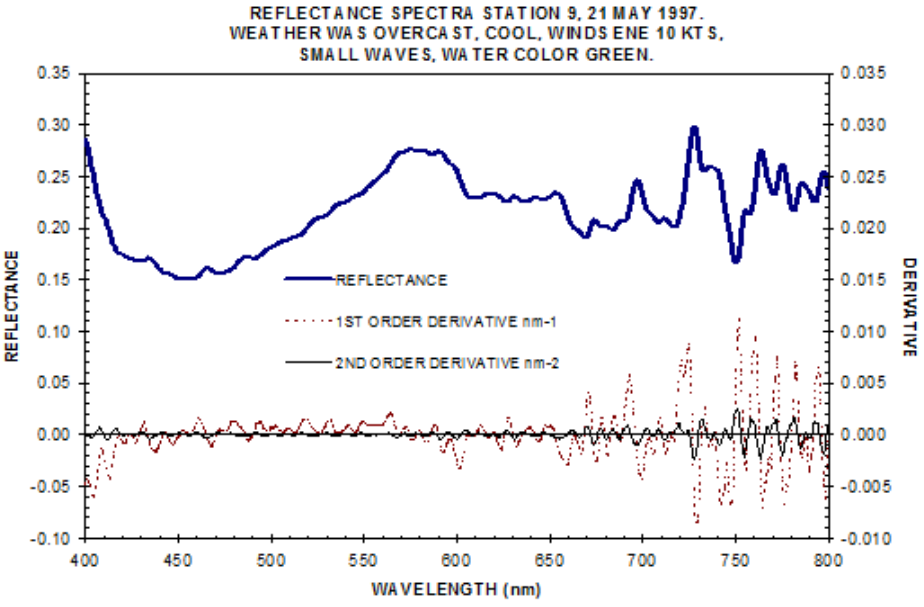
REFLECTANCE SPECTRA STATION 9, 21 MAY 1997.
WEATHER WAS OVERCAST, COOL, WINDS ENE 10 KTS,
SMALL WAVES, WATER COLOR GREEN.
REFLECTANCE
1ST ORDER DERIVATIVE nm-1
2ND ORDER DERIVATIVE nm-2
REFLECTANCE
DERIVATIVE
WAVELENGTH (nm)

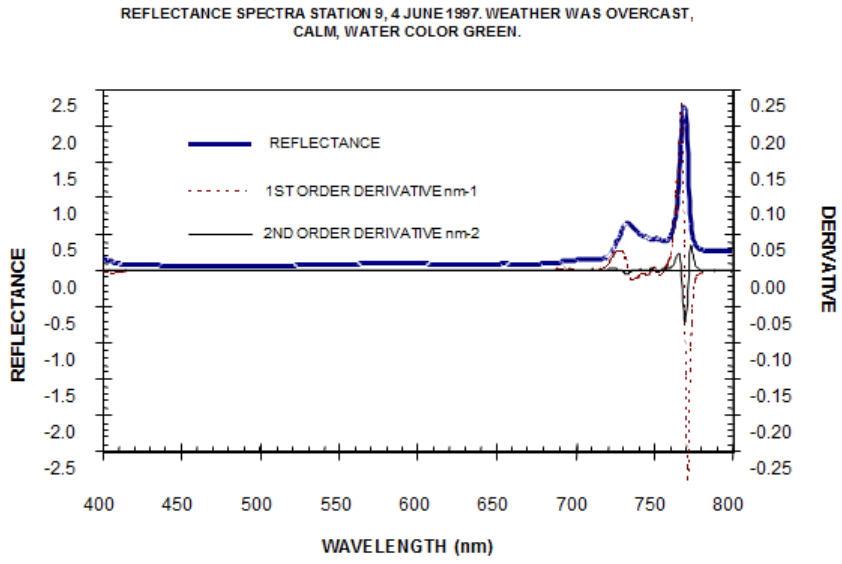

Station 9

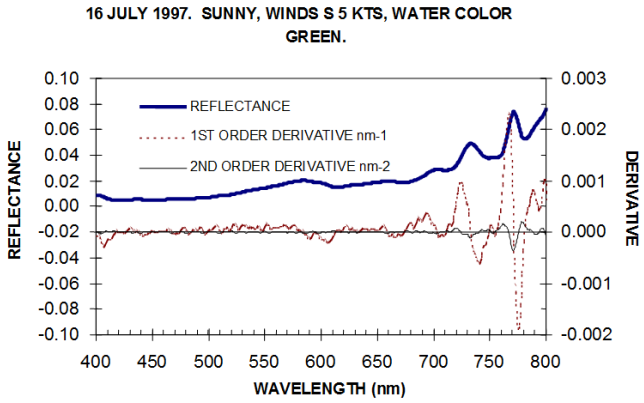

Station 9

b. Reflectance spectra and their first and second-order derivatives at Station 9, September 1996-July 1997.

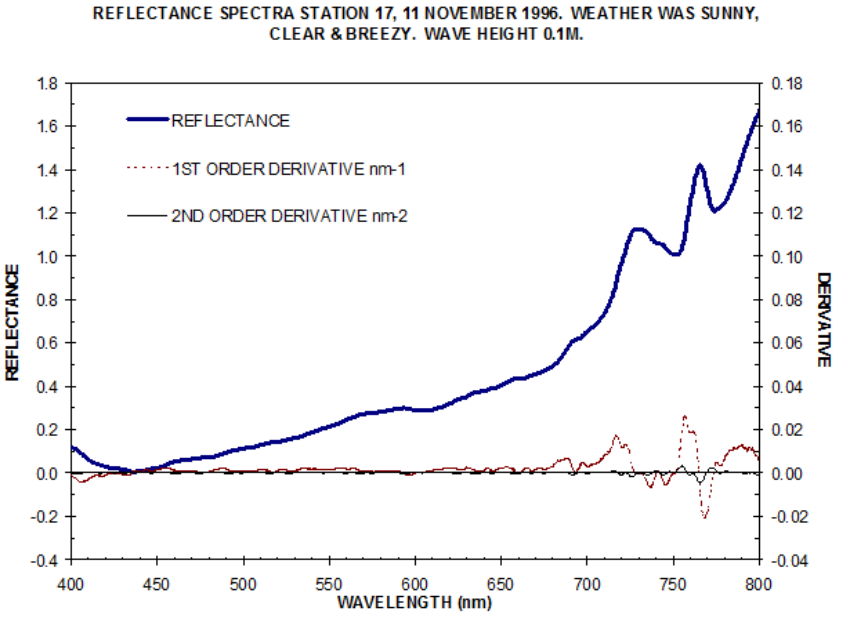

Station 17

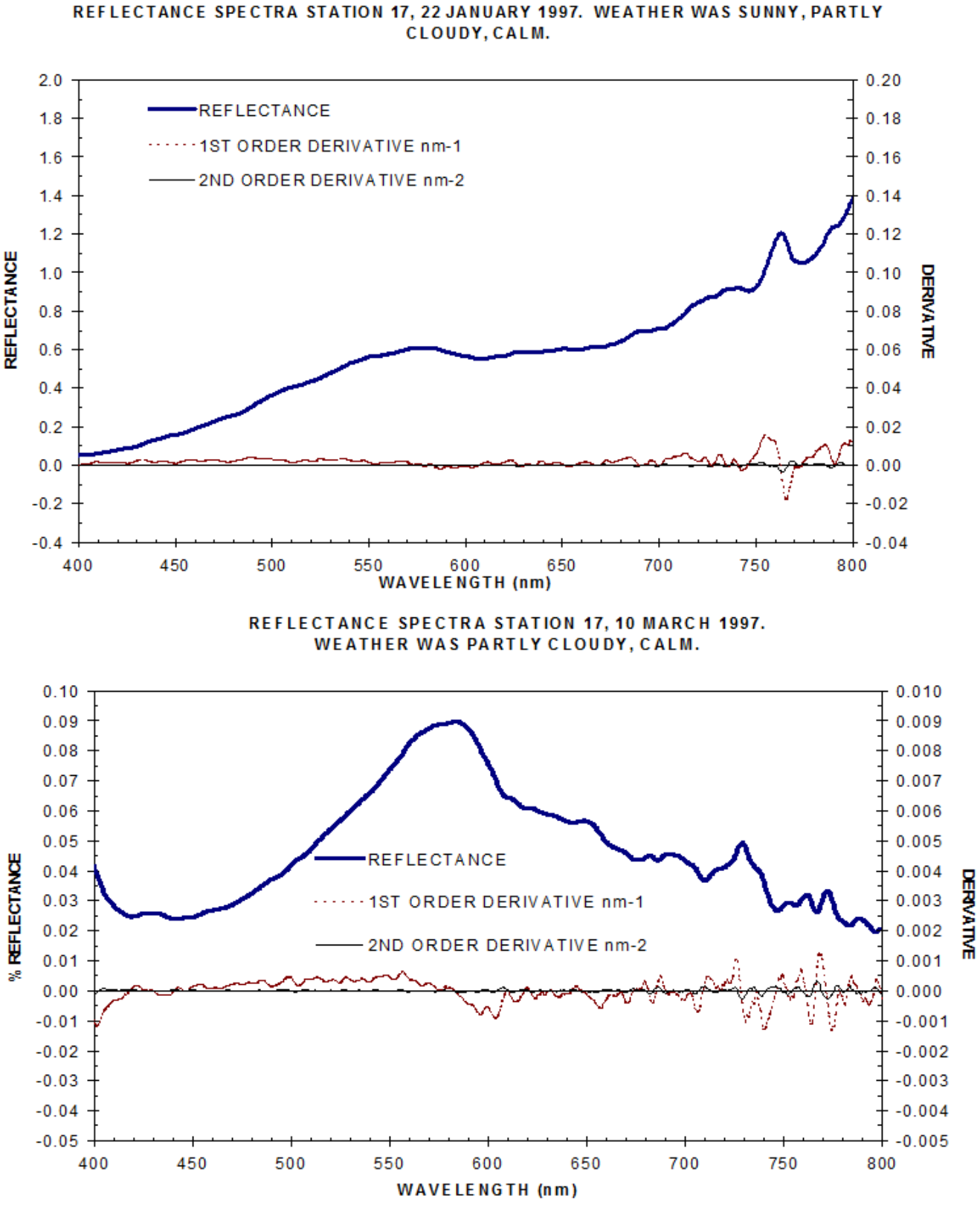
REFLECTANCE SPECTRA STATION 17, 22 JANUARY 1997. WEATHER WAS SUNNY, PARTLY CLOUDY, CALM.
REFLECTANCE
1ST ORDER DERIVATIVE nm-1
2ND ORDER DERIVATIVE nm-2
REFLECTANCE
DERIVATIVE
WAVELENGTH (nm)
REFLECTANCE SPECTRA STATION 17, 10 MARCH 1997.
WEATHER WAS PARTLY CLOUDY, CALM.
% REFLECTANCE
REFLECTANCE
1ST ORDER DERIVATIVE nm-1
2ND ORDER DERIVATIVE nm-2
DERIVATIVE
WAVELENGTH (nm)

Station 17

REFLECTANCE SPECTRA STATION 17, 14 APRIL 1997.
WEATHER WAS CLEAR, CALM, WINDS-ESE 0-5 KTS.

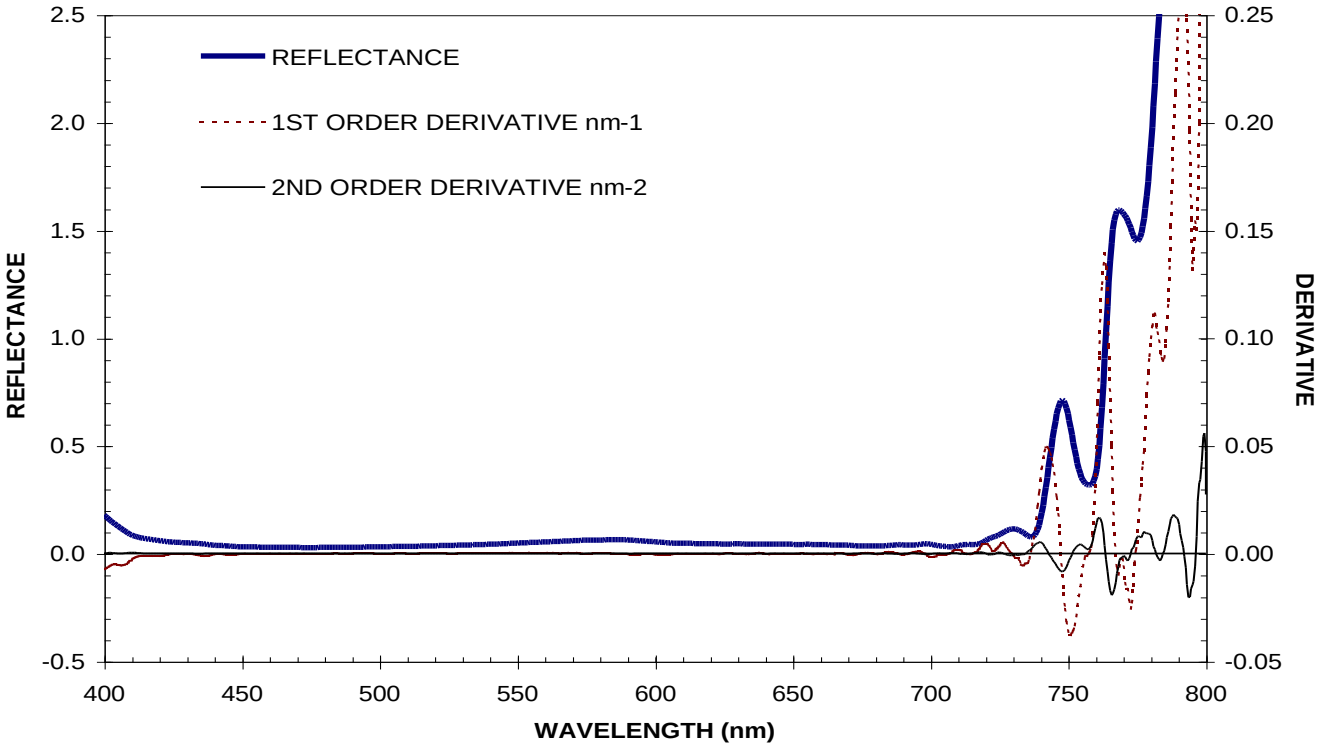

REFLECTANCE SPECTRA STATION 17, 07 MAY 1997.
WEATHER WAS OVERCAST, INTERMITTENT SUN,
WINDS S-15 KTS. WATER COLOR GRAY-GREEN.

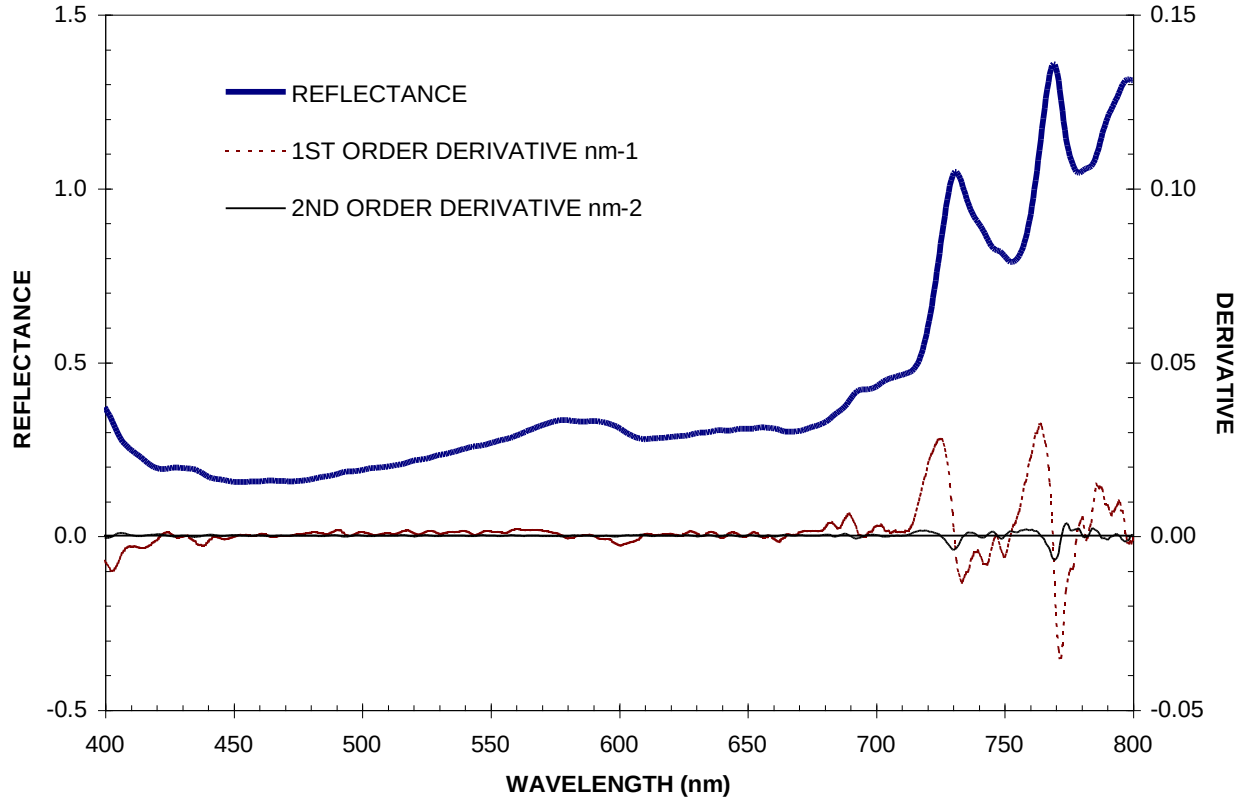

REFLECTANCE SPECTRA STATION 17, 19 MAY 1997.
WEATHER WAS OVERCAST, CALM, WINDS S - 5 KTS.
WATER COLOR GREEN.

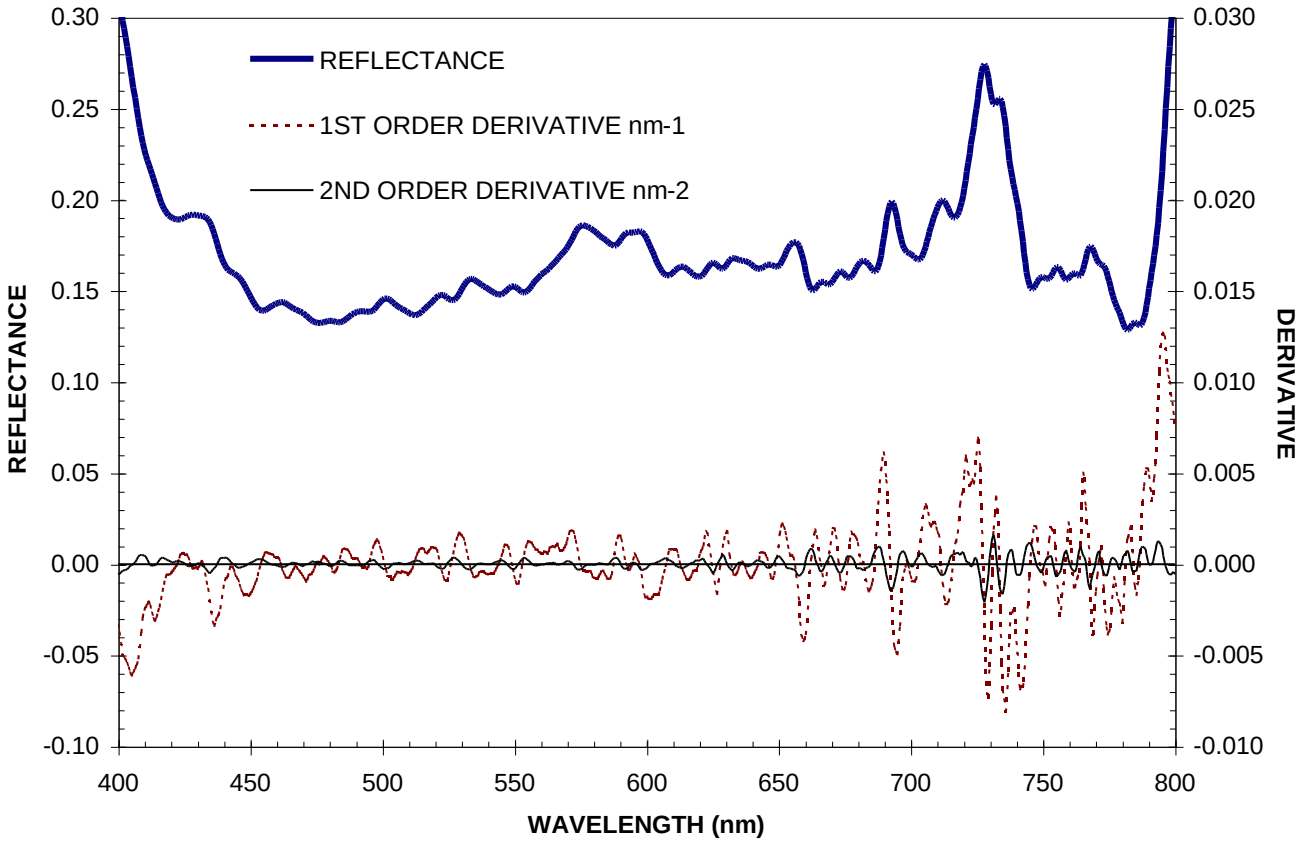

02 JUNE 1997. SUNNY, PARTLY CLOUDY, WINDS NNE - 5 KTS.
WATER COLOR GREEN.

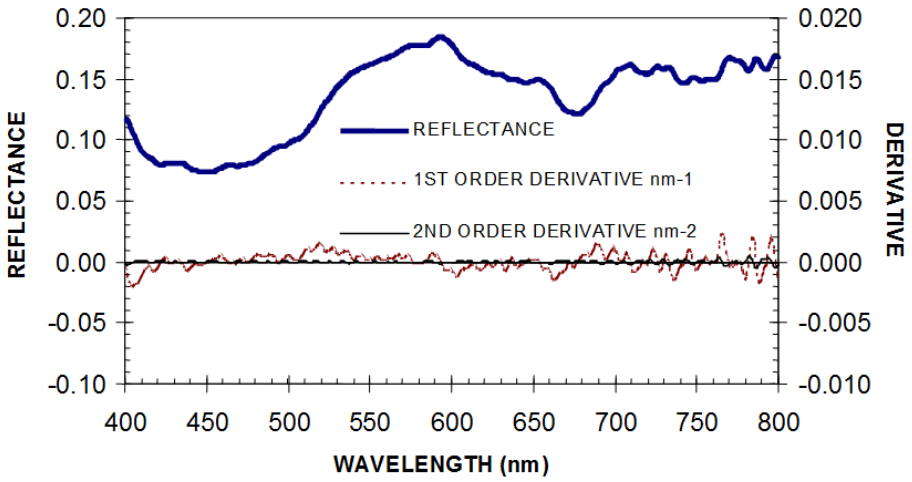

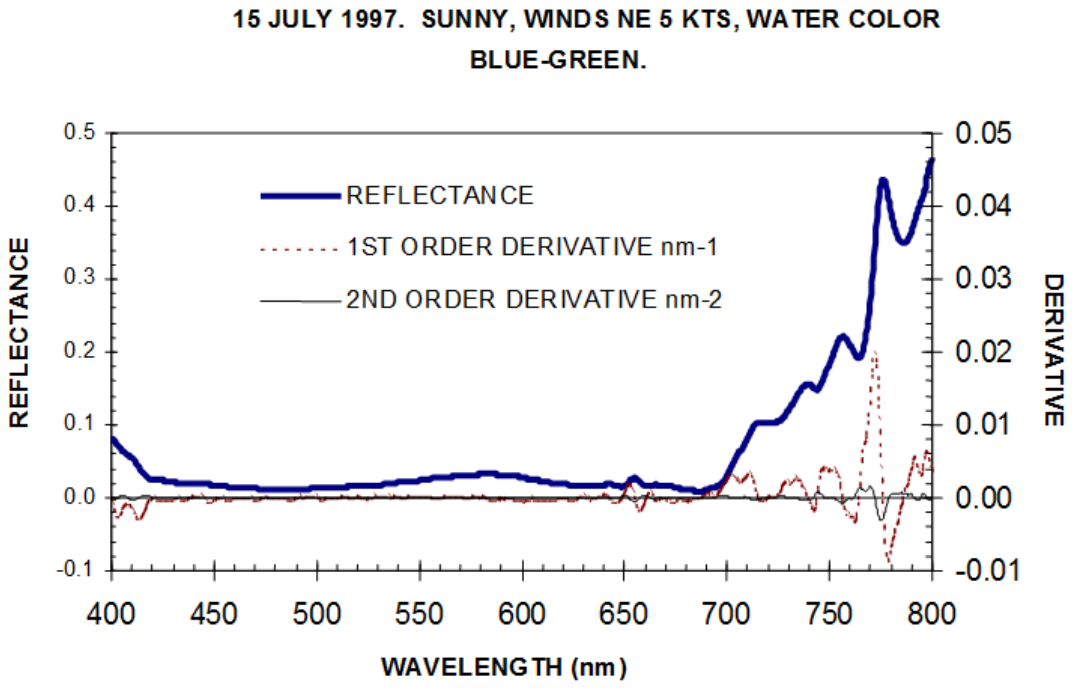

Station 17

c. Reflectance spectra and their first and second-order derivatives at Station 17, September 1996-July 1997.

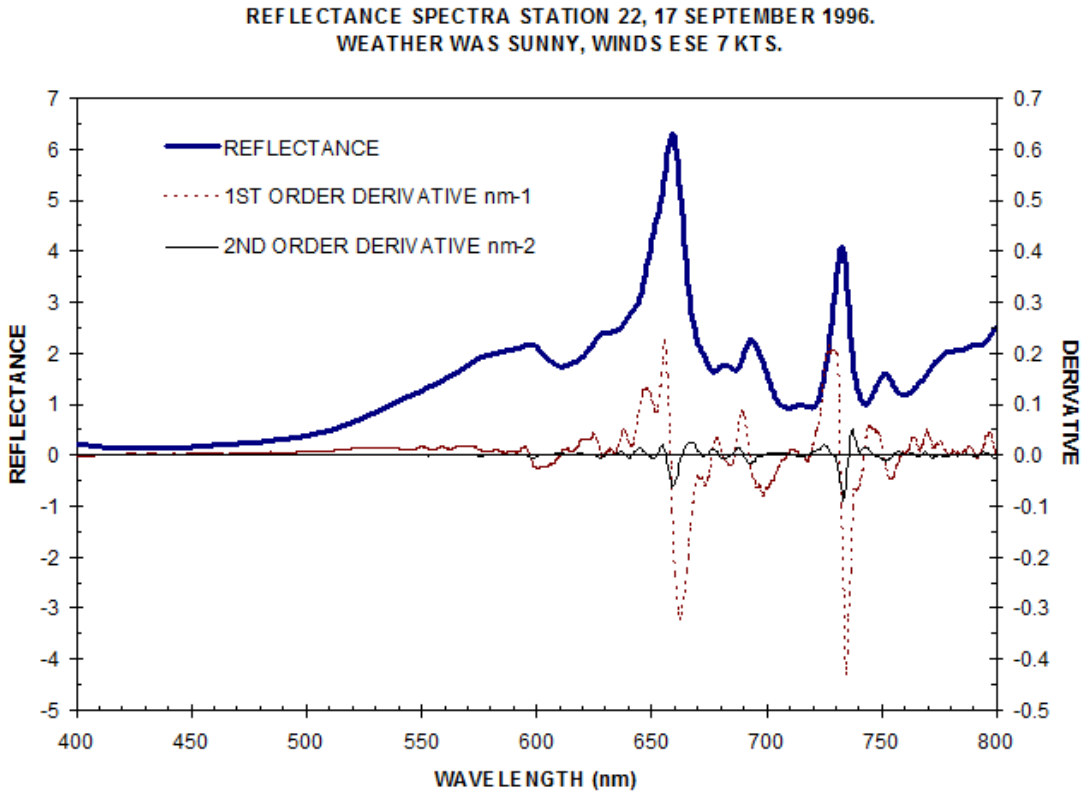

Station 22

REFLECTANCE SPECTRA STATION 22, 10 NOVEMBER 1996.
WEATHER WAS SUNNY, WINDY, CHOPPY WAVES, COLD.

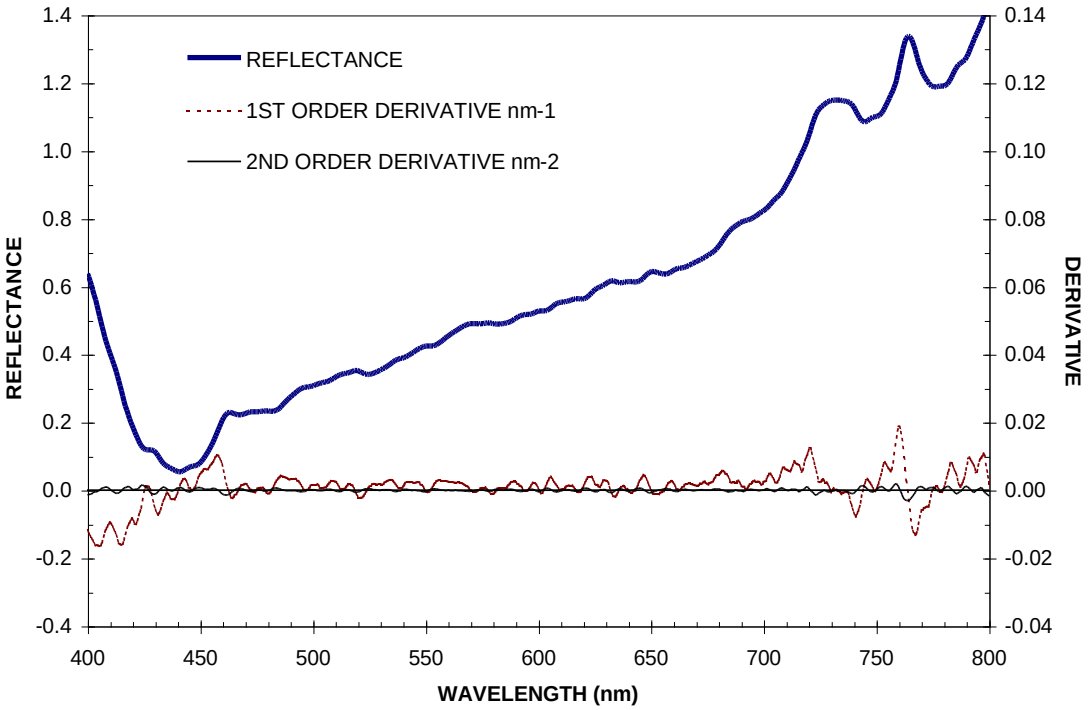

REFLECTANCE SPECTRA STATION 22, 19 JANUARY 1997.
WEATHER WAS SUNNY AND CALM.

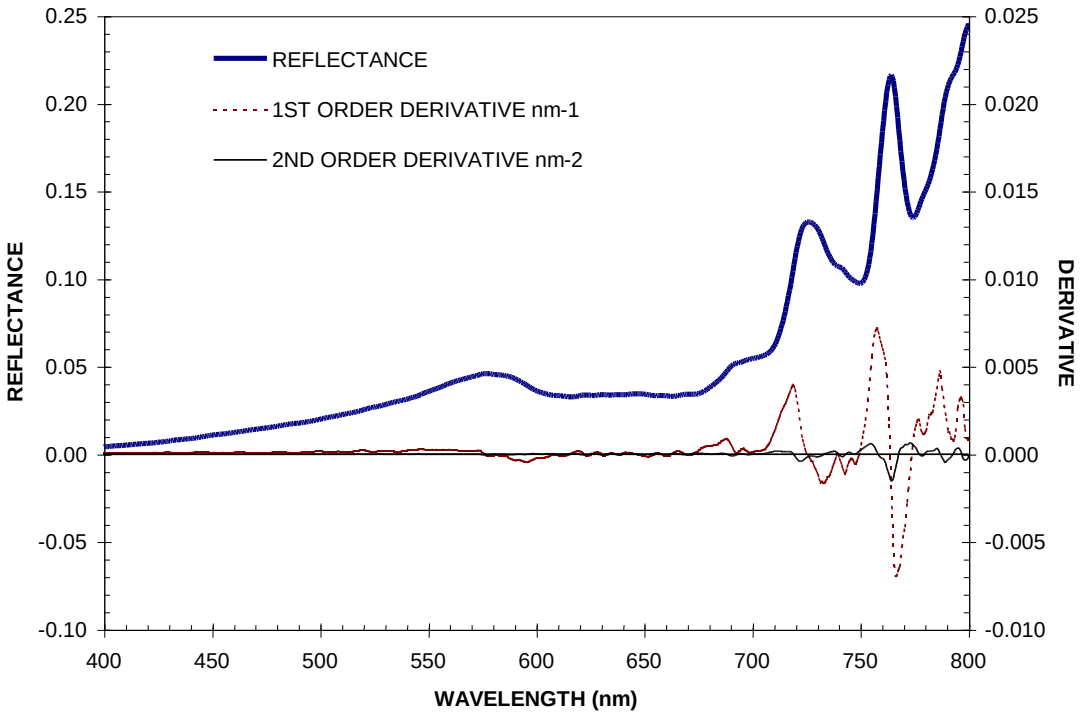

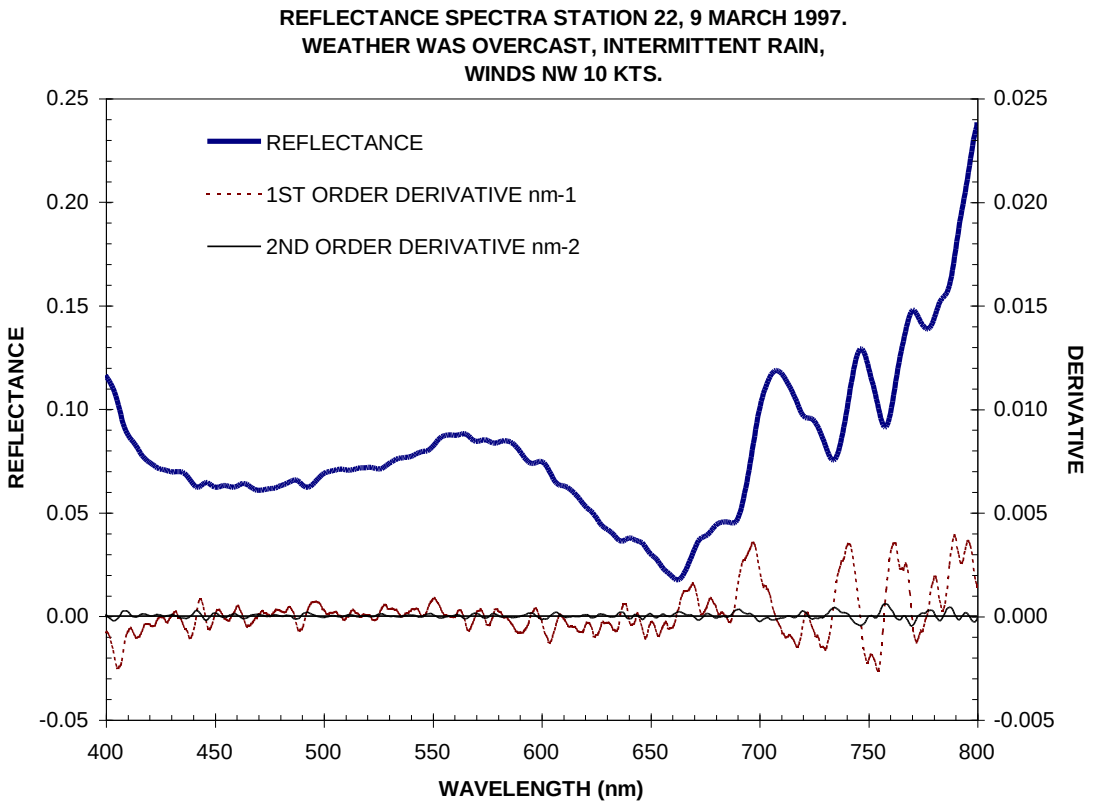
REFLECTANCE SPECTRA STATION 22, 9 MARCH 1997.
WEATHER WAS OVERCAST, INTERMITTENT RAIN,
WINDS NW 10 KTS.
REFLECTANCE
1ST ORDER DERIVATIVE nm-1
2ND ORDER DERIVATIVE nm-2
REFLECTANCE
DERIVATIVE
WAVELENGTH (nm)
0.25
0.20
0.15
0.10
0.05
0.00
-0.05
0.025
0.020
0.015
0.010
0.005
0.000
-0.005
400
450
500
550
600
650
700
750
800

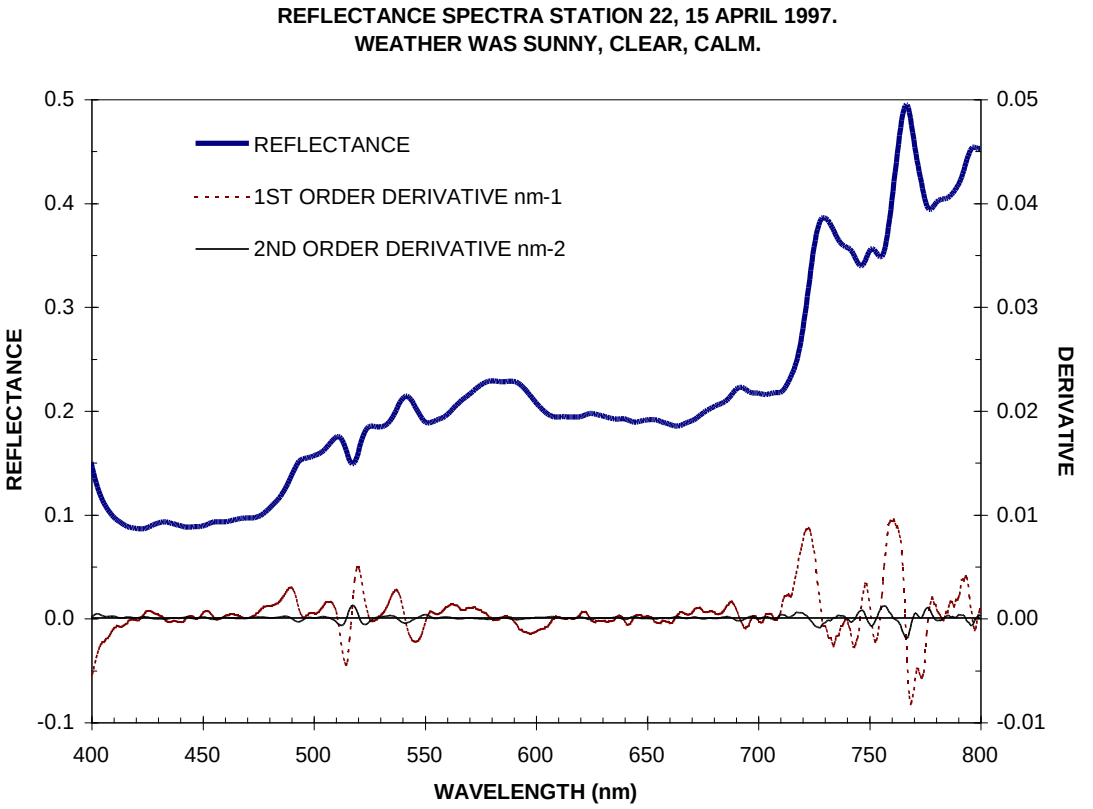
REFLECTANCE SPECTRA STATION 22, 15 APRIL 1997.
WEATHER WAS SUNNY, CLEAR, CALM.
REFLECTANCE
1ST ORDER DERIVATIVE nm-1
2ND ORDER DERIVATIVE nm-2
REFLECTANCE
DERIVATIVE
WAVELENGTH (nm)
0.5
0.4
0.3
0.2
0.1
0.0
-0.1
0.05
0.04
0.03
0.02
0.01
0.00
-0.01
400
450
500
550
600
650
700
750
800

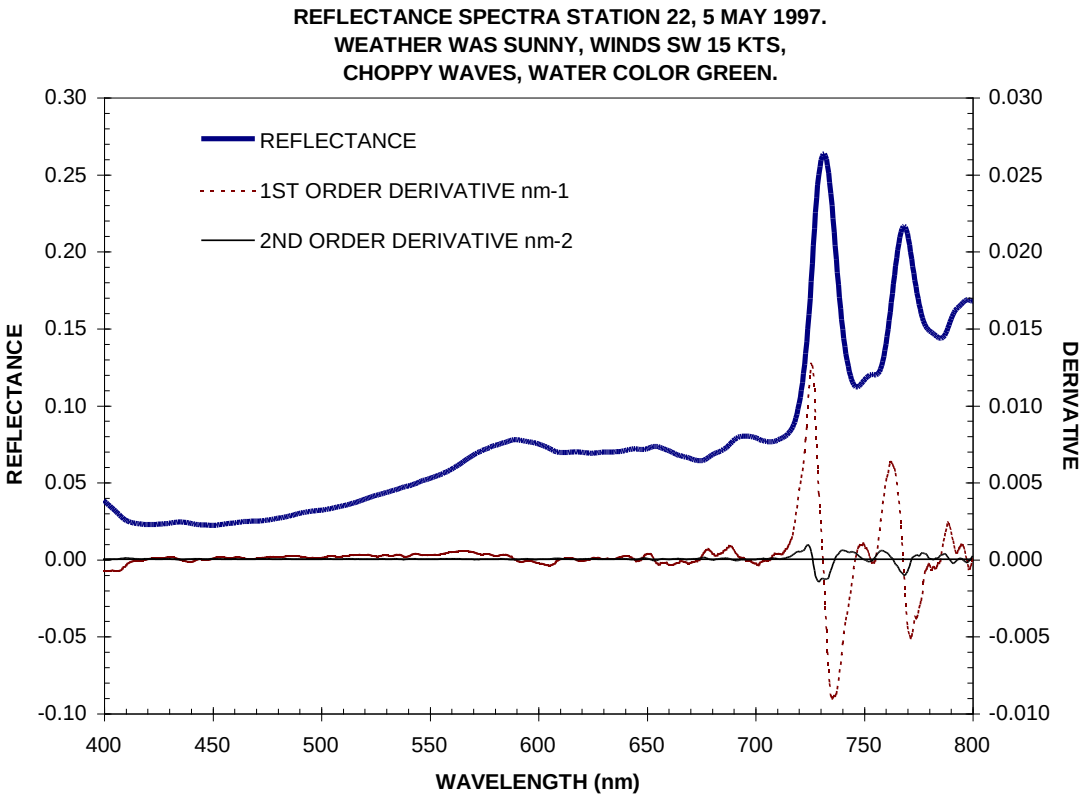
REFLECTANCE SPECTRA STATION 22, 5 MAY 1997.
WEATHER WAS SUNNY, WINDS SW 15 KTS,
CHOPPY WAVES, WATER COLOR GREEN.
REFLECTANCE
1ST ORDER DERIVATIVE nm-1
2ND ORDER DERIVATIVE nm-2
REFLECTANCE
DERIVATIVE
WAVELENGTH (nm)
0.30
0.25
0.20
0.15
0.10
0.05
0.00
-0.05
-0.10
0.030
0.025
0.020
0.015
0.010
0.005
0.000
-0.005
-0.010
400
450
500
550
600
650
700
750
800

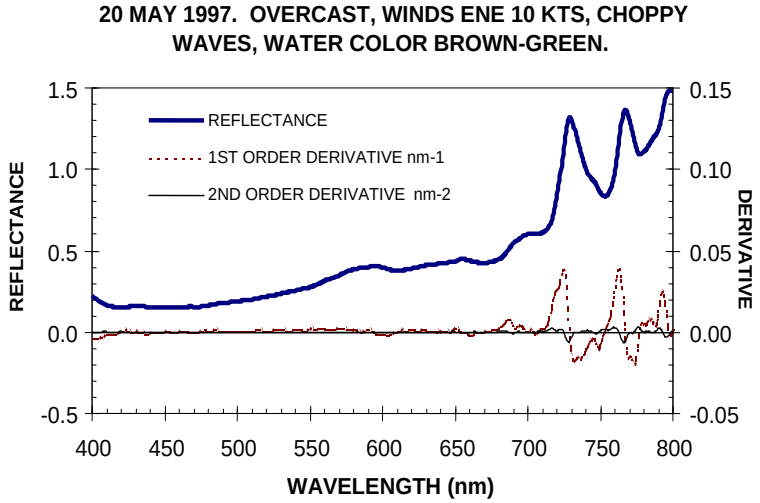
20 MAY 1997. OVERCAST, WINDS ENE 10 KTS, CHOPPY
WAVES, WATER COLOR BROWN-GREEN.
REFLECTANCE
1ST ORDER DERIVATIVE nm-1
2ND ORDER DERIVATIVE nm-2
REFLECTANCE
DERIVATIVE
WAVELENGTH (nm)
1.5
1.0
0.5
0.0
-0.5
0.15
0.10
0.05
0.00
-0.05
400
450
500
550
600
650
700
750
800

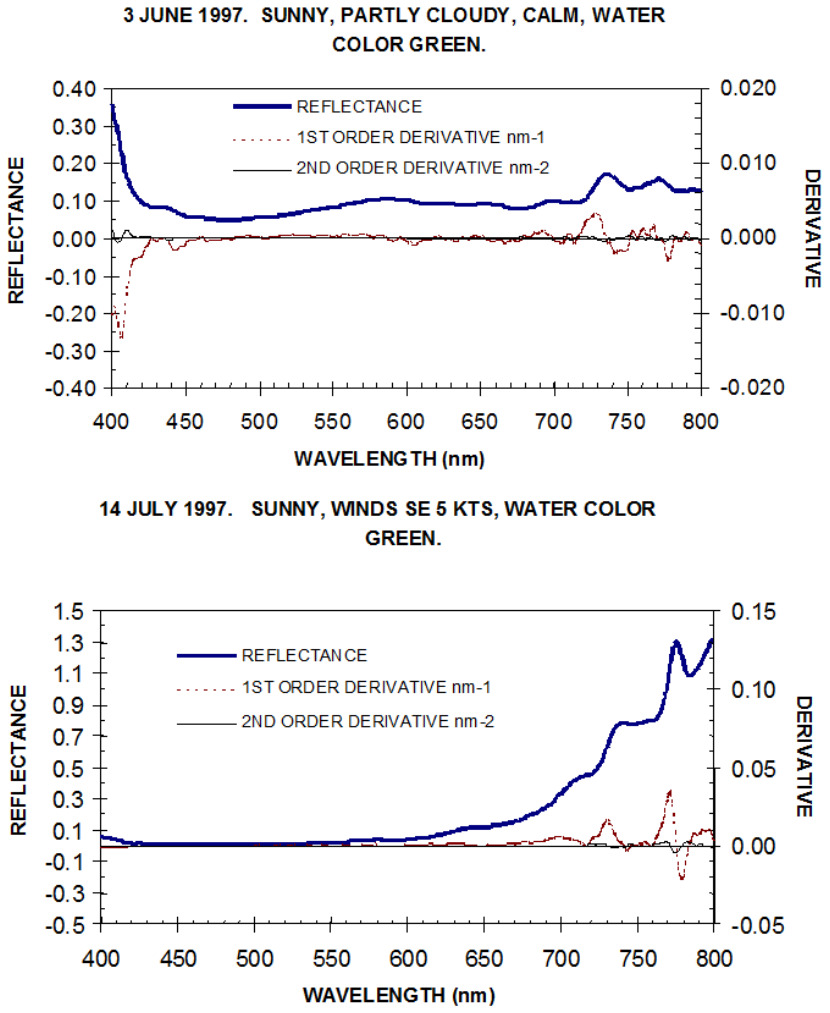

Station 22

d. Reflectance spectra and their first and second-order derivatives at Station 22, September 1996-July 1997.

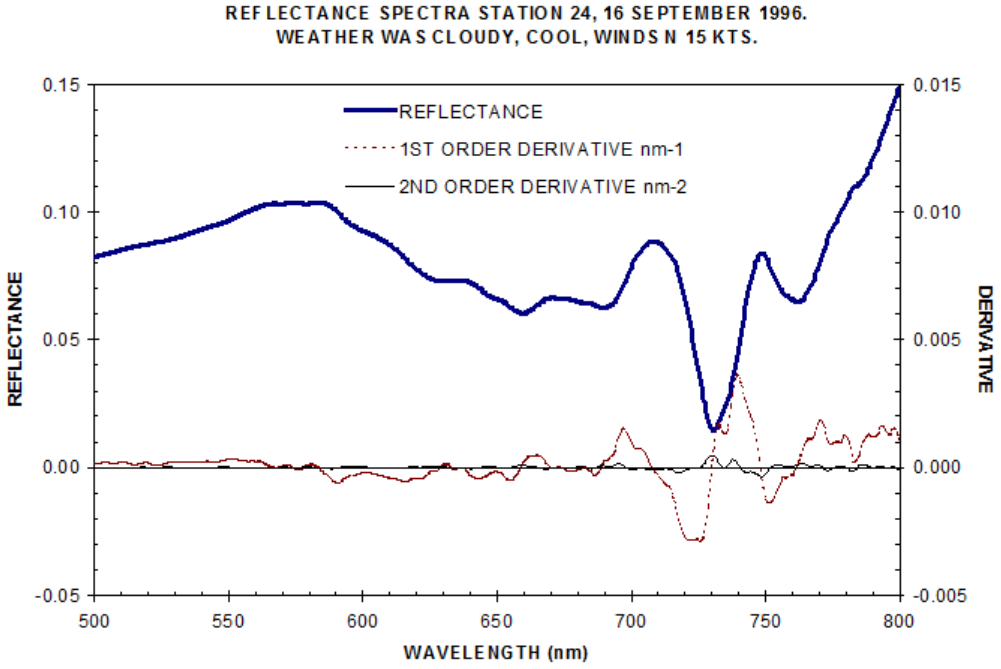

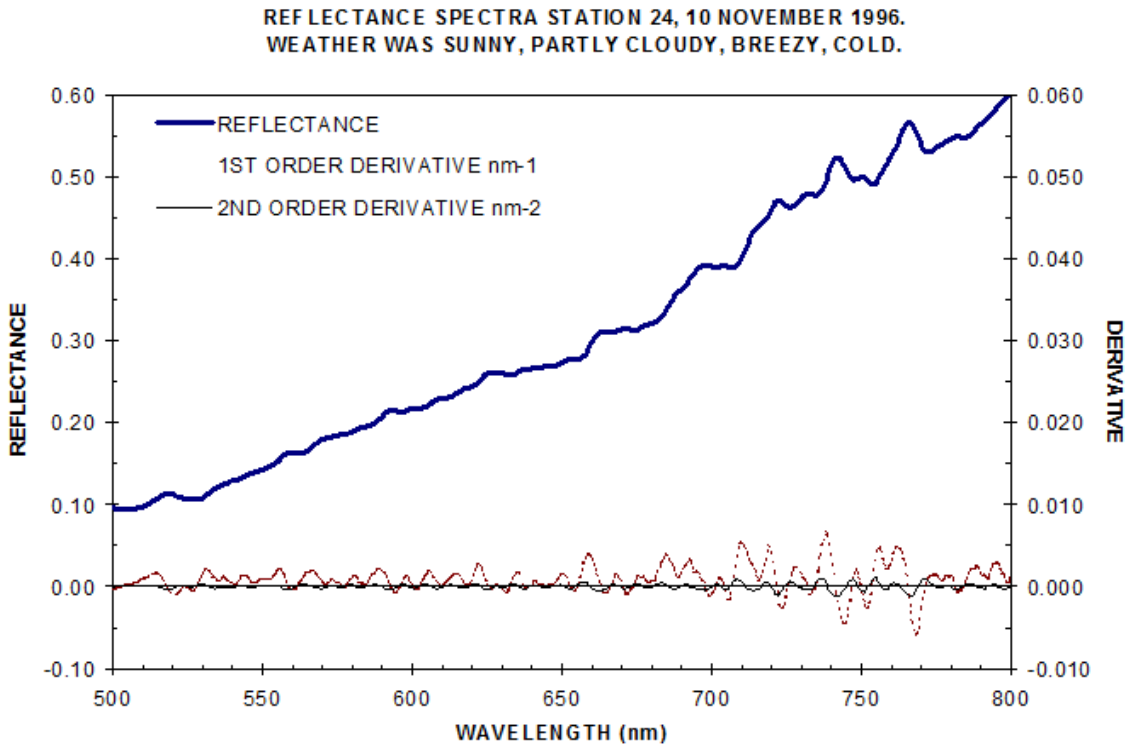
REFLECTANCE SPECTRA STATION 24, 10 NOVEMBER 1996.
WEATHER WAS SUNNY, PARTLY CLOUDY, BREEZY, COLD.
REFLECTANCE
1ST ORDER DERIVATIVE nm-1
2ND ORDER DERIVATIVE nm-2
REFLECTANCE
DERIVATIVE
WAVELENGTH (nm)
0.60
0.50
0.40
0.30
0.20
0.10
0.00
-0.10
0.060
0.050
0.040
0.030
0.020
0.010
0.000
-0.010
500
550
600
650
700
750
800

Station 24

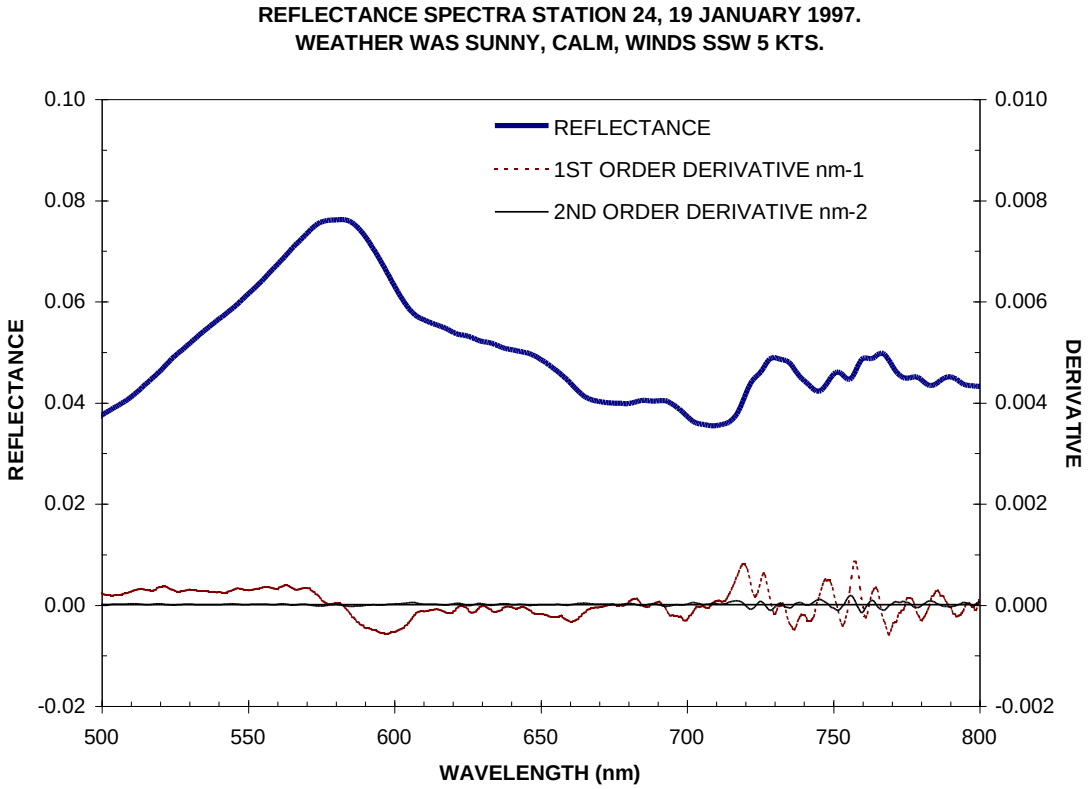
REFLECTANCE SPECTRA STATION 24, 19 JANUARY 1997.
WEATHER WAS SUNNY, CALM, WINDS SSW 5 KTS.
REFLECTANCE
1ST ORDER DERIVATIVE nm-1
2ND ORDER DERIVATIVE nm-2
REFLECTANCE
DERIVATIVE
WAVELENGTH (nm)
0.10
0.08
0.06
0.04
0.02
0.00
-0.02
0.010
0.008
0.006
0.004
0.002
0.000
-0.002
500
550
600
650
700
750
800

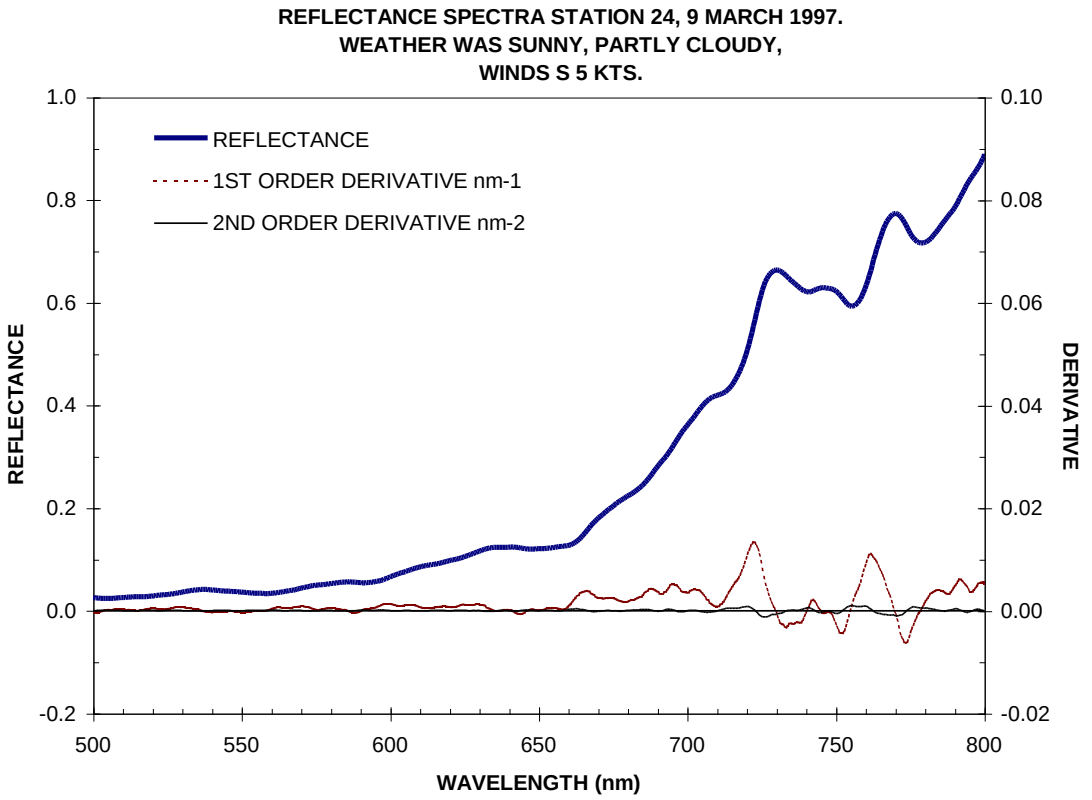
REFLECTANCE SPECTRA STATION 24, 9 MARCH 1997.
WEATHER WAS SUNNY, PARTLY CLOUDY,
WINDS S 5 KTS.
REFLECTANCE
1ST ORDER DERIVATIVE nm-1
2ND ORDER DERIVATIVE nm-2
REFLECTANCE
DERIVATIVE
WAVELENGTH (nm)
1.0
0.8
0.6
0.4
0.2
0.0
-0.2
0.10
0.08
0.06
0.04
0.02
0.00
-0.02
500
550
600
650
700
750
800

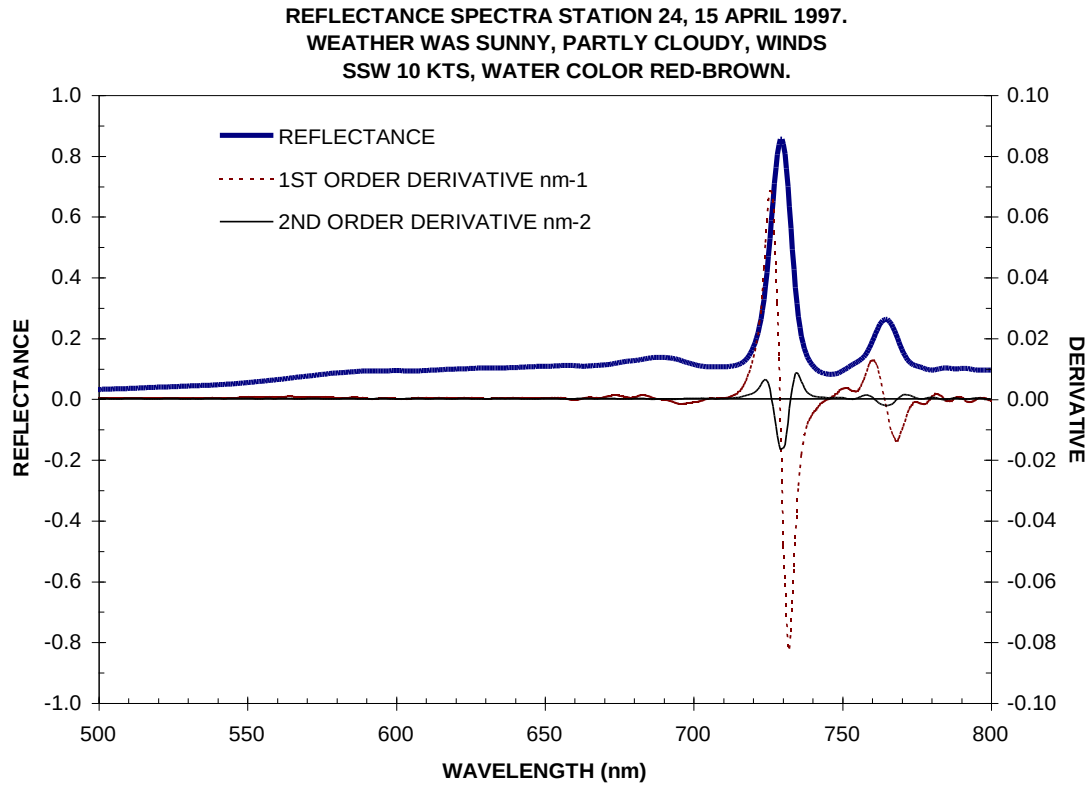
REFLECTANCE SPECTRA STATION 24, 15 APRIL 1997.
WEATHER WAS SUNNY, PARTLY CLOUDY, WINDS
SSW 10 KTS, WATER COLOR RED-BROWN.
REFLECTANCE
1ST ORDER DERIVATIVE nm-1
2ND ORDER DERIVATIVE nm-2
REFLECTANCE
DERIVATIVE
WAVELENGTH (nm)
1.0
0.8
0.6
0.4
0.2
0.0
-0.2
-0.4
-0.6
-0.8
-1.0
0.10
0.08
0.06
0.04
0.02
0.00
-0.02
-0.04
-0.06
-0.08
-0.10
500
550
600
650
700
750
800

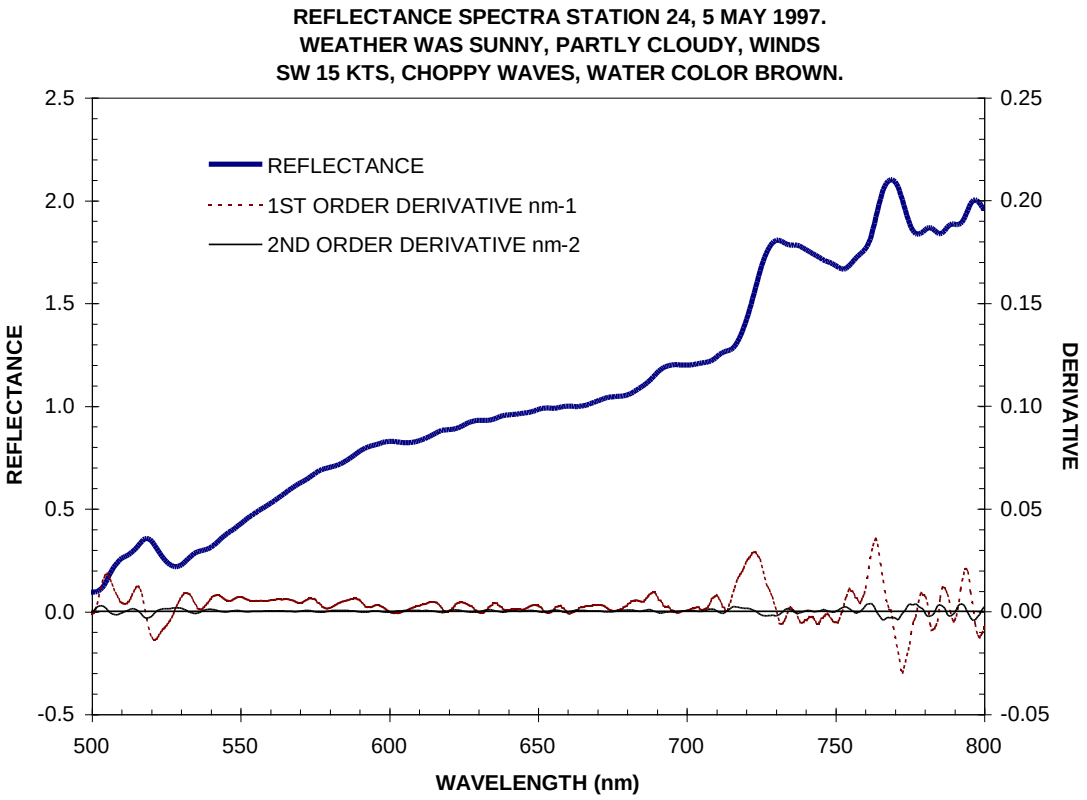
REFLECTANCE SPECTRA STATION 24, 5 MAY 1997.
WEATHER WAS SUNNY, PARTLY CLOUDY, WINDS
SW 15 KTS, CHOPPY WAVES, WATER COLOR BROWN.
REFLECTANCE
1ST ORDER DERIVATIVE nm-1
2ND ORDER DERIVATIVE nm-2
REFLECTANCE
DERIVATIVE
WAVELENGTH (nm)
2.5
2.0
1.5
1.0
0.5
0.0
-0.5
0.25
0.20
0.15
0.10
0.05
0.00
-0.05
500
550
600
650
700
750
800

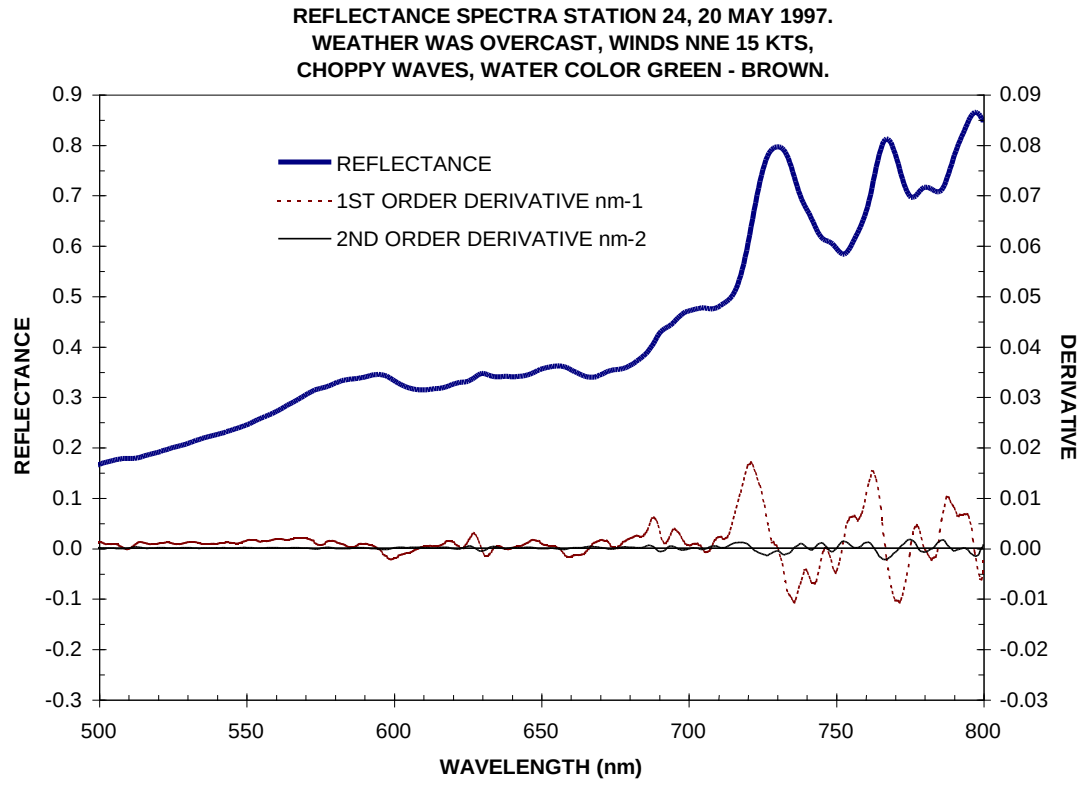
REFLECTANCE SPECTRA STATION 24, 20 MAY 1997.
WEATHER WAS OVERCAST, WINDS NNE 15 KTS,
CHOPPY WAVES, WATER COLOR GREEN - BROWN.
REFLECTANCE
1ST ORDER DERIVATIVE nm-1
2ND ORDER DERIVATIVE nm-2
REFLECTANCE
DERIVATIVE
WAVELENGTH (nm)
0.9
0.8
0.7
0.6
0.5
0.4
0.3
0.2
0.1
0.0
-0.1
-0.2
-0.3
0.09
0.08
0.07
0.06
0.05
0.04
0.03
0.02
0.01
0.00
-0.01
-0.02
-0.03
500
550
600
650
700
750
800

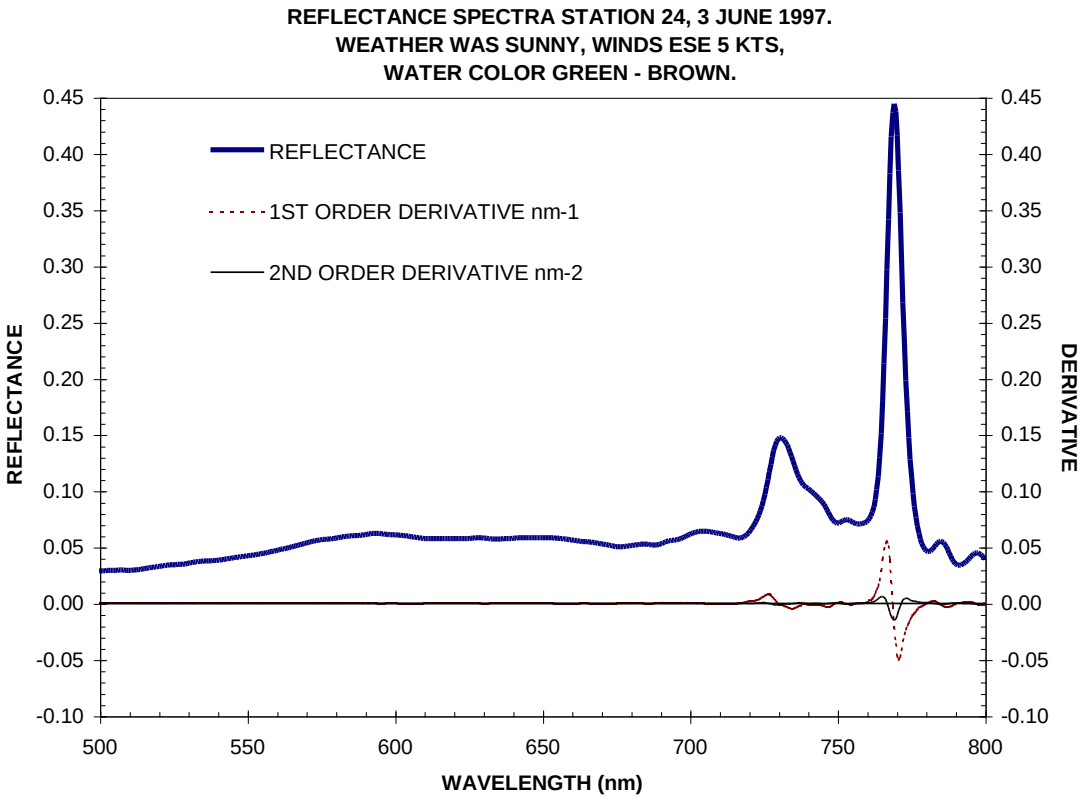

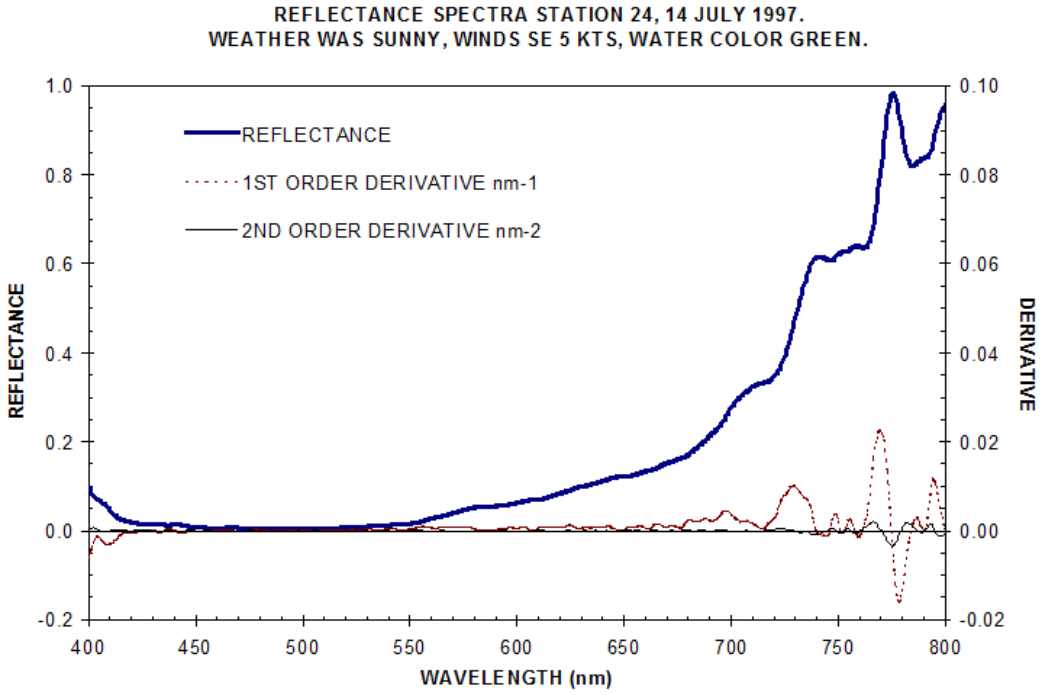

Station 24

e. Reflectance spectra and their first and second-order derivatives at Station 24, September 1996-July 1997.

Figure 8. *Reflectance spectra at 0.1-meter depth and their corresponding first and second-order derivatives for Stations 3, 9, 17, 22 and 24, Lake Texoma from September 1996 to July 1997. Reflectance values shown on left Y-axis; derivative values shown on right Y-axis. The following figures correspond to each station. Figure 8a: Station 3. Figure 8b: Station 9. Figure 8c: Station 17. Figure 8d: Station 22. Figure 8e: Station 24.*

4. Discussion

4.1. Changes in Optical Properties over Space and Time

Lake Texoma exhibits a steep longitudinal gradient of water clarity from the shallow river zones to the deep body of the main lake. Water turbidity is greatest in the river zones, becoming diluted as water flows into the main lake zone. Water visibility is greatly affected by run-off in the Red and Washita River zones whose shorelines are predominantly steep and bare-soiled. During rainfall events, especially in the spring and fall, erosion takes place (particularly in the river zones and the Red River itself) where soil is deposited directly into the lake, giving it a characteristic red color; hence the name Red River. Water clarity improves from the lakes' transition zones to the main lake zone as currents move sediments into deeper waters to settle out.

Changes in the apparent optical properties also follow spatial and temporal patterns. Light attenuation (η") is greatest in the Red and Washita River zones, decreasing in magnitude to the main lake zone (Figure 2). Conversely, SD and Z_{eu} values start out low in the river zones arriving at their maximum values in the main lake zone (Figure 9). Spring and fall bring about maximum values for η", and minimum values for SD and $Z_{eu,}$, whereas winter and summer months reverses the trend (Table 3). Spring and fall months experience mixing and turnover brought on by seasonal rain, wind and temperature changes [59]. Although winter months did not produce stratification in Lake Texoma (unpublished WQMP data), stratification did occur from June to August, where the water column was less agitated and allowed suspended matter to settle in the hypolimnion thus improving water clarity.

4.2. Implications of SD, η", Z_{eu} and PAR

In considering the lake as a whole over the entire year, median values of η", SD and Z_{eu} were compared to published values from other lakes, estuaries and oceans from around the world (Table 15). The best agreement was with 28 lakes of diverse optical properties in New Zealand [14]. Median values of η" and SD between Lake Texoma and the New Zealand lakes were 1.29· m^{-1} and 1.15 · m^{-1}, and 0.90 m and 1.35 m, respectively. Davies-Colley and Vant [14] did not report Z_{eu} values directly, therefore an estimate was made using the formula from Jones et al. [30] where Z_{eu} = ln100 ÷η". Median Z_{eu} at Lake Texoma was 3.48 m versus 4.00 m for the New Zealand lakes. Similar patterns were found among turbid lakes and estuaries; e.g., shallow, turbid lakes in the Netherlands [7], and in turbid, Chesapeake Bay [23]. Data from the eutrophication study of Cairns [8] show median values of SD and Z_{eu} were greater in Lake Ray Roberts than Lake Texoma, by as much as 0.55 and 1.02 meters, respectively. Water transparency in Lake Ray Roberts is expected to be low since it was (and still considered) a new impoundment with sediments still settling out. Water chemistry data [8] taken two year after its impoundment show mean turbidity (NTU) in Lake Ray Roberts was 13 versus 11 for Lake Texoma (this study). TDS (mg ·l^{-1}) was much greater at the eleven sampling stations in Lake Texoma with a mean of 1055 versus 203 at Lake Ray Roberts, suggesting absorption properties and light attenuation are much greater in Lake Texoma. Because there is a tendency for an artificial impoundment to have greater turbidity due to clays and silts, water transparency will usually differ from natural lakes [21]. This is evident when comparing turbid reservoirs to clear, natural lakes such as Lake Huron [4], Loch Ness [30], and clear, subarctic lakes in Alaska [34], where water transparency significantly improves.

Values of Z_{eu}: SD, η" x SD and percent PAR transmission at SD (%PAR) from this study were also compared to published values reported from around the world (Table 16). Values from turbid waters were generally consistent with Lake Texoma values. A grand median Z_{eu}: SD of 3.98 from Lake Texoma was closest to 3.05 at Lake Ray Roberts [8] and 4.93 found in turbid, subarctic Alaskan lakes [34]. Median η" x SD values of 1.15 from this study agreed with the empirical value of 1.16 [21] derived from turbid reservoirs in South Dakota and 11 others throughout the United States. An increase in η" x SD and a decrease in Z_{eu}: SD values from turbid to clear waters also become readily apparent in Table 16, having diagnostic use to water quality managers [34]. The empirical relationships of Z_{eu}: SD and η" x SD allows the water quality manager with only a secchi disk to use a simple conversion factor to predict Z_{eu} and η" for the water bodies shown; however, caution should be used when using it on different water bodies.

The overall median value 25.1% PAR at SD in Lake Texoma was consistent with 21.7% found in the turbid, subarctic Alaskan lakes [34], and the assumption that the depth of 20% surface light approximates SD [39]. This value, however, does not agree with the traditional assumption of Carlson [9] where irradiance at SD is about 10%, and could be used as a constant. Although, Carlson [9] readily admits that relating secchi depth to chlorophyll-*a* may not be accurate in lakes containing high amounts of non-algal particulate matter, or in highly colored lakes where η" is high. Values of 7.4% and 14.7% in Lake Huron [4] and clear, Alaskan lakes [34], respectively, are consistent with Carlson's [9] 10% assumption. In this study, the closest value to 10% were median values of 18.2% and 21.0% coming from the main lake zone (Stations 17 and 19, respectively) having traditionally low turbidity. It is more likely that% PAR at SD is greater in turbid waters because of the increased scattering due to suspended matter [4]. Also, consider the fact that the secchi disk is closer to the water's surface than in clear waters where blue and green light usually can still penetrate to the photoelectric cell of a submarine photometer, whose maximum efficiency is around 550nm, the area most sensitive to the human eye [38]. Values for Z_{eu} and% PAR at SD were not directly measured in this study. Instead, I calculated them by regressing depth against

the natural logarithm of percent light transmission obtained from the submarine photometer (Figure 10).

4.3. The Link Between SD, η", Z_{eu} and Water Quality Parameters

Despite the presence of chlorophyll-*a* in Lake Texoma, a significant correlation was not found between SD nor η". Turbidity and suspended matter dominated spatial and temporal variations in the light regime (Table 10). Secchi depth was only mildly correlated to turbidity whereas η" showed a significantly stronger correlation in all zones, explaining 76% of the variation in η" over the course of the sampling year. It has been argued that variations in secchi transparency can be related to chlorophyll-*a* only in the absence of nonalgal light attenuation [9, 34, 39, 45]. This study shows that using secchi depth is not a good indicator to the presence of chlorophyll-*a* in Lake Texoma, nor would it be useful as an indicator of trophic status [9]. Because of the propensity for Lake Texoma to remain turbid, use of the secchi disk is limited. However, secchi transparency is useful in estimating Z_{eu} and η" in Lake Texoma. Data from this study (Table 9) show good spatial and seasonal correlation between Z_{eu} and SD and for the entire year (r_s = 0.89; p = 0.0001). Moreover, a good database of η" and Z_{eu} values has been established (e.g., Figure 10) so that conversion factors of Z_{eu}: SD and η" x SD can be applied to future SD readings in the absence of a submarine photometer.

4.4. Applications of High-resolution Derivative Spectra and Inherent Optical Variability

Derivative spectroscopy has been used extensively in applications such as analytical chemistry [16, 17], obtaining reflectance and transmittance spectra in bacterial colonies [60], detecting red-tide blooms in coastal waters [46], and estimating suspended sediment concentrations [11, 25]. High-resolution spectroscopy enables the investigator to detect sharp changes in the spectral signature as potential indicators of the target species. Much of the research in derivative spectroscopy takes place in the laboratory, where effects of environmental variability are small. Problems with high variability arise when the experiment is moved from a controlled laboratory environment to an in situ environment (e.g., from laboratory holding tanks to open seawater). The in situ underwater light field is subject to instability caused by winds and currents, creating high frequency fluctuations of underwater irradiance [48]. Waves can act as lenses, focusing light into high intensity 'light flashes' [48] near the surface making it a challenge to characterize the light field just below the surface. Problems associated with environmental variability include decrease in the signal to noise ratio (S/N) of the spectral signal, especially in the longer wavelengths [11]. The wind-induced wave motion can affect concentrations of water quality parameters, which reduce the homogeneity of their concentrations leading to high variability particularly near the surface. The theories behind PAR variability are beyond the scope of this study; however, extensive coverage of this subject matter may be found in Spinrad et al. [53].

4.5. The Relationship Between High-resolution Derivative Spectra and Water Quality Parameters in Lake Texoma

Despite the problems associated with underwater variability, distinct, orderly spectral patterns still emerge. Each month's reflectance spectra produced patterns that showed up in the same region of the spectrum every time. Reflectance below the surface produced spectral peaks in the green-yellow (590-610nm), and infrared (725-735 and 765-775nm) regions of the spectrum (Figures 8a – 8e). The green-yellow signature was not as intense as the prominent features displayed in the infrared region, which suggests the majority of reflection may be attributed to turbidity and backscattering. Nevertheless, discrimination of the chlorophyll signature at 590-610nm was possible in the second-order derivative, explaining as much as 99% of the variation in the best single and multi-variable regression models (Table 11). Estimates of chlorophyll-*a* concentrations agreed well with absorption in the reflectance spectra at 670, 750 and 780nm (Table 12). In the summer, when phytoplankton growth reaches its maximum, chlorophyll-*a* can be predicted with good accuracy. The absorption trough of chlorophyll-*a* at 670nm [16, 25] was significant in June, explaining 92% of the variation in the single-variable model. Turbidity concentration was estimated using the second-order derivative with reasonable accuracy (Table 13). Goodin et al. [25] stated waters containing both turbidity and algal chlorophyll are more complex that either clear or turbid waters, and that turbidity is a first-order effect, which is removed in the second-order derivative leaving the remaining effects to chlorophyll-*a*. The data in this study, however, suggest the turbidity signal is still present in the second-order derivative, explaining as much as 96% of the variation in a single-variable regression model (April 1997). In the presence of both turbidity and chlorophyll-*a*, the regression coefficient is greater for chlorophyll-*a* than for turbidity when chlorophyll-*a* concentrations increase, and turbidity concentrations decrease. When both turbidity and chlorophyll-*a* concentrations are low, as in April, the regression coefficient is greater for turbidity.

In all, improvement in the regression coefficient was gained with multiple-variable models. The independent variables chosen were the second-order derivatives consistently located at reflectance peaks and troughs showing up in the reflectance spectra each month. The goal in multiple linear regression is to produce the smallest, most simple model that adequately describes the data [5], personal communication, [63]; i.e., more variables are not necessarily better. However, in this study, more proved to be better. To further validate the best single and multiple-variable regression models, I used the replicates of chlorophyll-*a* that were deleted in the

trimmed-mean analysis and compared them to the regression models of 590-610nm (Table 11). A good agreement exists between mean values of measured concentrations and the predicted values (Figure 11), making both single and multi-variable models a robust estimator of chlorophyll-*a*.

4.6. Summary and Conclusions

The underwater optical climate of Lake Texoma was characterized by using secchi depth, submarine photometry and high-resolution spectroscopy at eleven fixed stations. Following a year's worth of collection effort, the original objectives of this study are recalled and the results summarized:

Objective 1 – Determine the depth of the euphotic zone (Z_{eu}) at each station and the attenuation coefficient (η), and

Objective 2 – Determine secchi transparency at each station.

1) A distinct longitudinal gradient was apparent in secchi depth (SD), attenuation coefficients (η") and depth of the euphotic zone (Z_{eu}), from the Red and Washita River zones to the main lake body. Attenuation was highest in the river zones of the lake, and lowest in the main lake zone.
2) An inverse relationship existed for both SD and Z_{eu}, which were lowest in the river zones and highest in the main lake zone.
3) Differences both spatially and temporally were found among η", SD and Z_{eu}. By zone, η", SD and Z_{eu} were separated into three statistically distinct groups: Group 1 – Red River, Big Mineral, and Washita River zones; Group 2 – Red River and Washita River Transition zones; Group 3 – Main Lake zone. By season, η", SD and Z_{eu} were placed into two distinct groups: Group 1 – winter and summer; Group 2 – spring and fall.

Objective 3 – Compare secchi depth (SD), Z_{eu}, and η with published data taken from other water bodies.

1) Values of SD, Z_{eu}, and η from this study were similar to optical properties found in turbid reservoirs in the United States, Netherlands, and New Zealand.
2) By using estimates from the submarine photometer readings taken during this study, standard conversions to estimate Z_{eu} and η" using only a secchi disk were developed and compared. Ratios of Z_{eu}: SD in this study were greatest in the river zones and least in the river transition and main zones of Lake Texoma, following traditional assumptions that Z_{eu}: SD *increases* in zones of high turbidity.
3) An empirical value of 3.98 can be used to estimate Z_{eu} in Lake Texoma using only a secchi disk.
4) The product of η" x SD also followed traditional assumptions that η" x SD *decreases* in zones of high turbidity and were consistent with values for turbid waters from around the world.
5) An empirical value of 1.15 can be used to estimate η" in Lake Texoma with a secchi disk.
6) Percent transmission of PAR at the secchi depth was greatest in the Red and Washita River zones and lowest in the Main Lake zone. An overall median value of 25.1% was consistent with published data for turbid waters in the United States. Turbidity causes scattering and reflectance upward, consequently making it more difficult to see the secchi disk at lower depths. A greater percentage of light transmission at the SD in turbid waters is a result of the secchi disk being kept closer to the surface.

Objective 4 – Model SD and η with water quality parameters taken during the sampling periods.

1) Correlation among water quality parameters showed a strong, positive association with turbidity and total suspended solids (TSS) suggesting turbidity contributes strongly to reflectance and scattering.
2) Chlorophyll-*a* was not significantly related to η" and SD.
3) SD was not a good indicator of algal chlorophyll due to the high presence of turbidity, limiting its use as a tool for estimating trophic status.
4) Overall, turbidity explained 76% of the variation in η", and 43% of the variation in SD.

Objective 5 – Obtain spectral data in narrow bandwidths from 300 to 800nm using high-resolution spectroscopy.

Objective 6 – Examine spectral irradiance, reflectance, and attenuation in the green (500-600nm), red (600-700nm), and near-infrared (700-800nm) spectrum, and Objective 7 – Model reflectance spectra with water quality parameters taken during the sampling periods.

1) High-resolution spectroscopy revealed distinct spectral patterns in the green-yellow, red, and infrared regions of the PAR spectrum.
2) Stations with low turbidity exhibited a distinct green reflectance peak at 590-610nm indicating presence of chlorophyll-*a*.
3) Stations with high turbidity exhibited a shift in the reflectance peak to the red-infrared region, masking the chlorophyll signature.
4) Second-order derivatives of the reflectance signal at 590-610, and 720-780nm were able to discriminate the chlorophyll signature from those of turbidity.
5) Using multiple linear regression, second-order derivatives of reflectance spectra accounted for up to 99% of the variation in chlorophyll-*a*, even in the presence of background turbidity.
6) High-resolution derivative spectroscopy therefore becomes a robust tool for estimating algal chlorophyll in Lake Texoma.

Table 15. *Summary of Zeu, η" and SD values comparing this study to various lakes, estuaries and oceans from around the world. Locations and site descriptions specific to each cited source are given.*

reference source	Z_{eu} (m)	η" (m^{-1})	SD (m)	location	site description
this study	3.48†	1.29†	0.90†	Lake Texoma, U.S.	turbid reservoir
Beeton 1957 [4]	—	—	7.98	Lake Huron, U.S.	deep, glacially-formed
Bowling 1988 [6]	1.71†	2.42†	1.35†	Queensland, Australia	6 coastal dune lakes
Buiteveld 1995 [7]	1.40*	3.3	0.53†	Netherlands	shallow, turbid, eutrophic
Cairns 1993 [8]	4.5†	—	1.48†	Lake Ray Roberts, U.S.	new reservoir (1987)
Davies-Colley and Vant 1988 [14]	4.00*	1.15†	1.35†	New Zealand	27 lakes and 7 sites on Lake Whangape
Gallagos et al. 1990 [23]	2.40*	1.92†	0.70†	Chesapeake Bay, U.S.	turbid estuary
Graham 1966 [26]	32.89*	≈ 0.14	15.2	West coast U.S.; three cruises by Smith & Manning	ocean water, coastal influence
Jones et al. 1996 [30]	6.58*	0.7	—	Loch Ness, Scotland	deep, oligotrophic lake
Knowlton and Jones 1993 [33]	—	—	1.40†	Oklahoma, U.S.	12 turbid reservoirs
Koenings and Edmundson 1991 [34]	7.4	0.62	1.5	Alaska, U.S.	subarctic, turbid glacial lakes
Koenings and Edmundson 1991 [34]	7.3	0.62	4.3	Alaska, U.S.	subarctic, humic stained lakes
Koenings and Edmundson 1991 [34]	16.1	0.27	6.9	Alaska, U.S.	subarctic, clear lakes
Schwarz et al. 1996 [51]	15.35*	0.30†	8.78†	South Island, New Zealand	clear lakes with macrophyte colonization

* calculated for this summary using method by Jones et al. [30] where $Z_{eu} = \ln 100 \div \eta"$
† median values

Table 16. *Summary of Z_{eu}: SD, η" x SD and percent PAR transmission at SD (%PAR) values comparing this study to various lakes, estuaries and oceans reported from around the world. Locations and site descriptions specific to each cited source are given.*

reference source	Z_{eu}: SD	η" x SD	% PAR	location	site description
this study	3.98	1.15	25.1	Lake Texoma, U.S.	turbid reservoir
Beeton 1957 [4]	—	—	14.7	Lake Huron, U.S.	deep, glacially-formed
Birge and Juday 1934*	—	—	5	N Wisconsin, U.S.	humic stained acid bog lakes
Bowling 1988 [6]	1.27	3.27	—	Queensland, Australia	6 coastal dune lakes
Buiteveld 1995 [7]	2.64**	1.75	—	Netherlands	shallow, turbid, eutrophic lakes
Cairns 1993 [8]	3.05	—	—	Lake Ray Roberts, U.S.	new reservoir (1987)
Davies-Colley and Vant 1988 [14]	2.96**	1.55	—	New Zealand	27 lakes and 7 sites on Lake Whan gape
French et al. 1982 [21]	2.81	1.16	—	Lahontan Res. South Dakota and 11 other states, U.S.	turbid reservoirs
Gallagos et al. 1990 [23]	1.25**	1.34	—	Chesapeake Bay, U.S.	turbid estuary
Graham 1966 [26]	2.16**	2.13	—	West coast U.S.; three cruises by Smith & Manning	ocean water, coastal ocean water, coastal influence
Koenings and Edmundson 1991 [34]	4.93	0.93	21.7	Alaska, U.S.	subarctic, turbid glacial lakes
Koenings and Edmundson 1991 [34]	1.75	2.7	3.6	Alaska, U.S.	subarctic, humic stained lakes

reference source	Z_{eu}: SD	η" x SD	% PAR	location	site description
Koenings and Edmundson 1991 [34]	2.42	1.86	7.4	Alaska, U.S.	subarctic, clear lakes
Schwarz et al. 1996 [51]	1.75**	2.63	—	South Island, New Zealand	clear lakes with macrophyte colonization
Walker 1982 [56]	—	1.46	—	NE Australia	coastal seawater

* from Koenings and Edmundson [34]** calculated for this summary

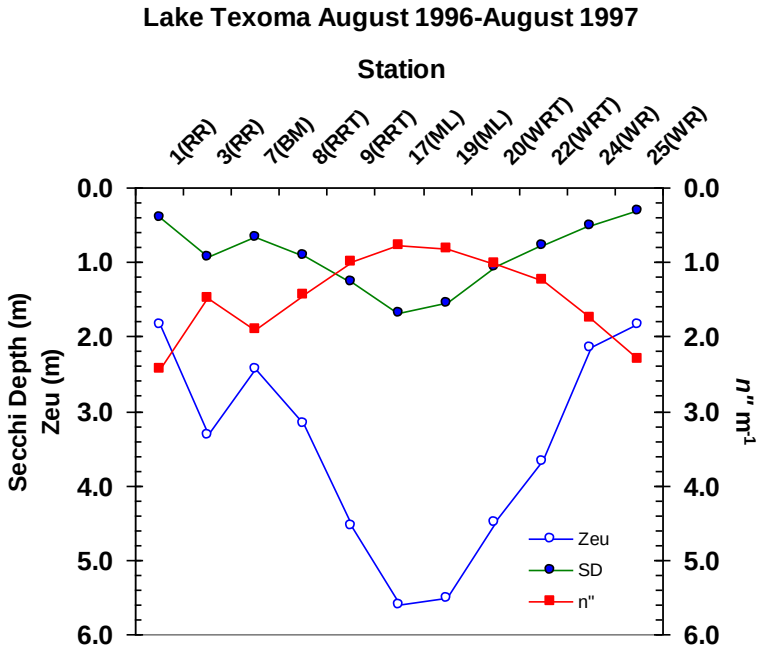

Figure 9. *Summary of secchi depth (SD), depth of euphotic zone (Z_{eu}) and vertical attenuation coefficients (η". m^{-1}) at eleven fixed sampling stations and their corresponding zones, Lake Texoma from August 1996-August 1997. Values for SD and Z_{eu} shown on left Y-axis, and values for n" shown on right Y-axis.*

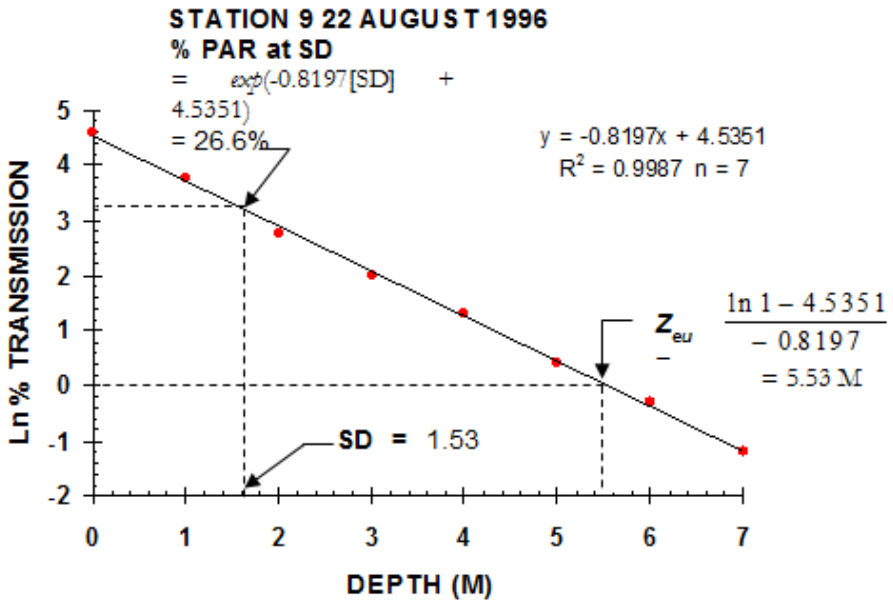

Figure 10. *Methodology in determining Z_{eu} and % PAR at SD.*

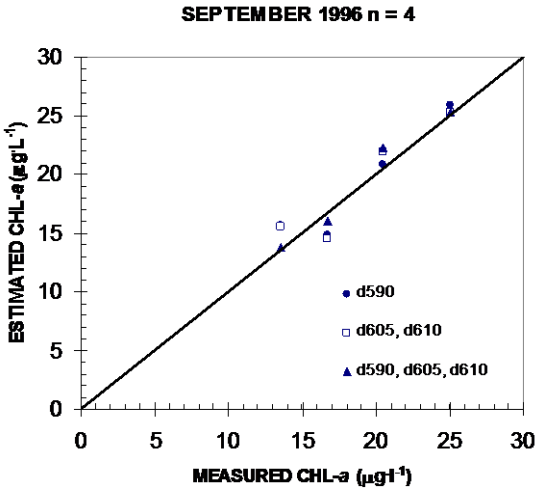

a. Estimated versus measured values of chlorophyll-a values in the green peak (590-610nm) spectrum from September 1996 to July 1997 using regression models in Table 11.

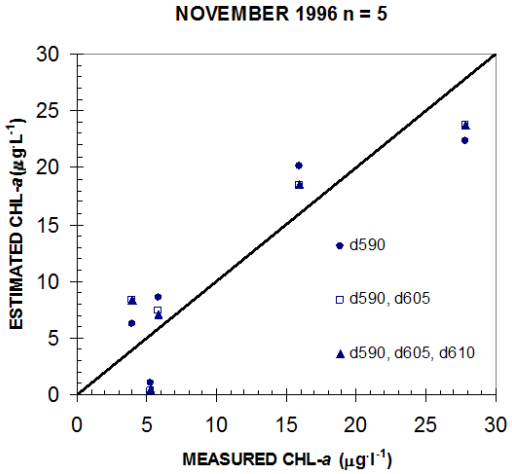

b. Estimated versus measured values of chlorophyll-a values in the green peak (590-610nm) spectrum from September 1996 to July 1997 using regression models in Table 11.

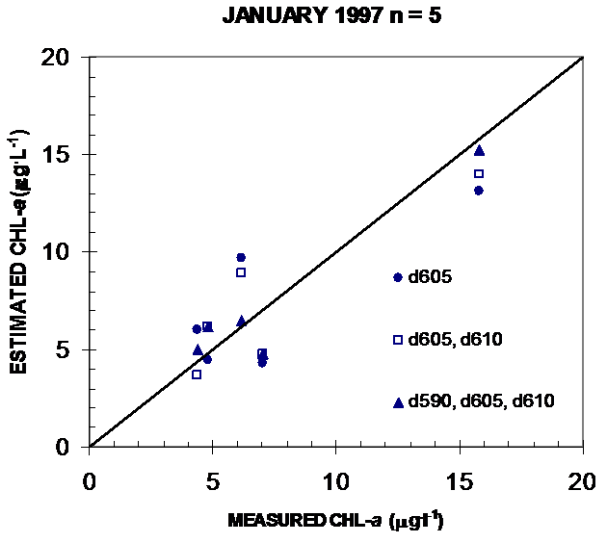

c. Estimated versus measured values of chlorophyll-a values in the green peak (590-610nm) spectrum from September 1996 to July 1997 using regression models in Table 11.

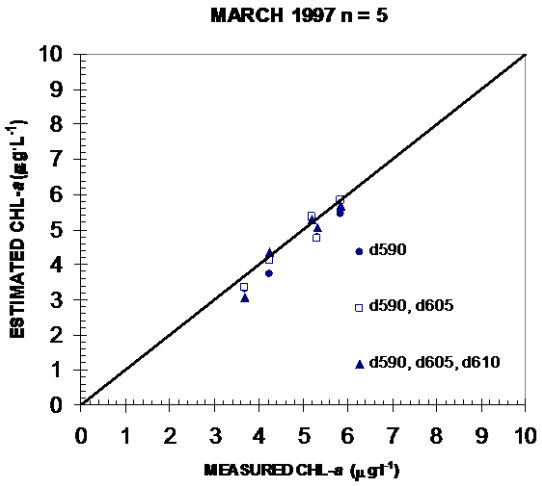

d. Estimated versus measured values of chlorophyll-a values in the green peak (590-610nm) spectrum from September 1996 to July 1997 using regression models in Table 11.

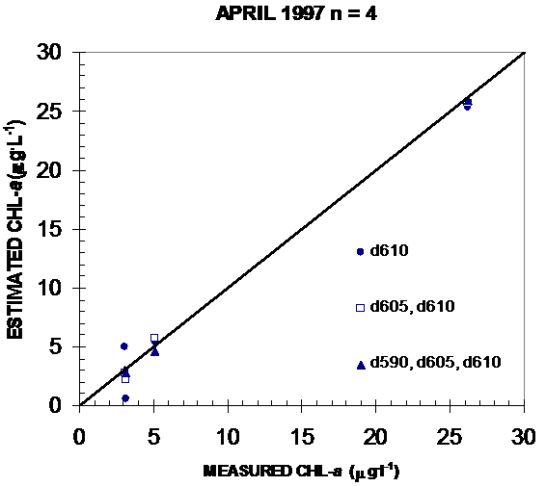

e. Estimated versus measured values of chlorophyll-a values in the green peak (590-610nm) spectrum from September 1996 to July 1997 using regression models in Table 11.

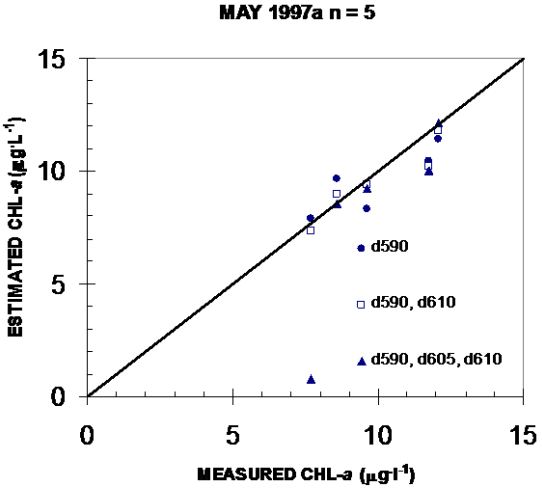

f. Estimated versus measured values of chlorophyll-a values in the green peak (590-610nm) spectrum from September 1996 to July 1997 using regression models in Table 11.

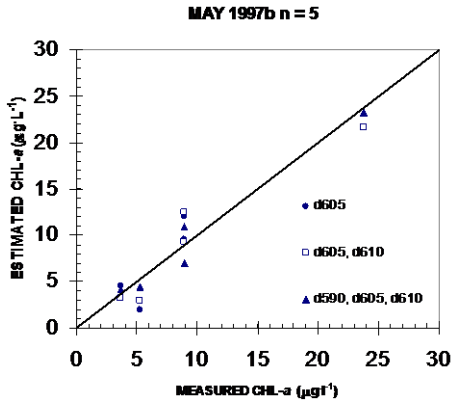

g. Estimated versus measured values of chlorophyll-a values in the green peak (590-610nm) spectrum from September 1996 to July 1997 using regression models in Table 11.

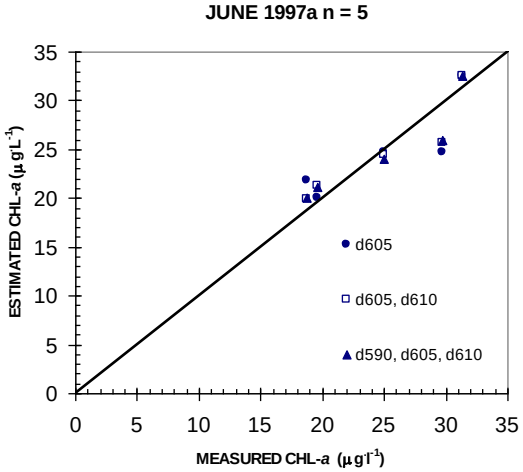

h. Estimated versus measured values of chlorophyll-a values in the green peak (590-610nm) spectrum from September 1996 to July 1997 using regression models in Table 11.

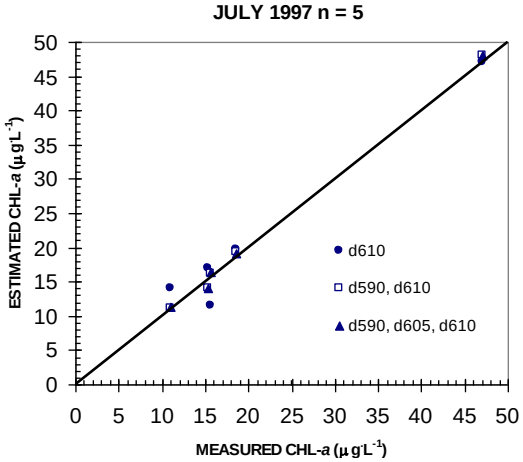

i. Estimated versus measured values of chlorophyll-a values in the green peak (590-610nm) spectrum from September 1996 to July 1997 using regression models in Table 11.

Figure 11. *Relationship between estimated versus the mean of measured chlorophyll-a concentrations (µg l^{-1}) from September 1996 to July 1997 using the max r^2 improvement multiple regression models of the chlorophyll green peak at 590-610nm.*

● = best single variable model, □ = best two variable model, ▲ = best multi-variable model from Table 11. Measured values were the excluded samples from the trimmed-mean analysis run on chlorophyll-*a* and other water quality parameters during multiple regression analysis.

Abbreviations

ANOVA	Analysis of Variance
ASCII	American Standard Code for Information Interchange
Chl-*a*	Chlorophyll-*a*, Key Pigment Found in Plants, Algae, and Cyanobacteria in Absorbing Light
FWHM	Full Width at Half the Maximum Peak
IR	Infra-red
H_o	Null Hypothesis
nm	Nanometer/Nanometers
m	Meter/Meters
NTU	Nephelometric Turbidity Unit
PAR	Photosynthetically Available Radiation
SD	Secchi Depth
TDS	Total Dissolved Solids
TSS	Total Suspended Solids
WQMP	Water Quality Monitoring Program
β	Population Regression Coefficient
η"	Attenuation Coefficient
Io	Irradiance at 0.1 Meter
Iz	Irradiance at Depth, z
λ	Wavelength of Light (Peak-to-Peak)
P	Probability Value
r^2	Coefficient of Determination in a Regression Model
r_s	Spearman's rho Coefficient, a Nonparametric Correlation Coefficient
μ	Mean Value
μg	Microgram
Zeu	Depth of Euphotic Zone

Acknowledgments

This paper is dedicated to my graduate chair and major professor, and esteemed limnologist, the late Dr. Kenneth L. Dickson, and to the other members of my graduate committee, Dr. Samuel ("*Looks Like Science*") F. Atkinson and Dr. Miguel F. Acevedo, for their support in allowing me to participate in the Lake Texoma Water Quality Monitoring Program (WQMP). This project provided me with hands-on experience in various aspects of limnology, both in the field and in the laboratory.

Author Contributions

David Alan Rolbiecki is the sole author. The author read and approved the final manuscript.

Data Available Statement

The data supporting the outcome of this research is available upon reasonable request.

Funding

This work was funded by the U.S. Army Corps of Engineers, Tulsa District from 1996-1998.

Conflicts of Interest

The author declares no conflicts of interest.

Appendix

Table A1. *Water quality parameters taken at eleven fixed sampling stations at Lake Texoma from August 1996 to August 1997.*

Mean Chlorophyll-*a* (mg. L^{-1})												
	Aug-96	**Sep-96**	**Nov-96**	**Jan-97**	**Mar-97**	**Apr-97**	**May-97a**	**May-97b**	**Jun-97a**	**Jun-97b**	**Jul-97**	**Aug-97**
1 (RR)	59.6	15.7	40.9	19.0	18.6	10.6	9.7	33.1	21.9	12.8	28.5	n/a
3 (RR) †	16.8	16.5	27.9	15.7	5.8	26.1	8.5	23.8	19.0	20.1	15.1	35.5
7 (BM)	29.2	25.4	48.6	17.9	16.6	8.8	10.9	5.1	42.2	25.1	41.6	n/a
8 (RRT)	14.0	18.1	19.2	9.9	7.6	14.3	13.8	6.0	27.3	19.3	20.8	n/a
9 (RRT)†	15.4	21.0	15.8	7.0	4.2	7.0	11.3	5.2	25.1	20.5	15.7	37.6
17 (ML)†	14.9	10.3	5.9	4.4	5.3	3.0	7.7	3.6	31.3	22.2	11.0	16.4
19 (ML)	12.7	13.4	7.1	4.6	5.9	2.3	17.7	11.1	30.0	34.6	9.8	n/a

Mean Chlorophyll-*a* (mg. L^{-1})												
	Aug-96	**Sep-96**	**Nov-96**	**Jan-97**	**Mar-97**	**Apr-97**	**May-97a**	**May-97b**	**Jun-97a**	**Jun-97b**	**Jul-97**	**Aug-97**
20 (WRT)	14.0	17.9	6.7	7.7	14.0	7.7	19.0	7.4	31.0	26.2	12.2	n/a

† = 10 replicate samples; otherwise, 3 replicates, * = not measured

Mean Chlorophyll-*a* (mg. L^{-1})												
	Aug-96	**Sep-96**	**Nov-96**	**Jan-97**	**Mar-97**	**Apr-97**	**May-97a**	**May-97b**	**Jun-97a**	**Jun-97b**	**Jul-97**	**Aug-97**
22 (WRT)†	29.3	25.1	3.9	4.6	3.5	3.1	12.1	8.9	29.3	34.8	18.5	26.1
24 (WR)†	26.6	13.6	5.2	6.2	5.2	5.0	9.5	8.9	19.5	40.2	47.5	30.7
25 (WR)	*	12.6	7.3	7.3	4.8	4.3	7.6	4.0	9.8	39.7	45.4	n/a

† = 10 replicate samples; otherwise, 3 replicates, * = not measured

Mean Turbidity (NTU)												
	Aug-96	**Sep-96**	**Nov-96**	**Jan-97**	**Mar-97**	**Apr-97**	**May-97a**	**May-97b**	**Jun-97a**	**Jun-97b**	**Jul-97**	**Aug-97**
1 (RR)	17	57	21	8	20	53	27	18	20	29	12	n/a
3 (RR) †	5	9	8	5	17	8	26	6	11	4	5	5
7 (BM)	8	11	25	7	28	23	12	7	7	6	8	n/a
8 (RRT)	4	6	7	5	17	9	11	6	7	5	3	n/a
9 (RRT)†	4	5	7	4	16	7	8	5	4	4	3	4
17 (ML)†	4	2	5	3	4	2	3	2	4	3	2	2
19 (ML)	4	3	5	3	5	3	4	3	5	4	3	n/a
20 (WRT)	4	5	13	3	6	5	5	5	6	5	4	n/a
22 (WRT)†	5	5	12	4	11	7	7	8	9	8	4	3
24 (WR)†	9	19	20	6	28	17	33	8	14	12	9	5
25 (WR)	*	26	29	6	38	30	39	27	73	11	8	n/a

† = 10 replicate samples; otherwise, 3 replicates, * = not measured

Table A2. *Secchi depth (SD), vertical attenuation coefficients (η”· m^{-1}) and depth of euphotic zone (Z_{eu}) taken at eleven fixed sampling stations at Lake Texoma from August 1996 to August 1997.*

Secchi Depth (m)												
	Aug-96	**Sep-96**	**Nov-96**	**Jan-97**	**Mar-97**	**Apr-97**	**May-97a**	**May-97b**	**Jun-97a**	**Jun-97b**	**Jul-97**	**Aug-97**
1 (RR)	0.52	0.20	0.35	0.75	0.38	0.15	0.25	0.45	0.42	0.25	0.55	0.25
3 (RR)	1.03	0.74	0.90	0.94	0.50	0.75	0.35	0.95	0.65	1.15	1.25	0.35
7 (BM)	0.52	0.56	0.23	0.82	0.35	0.41	0.75	1.05	0.85	0.85	0.75	0.75

Secchi Depth (m)

	Aug-96	Sep-96	Nov-96	Jan-97	Mar-97	Apr-97	May-97a	May-97b	Jun-97a	Jun-97b	Jul-97	Aug-97
8 (RRT)	0.92	0.97	0.93	1.15	0.45	0.75	0.58	0.91	0.85	0.85	1.50	0.58
9 (RRT)	1.53	1.06	0.93	1.31	0.51	1.01	0.60	1.80	1.35	1.35	1.85	0.60
17 (ML)	1.38	1.62	1.30	1.80	1.75	3.38	1.85	1.48	1.15	1.95	1.55	1.85
19 (ML)	1.30	1.67	1.68	2.15	1.67	1.71	1.40	1.85	0.60	1.45	1.75	1.33
20 (WRT)	1.20	1.13	0.55	0.65	1.05	1.09	1.10	1.21	1.05	1.05	1.01	1.07
22 (WRT)	0.90	0.95	0.57	1.45	0.75	0.75	0.80	0.76	0.65	0.75	1.25	1.40
24 (WR)	0.50	0.50	0.42	1.23	0.35	0.47	0.35	0.78	0.35	1.07	0.85	0.95
25 (WR)	*	0.31	0.27	0.92	0.32	0.25	0.15	0.35	0.29	0.45	0.65	0.85

Vertical Attenuation coefficient (h". m^{-1})

	Aug-96	Sep-96	Nov-96	Jan-97	Mar-97	Apr-97	May-97a	May-97b	Jun-97a	Jun-97b	Jul-97	Aug-97
1 (RR)	2.40	2.73	2.90	1.56	2.16	5.13	2.38	1.83	2.47	3.28	2.09	2.62
3 (RR)	1.03	1.69	1.96	1.15	3.73	1.68	2.62	1.19	1.68	1.23	1.00	1.29
7 (BM)	1.36	2.08	2.89	1.32	2.69	2.83	2.60	1.21	1.47	2.08	1.70	1.73
8 (RRT)	1.01	1.53	1.69	1.10	2.17	1.71	1.96	1.15	1.55	1.32	0.89	1.30
9 (RRT)	0.83	1.22	1.00	0.82	2.20	1.19	1.08	0.90	0.96	1.28	0.82	1.01
17 (ML)	0.67	0.90	0.86	0.75	0.62	0.74	0.84	0.54	1.21	0.90	0.75	0.82
19 (ML)	0.58	0.73	1.04	0.81	0.86	0.67	0.95	0.77	0.94	0.86	0.85	0.76
20 (WRT)	0.60	1.25	2.07	0.91	1.12	0.87	1.13	1.01	1.54	0.95	1.02	0.87
22 (WRT)	1.05	1.23	1.90	1.08	1.45	1.14	1.26	1.32	1.78	1.44	0.95	0.80
24 (WR)	1.21	1.94	2.66	1.11	1.72	1.79	3.58	1.64	2.62	2.27	1.35	1.16
25 (WR)	*	1.88	1.44	1.73	2.97	3.19	3.26	2.78	5.55	2.30	1.71	1.69

† = 10 replicate samples; otherwise, 3 replicates, * = not measured

Depth of Euphotic Zone, Z_{eu} (m)

	Aug-96	Sep-96	Nov-96	Jan-97	Mar-97	Apr-97	May-97a	May-97b	Jun-97a	Jun-97b	Jul-97	Aug-97
1 (RR)	1.91	1.67	1.54	2.85	2.12	0.92	1.87	2.53	1.80	1.43	2.14	1.72
3 (RR)	4.40	3.20	3.19	6.70	2.36	2.64	1.69	3.86	2.69	3.77	4.54	3.45
7 (BM)	3.35	2.22	1.59	3.46	1.69	1.51	1.77	3.82	3.07	2.15	2.67	2.66
8 (RRT)	4.58	2.92	2.71	4.26	2.20	2.57	2.38	4.01	2.91	3.46	4.98	3.43
9 (RRT)	5.53	3.78	4.61	5.72	2.13	3.63	4.25	5.11	4.83	3.48	5.40	4.45
17 (ML)	6.77	5.15	5.36	6.34	7.32	5.61	5.59	8.58	3.76	5.27	6.17	5.35
19 (ML)	7.90	6.25	4.39	5.62	5.35	6.38	4.90	6.01	4.58	5.39	5.23	6.00
20 (WRT)	7.60	3.58	2.14	5.14	4.12	5.31	4.07	4.59	2.92	4.92	4.38	5.16

Depth of Euphotic Zone, Z_{eu} (m)

	Aug-96	Sep-96	Nov-96	Jan-97	Mar-97	Apr-97	May-97a	May-97b	Jun-97a	Jun-97b	Jul-97	Aug-97
22 (WRT)	4.42	3.75	2.34	4.24	3.19	4.02	3.59	3.51	2.57	3.13	4.88	5.73
24 (WR)	3.80	2.37	1.70	4.14	1.52	1.87	1.22	2.87	1.74	1.93	3.42	3.94
25 (WR)	*	2.53	1.83	2.62	1.55	1.42	1.35	1.65	0.81	1.92	2.65	2.56

† = 10 replicate samples; otherwise, 3 replicates, * = not measured

References

[1] Acevedo, D. V., D. F. Bogs, M. F. Acevedo, S. F x. Atkinson, B. Qui, J. Hemming, K. L. Dickson, W. T. Waller, F. Mayer and M. Lewis. 1995. High-Resolution Spectral Characteristics of Light Attenuation and Reflectance Above Seagrass Beds. Publication pending.

[2] Atkinson, S. F., K. L. Dickson and W. T. Waller. 1996. Lake Texoma Water Quality Monitoring Program. A Proposal to the: U.S. Army Corps of Engineers and Red River Authority. *Environmental Science Program. University of North Texas, Denton, Texas.*

[3] Atlas, D. and T. T. Bannister. 1980. Dependence of Mean Spectral Extinction Coefficient of Phytoplankton on Depth, Water Color, and Species. *Limnol. Oceanogr.* 25(1): 157-159.

[4] Beeton, A. M. 1957. Relationship Between Secchi Disk Readings and Light Penetration in Lake Huron. *Trans. Am. Fish. Soc. 87: 73-79.*

[5] Beitinger, T. L. 1997. Professor of ichthyology, University of North Texas.

[6] Bowling, L. C. 1988. Optical Properties, Nutrients and Phytoplankton of Freshwater Coastal Dune Lakes in South-east Queensland. *Aust. J. Freshwater Res. 39: 805-815.*

[7] Buiteveld, H. 1995. A Model for Calculation of Diffuse Light Attenuation (PAR) and Secchi Depth. *Netherlands Journal of Aquatic Ecology. 29(1): 55-65.*

[8] Cairns, S. H. 1993. Eutrophication Monitoring and Prediction. Ph. D. Dissertation. University of North Texas. 161 pp.

[9] Carlson, R. E. 1977. Trophic State Index for Lakes. *Limnol. Oceanogr. 22: 361-369.*

[10] Carlson, R. E. 1980. More Complications in the Chlorophyll-Secchi Dish Relationship. *Limnol. Oceanogr. 25(2): 379-382.*

[11] Chen, Z., P. J. Curran and J. D. Hansom. 1992. Derivative Reflectance Spectroscopy to Estimate Suspended Sediment Concentration. *Remote Sens. Environ. 40: 67-77.*

[12] Clyde, G. A. 2004. Spatial and Temporal Patterns Exhibited by Select Physicochemical and Biological Water Quality Parameters in Lake Texoma, Oklahoma and Texas. Ph. D. Dissertation. University of North Texas. 157 pp.

[13] Davies-Colley, R. J., W. N. Vant and R. J. Wilcock. 1988. Lake Water Color: Comparison of Direct Observations With Underwater Spectral Irradiance. *Water Resources Bulletin. 24(1): 11-18.*

[14] Davies-Colley, R. J. and W. N. Vant. 1988. Estimation of Optical Properties of Water from Secchi Disk Depths. *Water Resources Bulletin. 24(6): 1329-1335.*

[15] Dekker, A. G., T. J. Malthus, M. M. Wijnen and E. Seyhan. 1992. The Effect of Spectral Bandwidth and Positioning on the Spectral Signature Analysis of Inland Waters. *Remote Sens. Environ. 41: 211-225.*

[16] Demetriades-Shah, T. H., M. D. Steven and J. A. Clark. 1990. High Resolution Derivative Spectra in Remote Sensing. *Remote Sens. Environ. 33: 55-64.*

[17] Dixit, L. and S. Ram. 1985. Quantitative Analysis by Derivative Electron Spectroscopy. *Applied Spectroscopy Reviews. 21(4): 311-418.*

[18] Dubinsky, Z. and T. Berman. 1976. Light Utilization Efficiencies of Phytoplankton in Lake Kinneret (Sea of Galilee). *Limnol. Oceanogr. 21(2): 226-230.*

[19] Dubinsky, Z. and T. Berman. 1979. Seasonal Changes in the Spectral Composition of Downwelling Irradiance in Lake Kinneret (Israel). *Limnol. Oceanogr. 24(4): 652-663.*

[20] Dubinsky, Z. and T. Berman. 1981. Light Utilization by Phytoplankton in Lake Kinneret (Israel). *Limnol. Oceanogr. 26(4): 660-670.*

[21] French, R. H., J. J. Cooper, and S. Vigg. 1982. Secchi Disk Relationships. *Water Resources Bulletin. 18(1): 121-123.*

[22] Gade, D., S. L. Burks and A. V. Zale. 1992. An Evaluation of the Effect of Decreased Chloride Concentration in the Red River Basin on Primary Production and Sport Fish Abundance in Lake Texoma. *Report to the U.S. Army Corps of Engineers Environmental Section, Tulsa District.*

[23] Gallegos, C. L., D. L. Correll and J. W. Pierce. 1990. Modeling Spectral Diffuse Attenuation, Absorption, and Scattering Coefficients in a Turbid Estuary. *Limnol. Oceanogr. 35(7): 1486-1502.*

[24] Gitelson. A. A., K. Ya. Kondratyev. 1991. Optical Models of Mesotrophic and Eutrophic Water Bodies. *Int. J. Remote Sensing. 12(3): 373-385.*

[25] Goodin, D. G., L. Han, R. N. Rolland, N. Fraser, D. C. Rundquist, W. A. Stebbins and J. F. Schalles. 1993. Analysis of Suspended Solids in Water Using Remotely Sensed High Resolution Derivative Spectra. *Photogramm. Eng. Remote Sens. 59(4): 505-510.*

[26] Graham, J. J. 1966. Secchi Disk Observations and Extinction Coefficients in the Central and Eastern North Pacific. *Limnol. Oceanogr. 11: 184-190.*

[27] Hambright, D. K, R. M. Zamor, J. D. Easton, K. L. Glenn, E. J. Remmel, and A. C. Easton. 2010. Temporal and spatial variability of an invasive toxigenic protist in a North American subtropical reservoir. *Harmful Algae. 9 (2010): 568–577.*

[28] Henderson-Sellers, A. and P. J. Robinson. 1987. Contemporary *Climatology. Longman Scientific & Technical, UK.*

[29] Jewson, D. H. and J. A. Taylor. 1978. The Influence Of Turbidity On Net Phytoplankton Photosynthesis In Some Irish Lakes. *Freshwater Biology. 8: 573-584.*

[30] Jones, R. L., J. M. Young, A. M. Hartley and A. E. Bailey-Watts. 1996. Light Limitation of Phytoplankton Development in an Oligotrophic Lake – Loch Ness, Scotland. *Freshwater Biology. 35: 533-543.*

[31] Juday, C. 1940. The Annual Energy Budget Of An Inland Lake. *Ecology. 21(4): 438-50.*

[32] Kiefer, D. A., R. J. Olson and W. H. Wilson. 1979. Reflectance Spectroscopy of Marine Phytoplankton. Part 1. Optical Properties as Related to Age and Growth. *Limnol. Oceanogr. 24(4): 664-672.*

[33] Knowlton, M. F. and J. R. Jones. Testing Models of Chlorophyll and Transparency for Midwest Lakes and Reservoirs. *Lake and Reservoir Management. 8(1): 13-16.*

[34] Koenings, J. P and J. A. Edmundson. 1991. Secchi Disk and Photometer Estimates of Light Regimes in Alaskan Lakes: Effects of Yellow Color and Turbidity. *Limnol. Oceanogr. 36(1): 91-105.*

[35] Lee, G. F., W. Rast and R. A. Jones. 1978. Eutrophication Of Water Bodies: Insights For An Age-Old Problem. *Environmental Sciences and Technology. 12(8): 900-908.*

[36] Lee, G. F. and R. A. Jones. 1991. Effects of Eutrophication on Fisheries. *Reviews in Aquatic Sciences. 5(3-4): 287-305.*

[37] Lee, G. F., A. Jones-Lee and W. Rast. 1995. Secchi Depth as a Water Quality Parameter. Publication pending.

[38] Lind, O. T. 1983. Handbook of Common Methods in Limnology, 2nd Edition. *Kendal / Hunt Publishing Co., USA.*

[39] Lorenzen, M. W. 1980. Use of Chlorophyll-Secchi Disk Relationships. *Limnol. Oceanogr. 25(2): 371-372.*

[40] Mather, P. M. 1991. Computer Processing of Remotely-Sensed Images. *John Wiley & Sons.*

[41] Matthews, W. J., L. G. Hill and S. M. Scellhaass. 1985. Depth Distribution of Striped Bass and Other Fish in Lake Texoma (Oklahoma-Texas) During Summer Stratification. *Transactions of the American Fisheries Society. 114: 84-91.*

[42] Matthews, W. J. and L. G. Hill. 1988. Physical and Chemical Profiles in Lake Texoma (Oklahoma-Texas) in Summer 1982 and 1983. *Proceedings of the Oklahoma Academy of Sciences. 68: 33-38.*

[43] McPherson, B. F. and R. L. Miller. 1987. The Vertical Attenuation of Light in Charlotte Harbor, a Shallow, Subtropical Estuary, Southwestern Florida. *Estuarine, Coastal and Shelf Science. 25: 721-737.*

[44] McPherson, B. F. and R. L. Miller. 1994. Causes of Light Attenuation in Tampa Bay and Charlotte Harbor, Southwestern Florida. *Water Resources Bulletin. 30(1): 43-53.*

[45] Megard, R. O., J. C. Settles, H. A. Boyer, and W. S. Combs, Jr. 1980. Light, Secchi Disks, and Trophic States. *Limnol. Oceanogr. 25(2): 373-377.*

[46] Millie, D. F., G. J. Kirkpatrick and B. T. Vinyard. 1995. Relating Photosynthetic Pigments and *in vivo* Optical Density Spectra to Irradiance for the Florida Red-Tide Dinoflagellate *Gymnodinium breve. Marine Ecology Progress Series. 120: 65-75.*

[47] Ritchie, J. C., C. M. Cooper and F. R. Schiebe. 1990. The Relationship of MSS and TM Digital Data with Suspended Sediments, Chlorophyll, and Temperature in Moon Lake, Mississippi. *Remote Sens. Environ.. 33: 137-148.*

[48] Rørslett, B., I. Hawes and A-M. Schwarz. 1997. Features of the Underwater Light Climate Just Below the Surface in some New Zealand Inland Lakes. *Freshwater Biology. 37: 441-454.*

[49] Sathyendranath, S., L. Lazzara and L. Prieur. 1987. Variations in the Spectral Values of Specific Absorption of Phytoplankton. *Limnol. Oceanogr. 32(2): 403-415.*

[50] Schindler, J. E., B. J. Speziale, S. P. Mellinchamp, E. E. Robertson and J. J. Hain. 1995. The Effect of Pump-Storage Power Generation on Water Column Optical Features and Plankton Dynamics in the Forebay of Richard B. Russell Reservoir. *Lake and Reservoir Management. 11(3): 245-253.*

[51] Schwarz, A.-M., I. I. Hawes, and C. Howard-Williams. 1996. The role of photosynthesis/light relationships in determining lower depth limits of Characeae in South Island, New Zealand lakes. *Freshwater Biology. 35(1): 69-80.*

[52] Smith, R. C. and K. S. Baker. 1978. The Bio-Optical State of Ocean Waters and Remote Sensing. *Limnol. Oceanogr. 23(2): 247-259.*

[53] Spinrad, R. W., K. L. Carder, and M. J. Perry. 1994. Ocean Optics. *Oxford University Press, New York. 283 pp.*

[54] Tilzer, M. M. 1983. The Importance of Fractional Light Absorption by Photosynthetic Pigments for Phytoplankton Productivity in Lake Constance. *Limnol. Oceanogr. 28(5): 833-846.*

[55] Townsend, S. A., J. T. Luong-Van and K. T. Boland. 1996. Retention Time as a Primary Determinant of Colour and Light Attenuation in Two Tropical Australian Reservoirs. *Freshwater Biology. 36: 57-69.*

[56] Walker, T. A. 1982. Use of a Secchi Disc to Measure Attenuation of Underwater Light for Photosynthesis. *Journal of Applied Ecology. 19: 539-544.*

[57] Wang, B., Y. Ma, Y. Wang, Lazhu, L. Wang, W. Ma, and B. Su. 2023. Analysis of Lake Stratification and Mixing and Its Influencing Factors over High Elevation Large and Small Lakes on the Tibetan Plateau. Water. *15(2094): 1-17*.

[58] Wattenberg, F. 1997. Estimating First Derivatives Numerically. *Department of Mathematics, Montana State University, Bozeman, MT*.

[59] Wetzel, R. G. 1983. Limnology, *2nd Edition. W. B. Saunders, Philadelphia, USA.*

[60] Wiggli, M., R. Ghosh and R. Bachofen. 1996. Optical Fiber-Based In Situ Spectroscopy of Pigmented Single Colonies. *Applied and Environmental Microbiology. 62(9): 3339-3343*.

[61] Wilson, W. H. and D. A. Kiefer. 1979. Reflectance Spectroscopy of Marine Phytoplankton. Part 2. A Simple Model of Ocean Color. *Limnol. Oceanogr. 24(4): 673-682*.

[62] Yacobi, Y. Z., A. Gitelson and M. Mayo. 1995. Remote Sensing of Chlorophyll in Lake Kinneret Using High-Resolution Radiometer and Landsat TM: Spectral Features of Reflectance and Algorithm Development. *Journal of Plankton Research. 17(11): 2155-2173.*

[63] Zar, J. H. 1984. Biostatistical Analysis, Second Edition. *Prentice-Hall. 718 pp.*